

First-principles simulations of atomic geometries, electronic properties and chemical reactions at interfaces

Fahdzi MUTTAQIEN, Yuji HAMAMOTO, Kouji INAGAKI, and Yoshitada MORIKAWA

*Department of Precision Science and Technology,
Osaka University, Yamada-oka, Suita, Osaka 565-0871*

Adsorption and reaction of CO₂ on solid surfaces are attracting growing interest because of their importance in industrial, energy and environmental management[1]. In industry, H₂, CO₂ and CO gas mixtures are used in methanol synthesis by using Cu/ZnO/Al₂O₃ catalysts, where CO₂ is considered to be the main carbon source on the basis of the results of an isotope labeling experiment.

Previous studies of CO₂ adsorption on single-crystal Cu surfaces have shown that CO₂ is adsorbed more strongly on defective Cu surfaces than on flat Cu surfaces. On flat copper surfaces, CO₂ is weakly adsorbed molecularly and needs high activation energy to dissociate: 0.69 eV for Cu(110)[2]. Using temperature programmed desorption (TPD) experiment, Fu and Somorjai found that CO₂ is adsorbed and dissociates to CO and O on the Cu(311) surfaces with a 4 L dose at 150 K[3]. Boenicke *et al.* showed by means of thermal desorption spectroscopy (TDS) experiment that CO₂ is chemisorbed and dissociates at 95 K over the Cu(332) surface[4]. Using infrared reflection absorption spectroscopy (IRAS), Koitaya and co-workers recently discovered

that CO₂ dissociates on the Cu(997) stepped surface at 83 K[5]. They exposed isotopically labelled ¹³CO₂ to the Cu(997) surface at 83 K and observed two absorption peaks at 2050cm⁻¹ and 2066 cm⁻¹, which are assigned to the C-O stretching mode of ¹³CO at terrace and step sites, respectively, clearly demonstrating the dissociation of CO₂. They also discovered that there is no CO₂ dissociation on the Cu(111) surface at 83K.

To investigate the minimum energy pathways of the CO₂ dissociation process, we considered the Cu(111), Cu(221), Cu(211), and Cu(11 5 9) surfaces. We used three close-packed layers for the slab models and a fixed bottom atomic layer. The slab surfaces were constructed by using a calculated equilibrium lattice constant of 3.65Å, which is close to the experimental value of 3.62Å.

The standard GGA Perdew-Burke-Ernzerhof (GGA-PBE) exchange-correlation functional was used for the DFT calculations. The dispersion correction (DFT-D2) proposed by Grimme was used to describe the dispersion interaction between metal atoms and molecules. All calculations were carried out by using the

STATE (Simulation Tool for Atom TEchnology) package, which previously had been applied to the synthesis of formate and its hydrogenation process.

To check the accuracy of our results, we used a van der Waals density functional (vdW-DF) proposed by Dion and co-workers. The vdW-DF calculations were applied to charge density data obtained from standard GGA calculations.

We found that CO_2 is weakly adsorbed on stepped surfaces and that the dissociated products are less stable than the initial ones even if the dissociated CO species are located at the on-top site of copper atoms. The characteristic of CO_2 adsorption in the initial states for all models is identified by its relative distance from the surface (more than 3\AA) and its vibrational frequencies, which are close to those in the isolated gas phase.

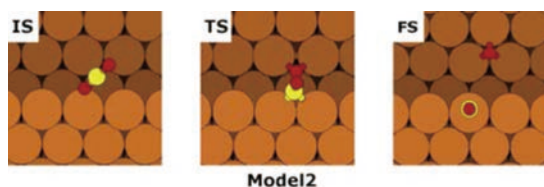


Fig. 1: CO_2 dissociation path on the Cu(221) surface.

We investigated the dissociation process of CO_2 to $\text{CO} + \text{O}$ on the Cu(111), Cu(221), Cu(211), and Cu(11 5 9) surfaces by using DFT-GGA and vdW-DF calculations. The

activation barrier for CO_2 dissociation on the flat Cu(111) surface is 1.33 eV, which agrees well with previous reports. For stepped surfaces, the activation energies are slightly lower, 1.06 eV, 0.67 eV, and 1.02 eV for the Cu(221), Cu(211), and Cu(11 5 9) surfaces, respectively. From our results, we conclude that CO_2 does not dissociate on the flat, stepped or kinked Cu surfaces at low temperature. We attribute the experimentally observed CO_2 dissociation on stepped Cu surfaces below 150 K to other factors such as Cu adatoms, gas phase or condensed CO_2 , or other gas phase molecules.

References

- [1] H.-J. Freund and M.W. Roberts, *Surf. Sci. Rep.*, **25**, 225 (1996).
- [2] J. Nakamura, J.A. Rodriguez, and C.T. Campbell, *J. Phys.: Condens. Matter* **1**, 149 (1989).
- [3] S. Fu and G.A. Somorjai, *Surf. Sci.* **262**, 68 (1992).
- [4] I.A. Boenicke, W. Kirstein, and F. Thieme, *Surf. Sci.* **307**, 177 (1994).
- [5] T. Koitaya, Y. Shiozawa, K. Mukai, S. Yoshimoto, and J. Yoshinobu, "14th International Conference on Vibrations at Surfaces in Kobe", (2012), and personal communication.

Atomic Structures and Electronic Properties of Hard- and Soft-Nanomaterials

Atsushi Oshiyama

Department of Applied Physics, The University of Tokyo
Hongo, Tokyo 113-8656

The two of our achievements in my group are reported in the following.

1. Magic Angle and Height Quantization in Nanofacets on SiC(0001) Surfaces

Nanostructures on surfaces are utilized as templates for subsequent nano-fabrications. A typical example is the faceting that is the unexpected and spontaneous appearance of the small-area surface on the substrate surface. SiC is one of the semiconductors which are most promising in power electronics. The epitaxial growth of SiC films plays a central role in the fabrication of SiC devices. In such epitaxial growth, the $(11\bar{2}n)$ nanofacets frequently appear on the (0001) surfaces. It is observed that such nanofacets consist of bunched atomic steps. Mysteriously, the facet angle φ which is the angle between the (0001) and the $(11\bar{2}n)$ planes is insensitive to the crystal polytype and the vicinal angle, being in the range of 12 - 16°, which we call *magic facet angle*. Moreover, the height of the nanofacet along the (0001) direction is interestingly *quantized* to a integer or a half-integer of the unit-cell height.

We have performed large-scale density-functional calculations using our real-space scheme (RSDFT code) [1,2]. We have found that the bunched single-bilayer steps are energetically favorable than equally spaced atomic steps, leading to the formation of the $(11\bar{2}n)$ nanofacets with a particular facet angle of $\varphi = 15^\circ$. We find that the balance between two factors, i.e., the step-step repulsive energy and the surface-energy variation, which comes from the different bilayer atomic sequence near the surface, is the reason for the *magic facet angle* and the *quantization* of the facet height.

Figure 1 shows the geometry optimized single-bilayer (SB) step on the 4H-SiC (0001) surface. In the SB step, the Si atom on the upper terrace rebonds with the partner Si atom on the lower terrace at the step edge. The energy gain from this rebonding is 2.1 eV per unit length a_0 ($a_0 = 5.27 \text{ \AA}$) along

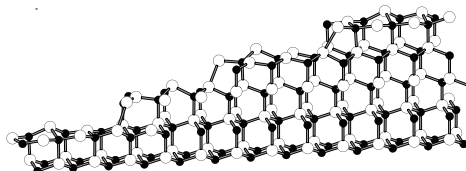


Figure 1: Geometry optimized single-bilayer height step on the 4H-SiC (0001) surface. Large open and small solid circles denote Si and C atoms, respectively. Step edge atoms are either three-fold or four-fold coordinated.

the step-edge direction. The formation energy for the SB step, λ_{SB} , is 0.31 eV/ a_0 in the present LDA calculations. We have also performed geometry optimization for the double-bilayer (DB) and quad-bilayer (QB) steps. On the contrary to the SB step, the rebonding between the upper-terrace and the lower-terrace atoms is unfeasible. As a result of this, the formation energies of the DB step and the QB step, λ_{DB} and λ_{QB} , are larger than λ_{SB} by about 1.8 eV/ a_0 and 4.9 eV/ a_0 , respectively.

We next explore a possibility of its bunching which leads to the nanofacet. We have constructed the $(11\bar{2}n)$ facet ($n = 32, 24, 16, 12, 8, 4$) consisting of the SB steps on the vicinal surface with $\theta = 5.9^\circ$ (968 atoms in a cell of the slab model). The facet angles of these six nanofacets are $\varphi = 5.9, 7.8, 11.6, 15.3, 22.3, 39.2^\circ$ respectively. We have performed the geometry optimization and obtained the stable structures for each nanofacet. The total energies of thus obtained nanofacets are plotted as a function of the facet angle in Fig. 2. We have found that there is a particular facet angle of $\varphi_0 = 15^\circ$ which makes the total energy minimum, indicating the existence of the *magic facet angle*. The calculated value $\varphi_0 = 15^\circ$ agrees with the experimental observation.

2. Interstitial Channels that Control Band

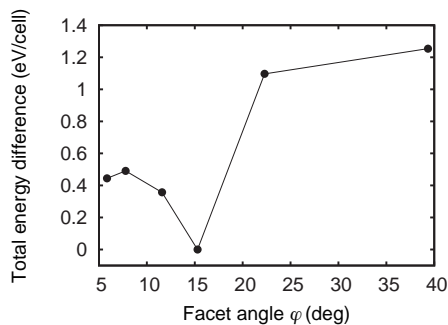


Figure 2: Total energy of the $(11\bar{2}n)$ nanofacet formed on the $4H$ -SiC (0001) vicinal surface as a function of the facet angle. The energies are relative to that of the most stable nanofacet with the facet angle $\varphi_0 = 15.3^\circ$ ($n = 12$). The total energy of the geometry optimized equally spaced SB steps (ESS) which corresponds to the facet angle of 5.9° is also shown.

Gaps and Effective Masses in Semiconductors

Most semiconductors, elemental or compound, have the four-fold coordinated tetrahedral structure caused by the hybridization of atomic orbitals. It is written in textbooks that the resultant hybridized sp^3 bonding orbitals constitute valence bands, whereas the anti-bonding counter parts do conduction bands. This is not necessarily true, however: We have recently found that the wavefunctions of the conduction-band minima (CBM) of the semiconductors are distributed not near atomic sites but in the interstitial channels [3]. The wavefunctions *float* in the internal space, i.e., the channels, inherent to the sp^3 -bonded materials.

Another structural characteristic in the semiconductor is the stacking of atomic bilayers along the bond axis direction such as AB (wurtzite) or ABC (diamond or zincblende). The different stacking sequence leads to the different polytype generally labeled by the periodicity of the sequence n and its symmetry, hexagonal (H) or cubic (C). The sequence determines the lengths and the directions of the interstitial channels: e.g., in the $3C$ polytype the channel along $\langle 110 \rangle$ extends infinitely, whereas in the $6H$ polytype the channel along $\langle 2\bar{2}01 \rangle$ has a finite length of $7a_0 / 2\sqrt{2}$ (a_0 : lattice constant). Hence the stacking affects the shapes of the wavefunctions of CBMs.

For SiC, dozens of polytypes of SiC are observed and the band gaps vary by 40 %, from 2.3 eV in $3C$ to 3.3 eV in $2H$ despite that the structures are locally identical to each other in the polytypes. This

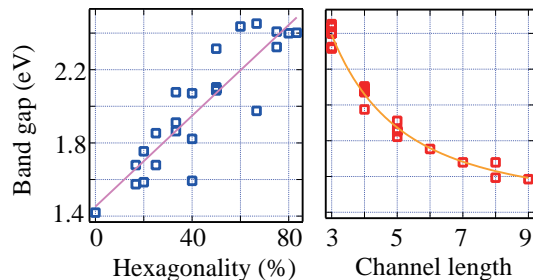


Figure 3: Band gaps for 24 representative SiC polytypes calculated in GGA as a function of the hexagonality (left panel) and a function of the channel length (right panel). In each panel, a fitting function is also shown. Each variance of the fitting is 355 (85) meV for a fitting curve as a function of hexagonality (channel length).

mysterious band-gap variation has been discussed in terms of an empirical quantity, hexagonality, for a half century: A bilayer sandwiched by the two same stacking indexes, as in $2H$ structure, is called a hexagonal layer and the ratio of the hexagonal layers in whole stacking sequence is called hexagonality; the band-gap variation in the polytypes is argued to be linear with respect to the hexagonality. Yet, the linearity is not satisfactory (see below) and moreover the underlying physics is totally lacking.

We have found, on the basis of the density-functional calculations, that the extent of the internal space, i.e., the length of the interstitial channel, in covalent semiconductors is decisive in the nano-scale shapes of the wavefunctions of the CBM and hereby explains the mysterious variation of the band gap in SiC polytypes (Fig. 3). We also find that the observed anisotropy of the effective masses in SiC, and the pressure dependence of the band gaps generally observed in most semiconductors, are naturally explained in terms of the channel length. Further, we find that the stacking control dramatically modifies the electronic properties, leading to generation of low-dimensional electron and hole systems in three-dimensional SiC.

References

- [1] K. Sawada, J.-I. Iwata and A. Oshiyama, Proc. ICSCRM **778-780**, 201 (2013).
- [2] K. Sawada, J.-I. Iwata and A. Oshiyama, APL **104**, 051605 (2014); submitted to PRB (2014).
- [3] Y. Matsushita and A. Oshiyama, PRL **112**, 136403 (2014); *ibid.*, **108**, 246404 (2012).

First-principles meta-dynamics analysis of Catalytic Referred Etching method (Reaction barrier in etching of GaN, SiC and SiO₂)

Kouji INAGAKI

Graduate School of Engineering, Osaka University

Yamadaoka 2-1, Suita, Osaka 565-0871

Step-and-terrace shaped smooth surfaces of wide-bandgap materials can be easily formed just by wiping the surface by a catalyst plate in an etching solution (named CARE(catalyst referred etching) method[1]), which is promising as an industrial surface finishing technique. To enhance etching rate and to find low-cost catalysts and/or safer etching materials is the current serious issue. In this project, we are investigating the reaction process in the atomic level to give a helping hand to experimentalists.

In this period, we have performed first-principles reaction barrier analysis of the initial stage of the etching process using the program package STATE[2,3] with Pt cluster placed near the reaction region. In the presence of Pt cluster, the energy barrier of dissociative adsorption of the etchant molecule found to become lower, in which the etchant molecule (H₂O or HF) is dissociatively absorbed on the process surface ([OH or F] to [SiC or SiO₂]) and Pt cluster (H to Pt). Figure 1 shows the schematic atomic structure of the intermediate meta-stable state of the reaction. The dissociative adsorption reaction finishes after

terminating C atom by H atom through a proton-relay-like reaction shown by arrows in Fig.1. The interaction between Pt (d orbital) and O (p orbital) is also found to be important for reducing the reaction barrier.

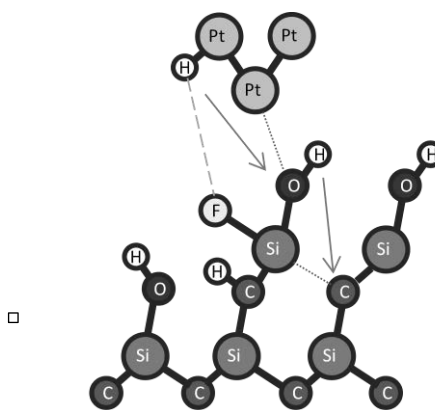


Fig. 1: Schematic view of the intermediate meta-stable atomic structure in the lower reaction barrier process.

References

- [1] H.Hara, et al., J.Electron.Mater. 35 (2006) L11.
- [2] Y. Morikawa, Phys. Rev. B 63 (2001) 033405.
- [3] T.Hayashi, Y. Morikawa, H. Nozoye, J. Chem. Phys. 114 (2001) 7615.
- [4] M.Oue, K.Inagaki, K.Yamauchi, Y.Morikawa, Nanoscale research lett. 8(2013) 323.

Ab Initio Study of Excited Electronic States and Nonadiabatic Processes of Nanostructures under External Fields

Kazuyuki WATANABE, Chunping HU, Keisuke TSUBONOYA,
Satoshi HAGIWARA, Taishi HIGUCHI
Department of Physics, Tokyo University of Science
1-3 Kagurazaka, Shinjuku-ku, Tokyo 162-8601

In the project we investigated the following five topics this year. 1) Laser-assisted field emission from silicene nanoribbons by time-dependent density functional theory (TDDFT), 2) Optical properties of boron nitride and graphene nanoribbons by TDDFT, 3) Low-energy electron wavepacket scattering with nanoflakes by TDDFT, 4) Field emission microscopy images of carbon nanotubes by TDDFT, 5) Evaluation of performance of Tamm-Dancoff approximation on nonadiabatic couplings by TDDFT.

1) *Laser-assisted field emission from silicene nanoribbons by TDDFT:*

We explored the laser-assisted field emission (LAFE) from graphene nanoribbons (GNR) in a previous study by the real-time TDDFT simulation, which is one of the most reliable and useful computational methods for describing dynamical phenomena associated with electronic excitations. We have shown the underlying physics of photoemission from GNRs that critically depends on the electric dipole transitions and the electronic properties of emitting states. In this study we further investigated the LAFE from silicene nanoribbons (SiNR) by the TDDFT for comparison with GNRs. The emission currents from SiNR are found to be much larger than from GNR for the same laser parameters in spite of the larger work function of SiNR than that of GNR. We have obtained the detailed results of electron emission and backward currents in real space and time under femtosecond laser pulses of various parameters. Large-scale TDDFT calculations have been performed using System A.

2) *Optical properties of boron nitride and graphene nanoribbons by TDDFT*[1]:

The dielectric functions of the armchair boron nitride nanoribbons with the comparison of their carbon analogues were investigated by the real-time TDDFT in the linear response regime. The energy dependence of dielectric functions changes very dramatically from hexagonal boron nitride to boron nitride white graphene (BNWG), while slightly changes from BNWG to BN nanoribbon (BNR). It was found that a remarkable difference appears in the imaginary part of dielectric function especially in the low energy region between BNR and graphene nanoribbons, which is attributed to the apparent difference in the energy band structures between them. Large-scale TDDFT calculations have been performed using System B.

3) *Low-energy electron wavepacket scattering with nanoflakes by TDDFT*[2]:

Low-energy electron scattering with nanoflakes was investigated using TDDFT simulation in real time and real space. By representing the incident electron as a finite-sized wave packet, we obtained diffraction patterns that show not only the regular features of conventional low-energy electron diffraction (LEED) for periodic structures but also special features resulting from the local atomic inhomogeneity. We also found a signature of π plasmon excitation upon electron impact on a graphene flake. The present study shows the remarkable potential of TDDFT for simulating the electron scattering process, which is important for clarifying the local

and periodic atomic geometries as well as the electronic excitations in nanostructures. Large-scale TDDFT calculations have been performed using System B.

4) *Field emission microscopy images of carbon nanotubes by TDDFT* [3]:

Theoretical field-emission (FE) patterns from pristine and H₂-adsorbed carbon nanotubes (CNTs) was simulated using the real-time TDDFT. The field-emitted electrons are treated in the equal footing with the electrons in the nanotubes and the spatial distributions of FE current densities are calculated directly by the time-propagated Kohn-Sham wave functions. The simulated results of pristine CNTs clearly show either five-fold or six-fold symmetries, corresponding to the symmetries of the features of pentagons on the CNT caps. Further simulations on the H₂ molecule adsorbed CNTs verify that the bright spots in the FE pattern are of signatures of atom adsorption onto CNTs, and the adsorption site should be close to the bright spots. Large-scale TDDFT calculations have been performed using System A.

5) *Evaluation of performance of Tamm-Dancoff approximation on nonadiabatic couplings by TDDFT*[4]:

We performed a systematic evaluation of the performance of the Tamm-Dancoff approximation for the TDDFT calculation of nonadiabatic couplings (NACs) between ground and excited states. In the cases we considered, the TDA performed better than the full TDDFT, contrary to the conjecture that the TDA might cause the NAC results to deteriorate and violate the sum rule. This was conjectured because it is well known that the sum rule of the oscillator strength is lost with the TDA, and the original formulation of NAC is similar to that for oscillator strength. The calculation results in the vicinity of Jahn-Teller and Renner-Teller intersections, as well as in an example of accidental conical intersections, show that the TDA can improve the accuracy of the NAC, since the TDA can give better excitation energies as a result of partially compensating for the LDA error when the intersections are approached. Our work also shows that the good performance of the TDA can only be achieved

on the basis of the rigorous TDDFT formulation of NAC. We believe that validation of the good performance of the TDA facilitates future nonadiabatic quantum simulations with TDDFT. Test of the parallel computing has been performed on System B, with the goal to parallelize the density-response calculations over atoms.

References

- [1] S. Hagiwara, H. Goto, C. Hu, and K. Watanabe: JPS. Conf. Proc. **1**, 012072 (2014).
- [2] K. Tsubonoya, C. Hu, and K. Watanabe, submitted.
- [3] C. Hu, R. Mori, and K. Watanabe, JPS Conf. Proc. **1**, 012067 (2014).
- [4] C. Hu, O. Sugino, and K. Watanabe, J. Chem. Phys. **140**, 054106 (2014).

First-principles calculation for light-matter interactions

Kazuhiro YABANA

Center for Computational Sciences,

University of Tsukuba, Tsukuba 305-8577

We have been developing a first-principles computational approach to describe electron dynamics in crystalline solid induced by intense and ultra-short laser pulses. We solve the time-dependent Kohn-Sham equation in real time.

This year we conducted a numerical simulation which mimics pump-probe experiments which are standard method to explore interactions between ultrashort laser pulse and matters [1]. It has been considered that the strong laser pulse immediately induces excitations of valence electrons, which bring an ultrafast change of dielectric properties of solids. The change of dielectric function is often modeled by a Drude model added to the dielectric function in the ground state. We numerically achieved pump-probe experiments, solving time-dependent Kohn-Sham equation which includes both pump and probe electric fields as external perturbation. Dielectric properties of excited materials can be examined by the current induced by the probe pulse. From the simulation, we have found that the dielectric properties change immediately after the laser pulse irradiation, and that the change of may be well described by the Drude model for the real part. However, we have found the

imaginary part of the dielectric function shows rather complex behavior, sometimes indicating amplification of the probe pulse. We also found there is a substantial difference of the response depending on the relative directions between the pump and probe pulses, although the material is isotropic in the ground state.

We also explore the ultrafast current induced by the strong laser pulse [2]. Recently, it has been found that the laser pulse irradiated on transparent oxide, SiO₂, at the laser intensity close to the threshold of radiation damage induces an electric current in the extremely short time scale. We have explored the mechanism of the generation of the current by the time-dependent density functional theory. We have found that qualitative features of observed current is very nicely reproduced by our calculation.

References

- [1] S.A. Sato, K. Yabana, Y. Shinohara, T. Otobe, G.F. Bertsch, *Phys. Rev. B* **89**, 064304 (2014).
- [2] G. Wachter, C. Lemell, J. Burgdorfer, S.A. Sato, X.M. Tong, K. Yabana, submitted.

Spontaneous Structural Distortion and Quasi-One-Dimensional Quantum Confinement in $\text{LaTiO}_{3.4}$

ZHONGCHANG WANG, MITSUHIRO SAITO, YUICHI IKUHARA

WPI, Advanced Institute for Materials Research, Tohoku University, Sendai, Japan

Institute of Engineering Innovation, The University of Tokyo, Tokyo, Japan

Two-dimensional electron gas at heterointerfaces between insulators is currently the subject of intensive research. The confined electrons, which are driven to minimize their free energy, often behave differently than in bulks. All of the unprecedented properties associated with the electrons rely critically on specific crystal structures and local chemistry at heterointerface, which are often not expected in respective bulks. Here we report that a single-phase $\text{LaTiO}_{3.4}$ bulk shows a quasi-1D quantum confinement and a fluctuation of valence over individual bulk layers by self-assembled structural distortions. We offer definitive evidence of a delicate structural distortion in the $\text{LaTiO}_{3.4}$ bulk unit cells and demonstrate that the energy band gap at Fermi level is almost closed in the spin-majority channel [1].

Figure 1 shows high-angle annular-dark-field (HAADF) image of the monoclinic $\text{LaTiO}_{3.41}$ from a direction with the corresponding spectrum imaging revealing individual EELS spectrum from the Ti sites 1 to 5. In the HAADF mode,

the contrast is proportional to $Z^{1.7}$ (Z : atomic number) at our predefined collection geometry [2]. In this case, the La column appears to be brighter than the Ti column. By acquiring EELS spectrum across the HAADF image, we obtained the elemental mapping of La and Ti at atomic resolution. By examining individual EELS spectrum from the Ti sites 1 to 5, we find that the Ti atoms at the site 3, which has a similar structural environment to that of the LaTiO_3 , display a 3^+ valence. Ti sites 1, 2, 4 and 5 display a nearly 4^+ valence, since the splitting of L_3 and L_2 peaks are readily visible. However, the valence of Ti at sites 2 and 4 differ that of the Ti in 1 and 5 by revealing a notably lower edge onset energy, indicating the local valence is yet not 4^+ , but slightly lower than that, which could be explained by the observed distortion from the HAADF image in comparison to the orthorhombic $\text{LaTiO}_{3.1}$. Further DFT calculations reveal that the quasi-1D quantum confinement system shows an extremely small band gap, a ferromagnetic ordering, a strong

anisotropy in the nonequilibrium quasi-1DEG.
quantum transport, and a spin-polarized

References

- [1] Z.C. Wang, L. Gu, M. Saito, S. Tsukimoto, M. Tsukada, F. Lichtenberg, Y. Ikuhara, and J. G. Bednorz, *Adv. Mater.* **25** (2013) 2186.
- [2] Z. Wang, M. Saito, K. P. McKenna, L. Gu, S. Tsukimoto, A. L. Shluger, and Y. Ikuhara, *Nature* **479** (2011) 380.

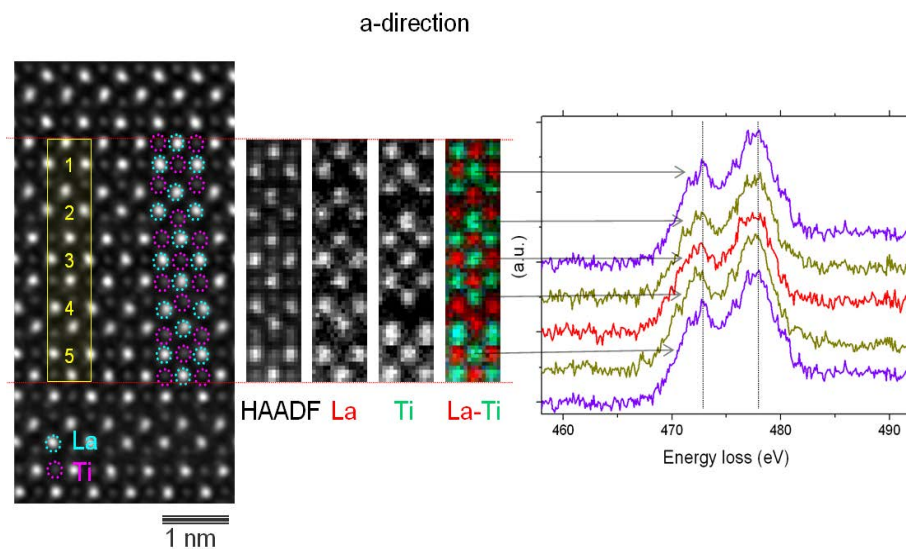


Fig. 1. HAADF and spectrum imaging of $\text{LaTiO}_{3.4}$ viewed from a direction with individual EELS spectrum from Ti sites 1 to 5.

Theoretical investigation on the magnetic polarization induced at organic/metal interfaces

Susumu YANAGISAWA¹ and Ikutaro HAMADA²

¹*Department of Physics and Earth Sciences, Faculty of Science, University of the Ryukyus, Senbaru 1, Nishihara, Okinawa, 603-0213, Japan*

²*International Center for Materials Nanoarchitectonics (WPI-MANA) and Global Research Center for Environment and Energy based on Nanomaterials Science (GREEN), National Institute for Materials Science, 1-1 Namiki, Tsukuba 305-0044, Japan*

There is growing interest in the field of organic spintronics. The spin-valve effect, i.e. charge injection with a preferential spin orientation from a ferromagnetic metal electrode into organic semiconductors has been observed [1]. However, there is a lack of understanding on the mechanism of the spin-valve effect, and thus the effect is hardly reproducible.

Recently, based on experimental results, it was suggested that the formation of spin-polarized hybridization between a ferromagnetic metal and organic molecules play a key role in the spin-valve effect [2].

The interface between Alq₃ molecule and a cobalt surface (Alq₃/Co) has attracted attention for the spin-valve effect [2]. Theoretically, first-principles density functional theory (DFT) calculations indicated formation of hybridized state at the interface [3]. The results indicated decrease in the charge injection barrier, which was induced by the molecular permanent dipole oriented upwardly to the vacuum side, as

proposed previously [4]. However, there is no consensus on the electronic mechanism of the preferential spin orientation upon the charge injection.

To clarify the mechanism of the spin-dependent electronic characteristics, we investigate the electronic states of Alq₃/Co interfaces by using spin-polarized DFT calculations. The adsorption configurations of Alq₃ on metal surfaces, i.e. up and down configurations, proposed by the authors in the previous works [4], are taken into account for initial adsorption geometries.

We use the STATE program code [5], with first-principles pseudopotentials for core states and a plane wave basis set for valence states. To optimize the adsorption geometries, we take into account the van der Waals (vdW) interaction in a semi-empirical manner [6].

To eliminate the artificial interaction between the slabs along the surface normal, we use the Effective Screening Medium (ESM) method [7]. By the ESM, the convergence of

DFT self-consistent cycles, which tends to be influenced by the fluctuation of electrostatic potential at the vacuum region, becomes stable. This treatment is advantageous over the conventional slab model or the dipole correction used in the previous similar studies.

First, we investigate the change in adsorption geometry and electronic state in AlQ_3 adsorbed on Mg (0001) substrate. Previously, we determined the stable chemisorbed configurations within the conventional GGA-PBE treatment [4]. Here, we find that inclusion of the vdW interaction slightly changes the chemisorption geometry. For the work function shift and the subsequent energy level alignment between the molecular and the substrate states, we find that the present ESM approach reproduces the previous result of the work function shift more efficiently.

Second, using the same methodology, we investigate the adsorption states of AlQ_3 on Co. We use the periodic slab model of a hcp Co (0001) surface in a 6×6 superstructure with six atomic-layers. We allow the upper four layers to relax during the optimization, and the lower layers are fixed to the bulk atomic positions. We sample the surface Brillouin zone by a 2×2

or 4×4 \mathbf{k} -point mesh.

Determination of the adsorption state of AlQ_3 on Co(0001) is in progress. After an optimized geometry is obtained, we go on to investigate the spin-dependent energy level alignment at the interface.

References

- [1] V. Dediu et al., Solid State Commun. **122**, 181 (2002); Z. H. Xiong, D. Wu, Z. Vally Vardeny, and J. Shi, Nature **427**, 821 (2004).
- [2] C. Barraud et al., Nat. Phys. **6**, 615 (2010); S. Steil et al., *ibid.* **9**, 242 (2013).
- [3] Y.-P. Wang, X.-F. Han, Y.-N. Wu, and H.-P. Cheng, Phys. Rev. B **85**, 144430 (2012); A. Droghetti et al., *ibid.* **89**, 094412 (2014).
- [4] S. Yanagisawa, K. Lee, and Y. Morikawa, J. Chem. Phys. **128**, 244704 (2008); S. Yanagisawa, I. Hamada, K. Lee, D. C. Langreth, and Y. Morikawa, Phys. Rev. B **83**, 235412 (2011).
- [5] Y. Morikawa, H. Ishii, and K. Seki, Phys. Rev. B **69**, 041403 (R) (2004).
- [6] S. Grimme, J. Comput. Chem. **27**, 1787 (1996).
- [7] M. Otani and O. Sugino, Phys. Rev. B **73**, 115407 (2006).

Intermolecular interaction as origin of red shifts in absorption spectra of Zinc-Phthalocyanine from first-principles

Susumu YANAGISAWA^{1,2}, Taiga YASUDA², Kouji INAGAKI², Yoshitada MORIKAWA²,
Kazuhiro MANSEKI³ and Shozo YANAGIDA⁴

¹*Department of Physics and Earth Sciences, Faculty of Science, University of the Ryukyus,
1 Senbaru, Nishihara, Okinawa, 903-0213, Japan*

²*Department of Precision Science and Technology, Osaka University, 2-1 Yamada-oka,
Suita, Osaka, 565-0871 Japan*

³*Graduate School of Engineering, Environmental and Renewable Energy System (ERES)
Division, Gifu University, 1-1 Yanagido, Gifu, 501-1193 Japan*

⁴*ISIR, Osaka University, 2-1 Mihoga-oka, Ibaraki, Osaka, 567-0047 Japan*

Zinc-phthalocyanines (ZnPc) have attracted much attention because of their photoelectric properties relevant to energy conversion in dye-sensitized solar cells and organic thin-film solar cells. For optimization of the excitation window, modification of the excited states of a chromophore molecule induced by molecularly stacked aggregation is of primary interest. Two stack configurations, *i.e.*, those with face-to-face cofacial configurations, referred to as H-type aggregates, and slipped-cofacially stacked configurations, known as J-type aggregates, are highlighted.

We investigate electronic origins of a redshift in absorption spectra of a dimerized ZnPc within the density functional theory [1]. We use the Gaussian 09 program code [2] installed on our own pc-cluster to calculate excitation spectra of the ZnPc monomer within the time-dependent density functional theory (TDDFT).

We also use the STATE program code [3] on the ISSP systems A and B to optimize the atomic geometry of the dimers of substituted ZnPc's taking into account the van der Waals (vdW) interaction with DFT-D2 [4] method.

In terms of the molecular orbital (MO) picture, the dimerization splits energy levels of frontier MOs such as the highest occupied molecular orbital (HOMO) and the lowest unoccupied molecular orbital (LUMO) of the constituent ZnPc molecules. Consequently, the absorption wavelength seems to become longer than the monomer as the overlap between the monomers becomes larger. However, for a ZnPc dimer configuration with its cofacially stacked monomer arrangement, the calculated absorption spectra within TDDFT indicates no redshift but blueshift in the Q-band absorption spectrum, *i.e.*, a typical H-aggregate.

The origin of the apparently contradictory

result is elucidated by the conventional description of the interaction between monomer transition dipoles in molecular dimers [4]. The redshift is caused by an interaction between the two head-to-tail transition dipoles of the monomers, while the side-by-side arranged transition dipoles result in a blueshift.

By tuning the dipole-dipole interaction based on the electronic natures of the HOMO and the LUMO, we describe a slipped-stacked dimer of unsubstituted ZnPc in which the Q-band absorption wavelength increases by more than 120 nm relative to the monomer Q-band.

However, there has been no experimental report of unsubstituted ZnPc dimer with large redshift. Actually, the binding energy of the slipped-stacked dimer calculated with DFT-D2 indicates that the dimer is meta-stable.

To simulate stable dimers of ZnPc's, we investigate dimer configurations of 1,4,8,11,15,18,22,25-octamethoxy Zinc phthalocyanine.

As a result, we find a stable dimer with a slipped-stack configuration. The binding energy is -2.1 eV. The resulting redshift of the

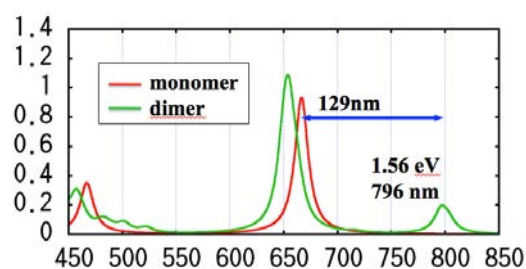


Fig. 1 Absorption spectra of the stable octamethoxy ZnPc with large redshift.

Q-band is 129 nm (Fig. 1). This finding may give us a hint to designing an aggregate of dye molecules with favorable long wavelength absorption.

References

- [1] S. Yanagisawa, T. Yasuda, K. Inagaki, Y. Morikawa, K. Manseki, and S. Yanagida, *J. Phys. Chem. A* **117**, 11246 (2013).
- [2] M. Frisch et al., *Gaussian 09*, revision C.01; Gaussian Inc.: Wallingford CT, 2009.
- [3] Y. Morikawa, H. Ishii, and K. Seki, *Phys. Rev. B* **69**, 041403 (R) (2004).
- [4] S. Grimme, *J. Comput. Chem.* **27**, 1787 (1996).
- [5] M. Kasha, *Radiat. Res.* **20**, 55 (1963).

Analyses on atomic structure, magnetism, and electronic structure in spintronics materials

Tatsuki ODA^{1,2}, Yuusaku TAGUCHI², Daiki YOSHIKAWA², Makoto NAKAMURA²,
Nurul IKUSAN², Masao OBATA²

Institute of Science and Engineering, Kanazawa University, Kanazawa, Ishikawa 920-1192
Graduate School of Natural Science and Technology, Kanazawa University, Kanazawa,
Ishikawa, 920-1192

We performed ab-initio electronic structure calculation in Co doped Fe/MgO interface on the basis of density functional theory. Two different slab models are considered, depending on the place of Co atom; at the interface and in the Fe layer. With using atomic forces, we obtained the optimized structure at the interface and discussed the layer distance of interface and the local structure around Co. Spin magnetic moments on Fe and Co atoms are also discussed. In the band dispersion at the Fermi level, distribution of the angular orbital component shows the possibility of perpendicular magnetic anisotropy.

This work takes two minimum slab models; MgO(3ML)/Fe₃Co(1ML)/Fe(2ML) and MgO(3ML)/Fe(1ML)/Fe₃Co(1ML)/Fe(1ML) (both are 36 atoms in 22 in-plane supercell configuration). In the former, the Co atom is placed at the interface (model A), and in the latter, at the inside of Fe layers (model B). Although the interface Fe/MgO has been fabricated in experiment, the in-plane lattice constant has not been determined even in the

clean interface. Therefore, for these slab models, two different in-plane lattice constants 5.74Å (= a_{Fe}) and 5.94Å (= a_{MgO}), which correspond to the bulk lattice constants of Fe and MgO respectively. There is the difference in lattice constant by 3.4%. totally we have four slab models.

For these models, we have carried out first-principles calculation which employs the density functional theory and ultra-soft pseudopotential. Energy cutoffs for electron density and wavefunction are 300Ry and 30Ry respectively. Here we used the 4x4x1 mesh of k space sampling. The generalized gradient approximation was adopted for exchange correlation energy. We optimized electronic wavefunctions and atomic positions by minimizing the total energy functional. The structural optimization has been performed by using atomic forces except for the in-plane lattice constant. The ESM method with zero external electric field condition was used to avoid artificial built-in electric field in the repeated slab model; ESM/vac./slab/vac. For

both vacuum layers, the width of 5.29\AA is taken.

We obtained the optimized structure after all the atomic forces reach equilibrium. The interface distance is compared to related works; 2.18\AA and 2.16\AA for model A with a_{MgO} and a_{Fe} lattice constants, respectively. In these results we observe that the smaller lattice constant produces slightly smaller interface distance. As another interesting point, we found that the Co atom moved from the Fe layer to the magnetic substrate by 0.03\AA and 0.04\AA for the model A with a_{MgO} and a_{Fe} , respectively. Even when we put the Co in the middle of Fe layer (model B), still we observed slight contracting distortion of Co to the bottom Fe layer. From these behaviors, we may deduce that Co prefers to be surrounded by Fe. We also observed that the model B has a slightly lower total energy than the model A by 3meV , implying that Co impurities in the middle Fe layer provides more stable system than those at the interface. The total magnetization and atomic magnetic moments were estimated. We observed that the Fe magnetic moment at interface, whose average is $2.8\mu_{\text{B}}$, is much enhanced from the value of second magnetic layer, the bulk value ($2.2\mu_{\text{B}}$), and the experimental value in the nano clusters. In contrast of this enhancement, the Co magnetic moments are similar to $1.8\mu_{\text{B}}$. Based on the discussion in the previous work, the enhancement on Fe magnetic moment is not

only attributed to the charge transfer to the oxygen at interface, but also understood as surface properties of Fe layer. Indeed, the Co magnetic moment has a similar value obtained by the monolayer model. At surface, electron wavefunction can be localized due to the lack of electron transfer to the open space while the electron transfer to the neighbors makes the wavefunction delocalized in the bulk. This localized electron contributes to larger magnetic moment. Electrons at interface are also easier to be localized compared to the middle layer and therefore, such interface accommodates the magnetic atom to a larger magnetic moment. Discussion mentioned above on delocalized electron also explains the smaller magnetic moment at the smaller lattice constant.

We discussed the possible origin of perpendicular magnetic anisotropy by analyzing the angular component in vicinity of the Fermi level. The angular orbital component in the band structure implies the possible contribution to positive MAE (favor of perpendicular magnetic anisotropy) due to $3d(xy)$ and $3d(x^2-y^2)$ orbital coupling below and above the Fermi level, in addition to the origin that the hybridization of $3d(3z^2-r^2)$ with oxygen $2p$ orbital can enhance the favor of perpendicular magnetic anisotropy.

Analyses on magnetic anisotropy and its electric field effect for magnetic thin films

Tatsuki ODA^{1,2}, Yuusaku TAGUCHI², Daiki YOSHIKAWA², Makoto NAKAMURA²,
Masao OBATA²

Institute of Science and Engineering, Kanazawa University, Kanazawa, Ishikawa 920-1192
Graduate School of Natural Science and Technology, Kanazawa University, Kanazawa,
Ishikawa, 920-1192

We have investigated magnetic anisotropy and its electric field (EF) effect in the thin Fe ferromagnetic films by using a first-principles approach of fully relativistic pseudo-potential spinor-planewave method. We have obtained a perpendicular magnetic anisotropy at zero EF for the isolated double Fe atomic layer. Around zero EF, the magnetic anisotropy energy (MAE) indicates a slight increase with respect to the EF. At the large variation to a few V/Å, the MAE decreases with a steep ratio. These behaviors in the EF dependence on MAE possibly explain the disagreement between experimental and theoretical results on the EF dependence for the interface magnetic anisotropy of MgO/Fe system.

For more than a decade, the spintronics has grown up intensively to realistic applications in the technology of magnetic random access memory (MRAM) development. Such development has been remarkable in memory density, reading-writing speed, and non-volatile property in cooperation with the technologies of spin-injection and physics of spin transfer

torque. Nowadays, the basic physics about magnetism has been developing in the response to electric field (EF). For thin films both of sensitivity or large response may be required in device applications, where the interface with a few metallic layers is critical to determine the response to the EF. The most promising system is the Fe layer attached with dielectric material, for example, MgO/Fe system. The most important microscopic interest is concentrated on the study of interface between Fe and MgO atomic layers.

Although the magnetic anisotropy and its EF effect for MgO/Fe have been already investigated, the part of ingredient layer, namely Fe layer of two atomic layers, was analyzed. The most important point in the computational results is that the largest MAE change is comparable to the corresponding experimental result within a several times. These results on the MAEs and its EF dependences will be contributed at the analysis of magnetic properties in the MgO/Fe interface.

Electronic Properties of Impurity Defects in Organic Molecular Semiconductors

Takashi NAKAYAMA

Department of Physics, Chiba University

1-33 Yayoi, Inage, Chiba 263-8522

Organic molecular semiconductors are key materials for future optical and electronic devices because of their unique characteristics such as softness and light mass. During the device fabrication, a variety of impurity atoms are often incorporated into semiconductor layers. Around metal-electrode interfaces, for example, metal atoms such as Al and Au easily diffuse into semiconductors. These impurities are believed to deteriorate semiconducting properties. However, there have been no systematic studies on how these impurities are located in semiconductors and what electronic states are produced by these impurities. The purpose of this project is to clarify these questions, by using the first-principles calculation based on the density functional theory. In this report, we show some of the results.

We first consider how the metal atoms are incorporated into insulating SAM (self assembled monolayer) film from its surface. Figures 1(a) and 1(b) show the top views of COOH and COOK terminated SAM surfaces, respectively. Adsorbed metal atom diffuses to penetrate the SAM film around crossed points. Figures 1(c) and 1(d) show calculated adiabatic potentials for Au and Al atom diffusions as a function of metal-atom position. It is seen that Au atom can enter the SAM without any potential barrier in case of COOH termination, while the potential has minimum and thus Au atom is trapped around the surface in case of COOK termination. This result well explains the experiments [1]. By analyzing the electronic structure, we found that the potential minimum around the SAM surface is produced by the ionic interaction between positive K and negative Au atoms. In case of Al-atom diffusion, on the other hand, because Al atom has small electronegativity

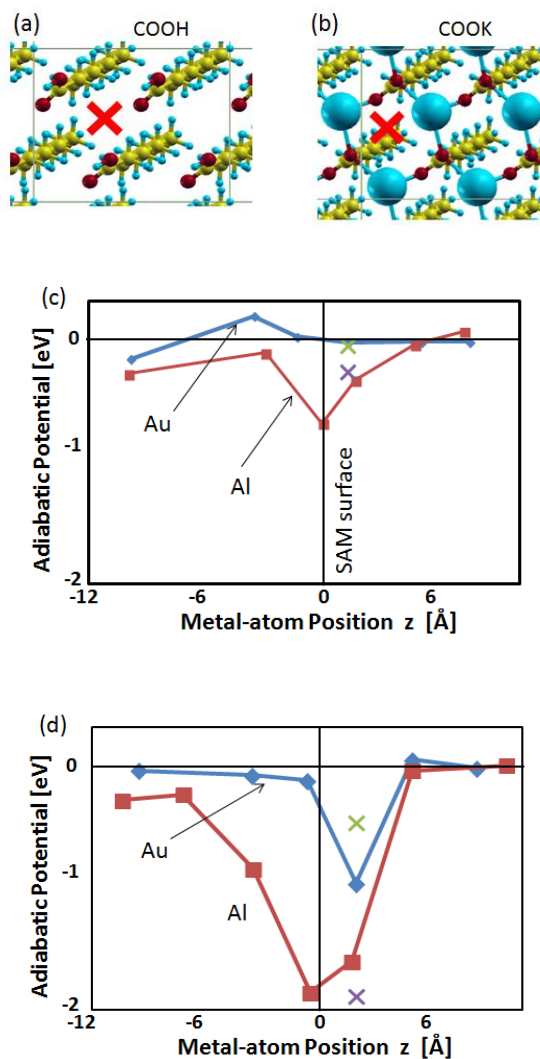


Fig.1. (a) and (b): Top views of COOH and COOK terminated SAM. Adsorbed metal atom diffuses into SAM around crossed point. (c) and (d): Calculated adiabatic potentials for Au and Al atoms around SAM surface. Metal-atom positions, $z=0$ and $z>0$, corresponds to SAM surface and vacuum, respectively.

compared to elements of organic molecules, much stronger ionic interaction appears between positive Al and negative O atoms. This is the reason why the potential for Al atom has large minima around

the SAM surface, which again explains the observations [2].

Next, we consider the interaction between metal atoms when metal atoms are located in organic systems. Figure 2(a) shows the calculated interaction energy between two Au (Al) atoms as a function of inter-atomic distance when metal atoms are adsorbed on a graphene sheet. In case of Au, the interaction is attractive and short range. This is because Au atoms are bound to the graphene substrate with weak covalent bonds and do not disturb the electronic states of graphene, thus the Au-Au interaction appearing only when two Au atoms approach nearby to produce a metallic bond [3]. In case of Al, on the other hand, the interaction is repulsive and long range. This is because the electron transfer occurs from Al to graphene due to small negativity of Al, and thus the adsorbed Al atoms are positively ionized. As a result, there appears a repulsive and long-range Coulomb interaction between Al atoms.

Then, we consider the interaction in case of one-dimensional molecule. Figure 2(b) shows the calculated interaction energy between two Au (Al) atoms as a function of inter-atomic distance when metal atoms are adsorbed on a polyacetylene chain. Similar to the case of graphene, roughly speaking, Au and Al atoms have attractive and repulsive interactions, respectively. The most interesting feature is the oscillation of interaction energy as a function of inter-atom distance. This oscillation occurs due to the same scenario as the Peierls transition; when the number of C atoms of polyacetylene skeleton between adsorbed metal atoms is even, the C-C bond shows dimerization and the system becomes stable, promoting negative interaction energy. When the number of such C atoms is odd, there appears no dimerization, thus producing little interaction energy. In this way, the interaction between metal atoms strongly depends on the dimensionality of host molecules.

In order to realize these calculations using the TAPP and xTAPP codes, because the target system

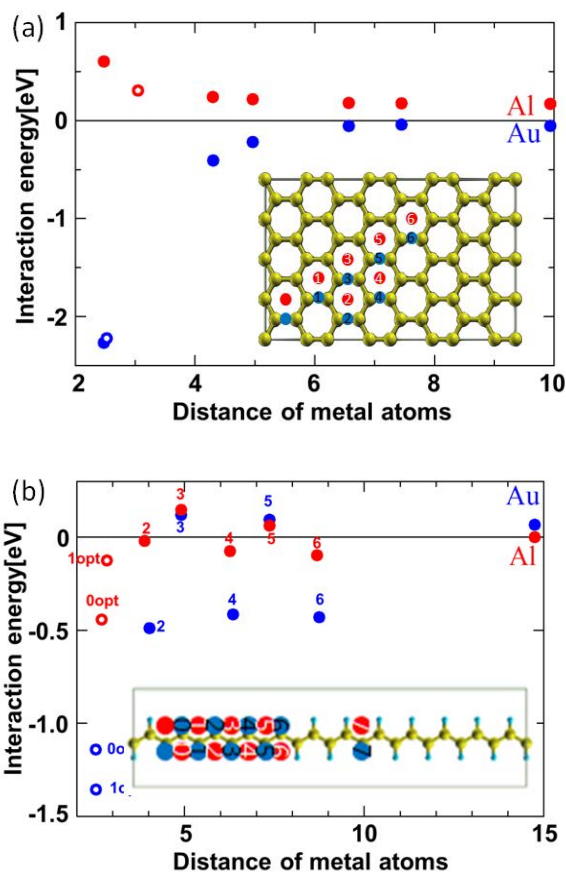


Fig.2. Calculated interaction energy between two metal atoms (a) on a graphene sheet and (b) on a polyacetylene chain as a function of distance, for Au and Al atom cases.

is very large (more than 150 atoms) and has a variety of geometries, the advanced computing facility that has higher-speed CPU than 100GFlops, larger-size memory around 100GB, larger-size storage than 1.0TB, and particularly a multi-task operation is indispensable. These conditions are never prepared in individual research laboratory. Only the present super-computing system of the ISSP can realize these calculations.

References

- [1] Z. Zhu et al., *J. Am. Chem. Soc.* **128** (2006) 13710.
- [2] H. Klauk et al., *Nature* **445** (2007) 745.
- [3] T. Park, Y. Tomita, T. Nakayama, *Surf. Sci.* **621** (2014) 7.

First-principles study of quantum transport in nanostructures

NOBUHIKO KOBAYASHI

Institute of Applied Physics, University of Tsukuba

1-1-1 tennodai Tsukuba Ibaraki 305-8573

Understanding and controlling quantum transport properties in nanostructures from atomistic levels is important for developments of nanoscale devices. A number of experimental studies have been performed on transport properties in nanostructures such as atomic wires, molecules and nano carbon systems to discuss the conductance and the current-voltage characteristics. Quantum nature is essential in nanoscale systems, and atomistic analysis based on detailed electronic states calculations are indispensable to discuss the transport property of such a system theoretically. In order to analyze transport properties, we have developed several methods such as the nonequilibrium Green's function (NEGF) method, and time dependent wave-packet diffusion (TD-WPD) method. Using these methods, we have investigated charge and heat transport properties of atomic wires, organic molecules, nano carbon systems and so on.

We have developed an efficient numerical calculation code for the ab-initio electron transport based on the DFT and NEGF formalism using Fortran and Message Passing Interface(MPI). The parallel computation technique with MPI is employed for efficient computations of density matrix via the the Green's functions, which depend on the energy and two-dimensional wave vectors, as shown in Fig.1. Since each matrix element of the Green's functions depends only on the single energy and two-dimensional wave vector point, it is possible to divide the calculations in the energy and wave vectors, which are carried out separately in each process. As a demonstration of the efficiency of the present code, the nu-

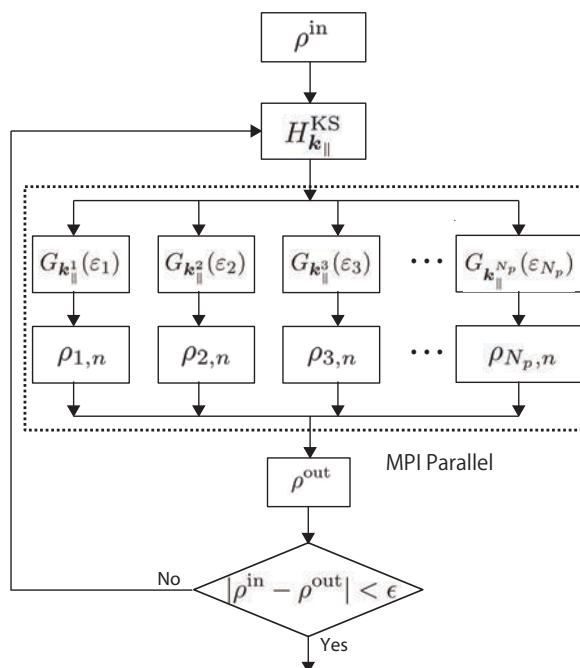


Figure 1: Flowchart of DFT-NEGF calculations with parallelization by MPI.

merical calculations of electron transport properties of Al(100)-Si(100)-Al(100) heterostructures are shown in Fig.2. The computational efficiency is seen to improve as the total number of processes becomes larger with the latency by the communication between whole process negligible. For an application, electron transport properties such as transmission spectra and total density of states are investigated for the systems with different thicknesses of Si layers.

We have also developed the $O(N)$ TD-WPD method for the quantum transport calculation

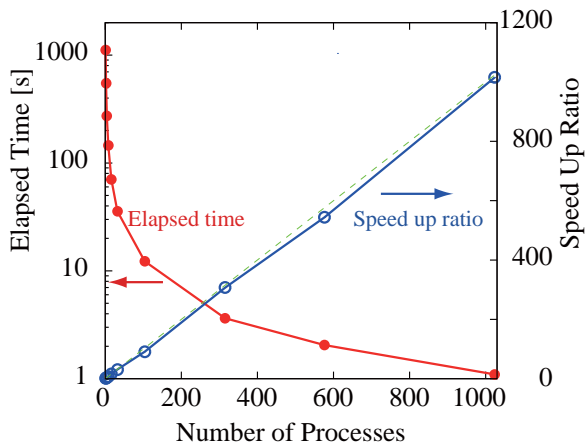


Figure 2: Speed-up ratio of total elapsed time by the parallelization of MPI in the ab-initio electron transport calculations in System B.

of huge systems of up to 100 million atoms. We calculated the conductance and the mobility of the system with micron-order lengths at room temperature based on the Kubo-Greenwood formula. Using this method we can study the transport properties from diffusive to ballistic regimes including the effect of realistic electron-phonon scattering, and determine the mean free path and relaxation time from an atomistic viewpoint. We performed DFT calculations of electronic structures and interactions between molecules of pentacene and rubrene single-crystal organic semiconductors including the effect of the van der Waals interaction, and applied the TD-WPD method to the analysis of transport properties of the organic semiconductors.

The realistic intermolecular-vibration effects on the anisotropic transport properties of pentacene and rubrene single-crystal organic semiconductors were analyzed by the systematic evaluations of the angle-resolved effective mass, mobility, carrier velocity, relaxation time, and mean free path, as shown in Fig. 3 and 4. We find that intermolecular vibrations induce the strong anisotropic relaxation time but moderate the anisotropy of carrier mobility, which increases with temperature, much more than that of inverse effective mass. We

also find that the main axis of mobility tensor rotates slightly with temperature in pentacene crystals. This clarifies the mechanism on the deviations of anisotropic ratio of mobility from that of effective mass observed in experiments.

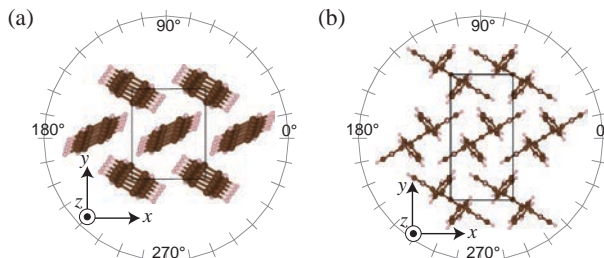


Figure 3: Crystal structures of pentacene (a) and rubrene (b) single-crystal semiconductors.

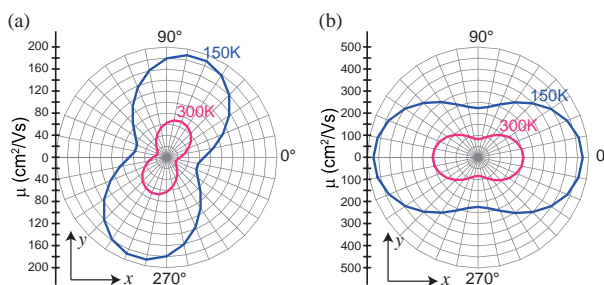


Figure 4: Calculated anisotropic mobilities of pentacene (a) and rubrene (b) single-crystal semiconductors.

References

- [1] H. Ishii, N. Kobayashi, K. Hirose, *Phys. Rev. B* 88 205208 (2013).
- [2] K. Yamamoto, H. Ishii, N. Kobayashi, K. Hirose, *Nano. Res. Lett.* 8 256 (2013).
- [3] K. Yamamoto, H. Ishii, N. Kobayashi, K. Hirose, *Open J. Comp. Mat.* 3 48 (2013).
- [4] K. Yamamoto, H. Ishii, N. Kobayashi, K. Hirose, *J. Nanomaterials* 2013 525070 (2013).
- [5] K. Hirose, K. Kobayashi, M. Shimono, H. Ishii, N. Kobayashi, *e-Journal Surf. Sci. Nanotechnol.* 12 (2014).

DFT statistical mechanics analysis of redox reaction mechanism at interfaces in catalysts and batteries

Y. Tateyama, H. Kino, K. Sodeyama, R. Jono, Z. Futera, L. Szabova, Y. Ootani, J. Haruyama, and K. Aikawa

International Center for Materials Nanoarchitectonics (WPI MANA),

National Institute for Materials Science (NIMS) 1-1 Namiki, Tsukuba, Ibaraki 305-0044

We have explored the chemical/redox reactions in solutions and at electrode-electrolyte interfaces via density functional theory based molecular dynamics (DFT-MD) analysis with explicit solvent molecules, for more understanding of cell, battery and catalysis. The advanced techniques for free energy calculations and redox reactions have been also used. Some results are described below.

(1) New reductive decomposition mechanism of carbonate-based electrolyte in Lithium Ion Battery [1]

Solid electrolyte interphase (SEI) on the electrode - electrolyte interfaces formed through the reductive decomposition of organic solvent molecules plays a crucial role in the stability and capability of lithium ion battery (LIB). Additives to the electrolyte often exhibit a large impact on the SEI quality. A typical example is vinylene carbonate (VC) additive to the ethylene carbonate (EC) solvent. Here we investigated the effects of VC additive to the EC solvent on the reductive decomposition and the initial stage of SEI formation. [1] Our focus

was put on kinetics as well as thermodynamics of the possible reduction processes. We used DFT-MD with explicit solvent molecules for the equilibrium properties at finite temperature, and carried out the free energy profile calculations along the reaction pathways using the blue-moon ensemble technique.

We found that 1e reduction induces breaking of C_E-O₂ bond in EC to produce ^oE-EC⁻ and CO, while d_{CO}-VC⁻ and CO are generated from VC through C_C-O₂ bond breaking in contrast to a previous study (Fig. (a)). When another electron is added to the system (2e reduction), EC decomposition produces CO₃²⁻ + C₂H₄ or CO + alkylcarbonate (Fig. (b)), whereas CO production occurs again at the 2e reduction of VC. We then examined the attack of anion radical made by 1e reduction to the nearby intact molecule, and found that the EC radical attack on the intact VC enhances the CO₂ production. These mechanisms on the atomic scale are in good agreement with the experimental observations of the gaseous products. Contrary to the conventional scenario that VC additive is

sacrificially reduced and makes a VC oligomer that seeds SEI formation, the present results provide a completely different mechanism: the VC additive preferentially reacts with the EC anion radical to suppress the 2e reduction of EC, the main initial stage of SEI formation in the VC-free EC electrolyte (Fig. (c)). Because this VC mechanism is realized via 1e reduction, the irreversible capacity at the SEI formation will decrease as well, which is also consistent with the experiments. These results not only reveal the primary role of the VC additive in the EC solvent, but also provide a new fundamental perspective for the reductive decomposition of carbonate-based electrolyte near the negative electrode.

(2) *Microscopic mechanism prediction with DFT simulations on unusual phenomena observed in experiments [2-4]*

With large-scale DFT-MD simulations and geometry optimizations on supercomputers, we have predicted the mechanisms of unusual swelling of nanosheets with specific electrolyte, unusual high mobility of hole in special organic crystals, and a novel type of molecular switch.

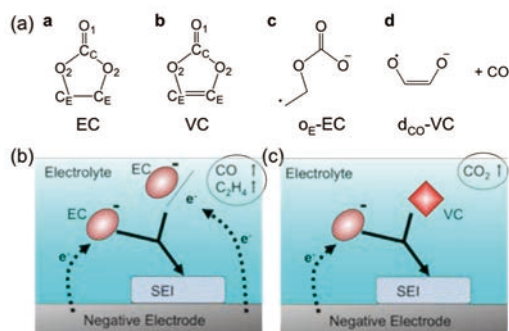


Figure (a) Structures of EC and VC with the atomic labels. Major reductive decomposition products of EC and VC ($\text{o}_E\text{-EC}$ and $\text{d}_{\text{CO}}\text{-VC}$) are also displayed. (b) Reductive decomposition mechanism for the electrolyte with EC only, confirmed in this work. (c) Novel reductive decomposition mechanism of the EC electrolyte with VC additives, found in this work.

References

- [1] K. Ushirogata, K. Sodeyama, Y. Okuno, Y. Tateyama. *J. Am. Chem. Soc.* **135**, 11967-11974 (2013).
- [2] F. Geng, R. Ma, A. Nakamura, K. Akatsuka, Y. Ebina, Y. Yamauchi, N. Miyamoto, Y. Tateyama, and T. Sasaki, *Nature Comm.* **4**, 1632 (2013).
- [3] Y. S. Yang, T. Yasuda, H. Kakizoe, H. Mieno, H. Kino, Y. Tateyama, C. Adachi, *Chem. Commun.*, 49, 6483 - 6485, (2013).
- [4] G. Pawin, A. Z. Stieg, C. Skibo, M. Grisolia, R. R. Schilittler, V. Langlais, Y. Tateyama, C. Joachim, and J. K. Gimzewski, *Langmuir*, 29, 7309-7317 (2013).

Doping Effect on Magnetism and Transport Property of Heterojunction between Carbon and Boron Nitride Nanotubes

Huy Duy NGUYEN and Tomoya ONO

*Department of Precision Science and Technology, Osaka University
Yamada-oka 2-1, Suita, Osaka 565-0871*

Honeycomb structures of carbon have emerged as promising candidates for spin-based switches and field-effect devices owing to their weak spin-orbit coupling and high carrier mobility. Theoretical investigations have demonstrated that graphene nanostructures exhibit local spin polarization along their zigzag edges. Recent first-principles calculations based on density functional theory revealed that graphene nanoflakes with a localized magnetic moment along their zigzag edges of carbon exhibit spin-dependent transport behavior (1).

Edge states are also observed in zigzag carbon nanotubes (CNTs). Choi et al. found that the alternate placement of zigzag CNTs and zigzag boron nitride nanotubes (BNNTs), which are possibly fabricated by the laser vaporization method (2), resulted in magnetic ordering by doping electrons or holes, and the magnetic ground states are associated with the zigzag edges of CNTs. However, electron or hole doping is not practical and the rotational symmetry mismatch between the conducting and edge states of a zigzag CNT prevents electron transport (3).

We study the electronic structures and electron-transport properties of the heterojunction formed by alternate placement of CNTs and BNNTs under atom substitutional doping by first-principles calculations using techniques described in Ref. 4. Figure 1 shows the our computational model of (9,0) nan-

otube and shall be referred as z-C/BNNT. Tetragonal supercells are adopted and periodic boundary conditions are imposed in all directions. The wall-to-wall distance between adjacent nanotubes is chosen so as to exceed 6 Å, which permits tube-tube interactions to be neglected. A grid spacing of 0.17 Å is used.

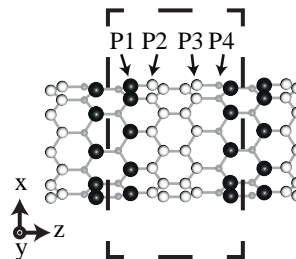


Figure 1: Computational model of a (9,0) z-C/BNNT. White, grey, and black balls are C, N, and B atoms, respectively. P1, P2, P3, and P4 indicate positions at which one B atom is replaced with one C atom, one C atom is replaced with one N atom, one C atom is replaced with one B atom, and one N atom is replaced with one C atom, respectively.

The electronic band structure of a z-C/BNNT is shown in Fig. 2(a). The edge states, which manifest themselves as doubly degenerate flat bands, are observed near the Fermi level. The charge density distributions of these edge states are localized at the zigzag boundaries of the CNT.

Since the edge states in the z-C/BNNT induce a large density of states closest to the

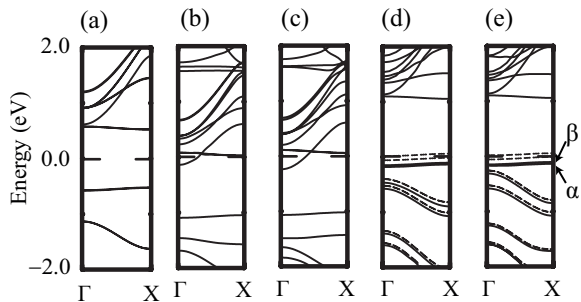


Figure 2: (a) Band structure of z-C/BNNT. (b)-(f) show the band structures of doped nanotubes associated with P1-P4 in Fig. 1. Zero energy was chosen as the Fermi level. Solid (dashed) curves indicate the spin-up (-down) states.

Fermi level, inserting or removing electrons causes spin polarization. We propose the atom substitutional doping, in which one C atom at the CNT/BNNT interface is replaced with one B (N) atom as shown in Fig. 1. As shown in Fig. 2, *p*-type substitutional doping gives rise to spin polarization with a magnetic moment of $1 \mu_B$, owing to the variation of the occupation number of the edge states. On the contrary, the $\sigma - \pi$ hybridization due to the curvature pulls down the energetically dispersive states, resulting in the nonmagnetic ground-state electronic structure for the *n*-type substitutional doping (5).

To study the electron-transport property, we employ a computational model shown in Fig. 3(a). The conductance spectra of the transport model for electrons coming from the left electrode is depicted in Fig. 3(b). Except for the peaks B_{\uparrow} and C_{\uparrow} , there is a one-to-one correspondence between spin-up and spin-down peaks. By plotting charge density of the scattering waves, we found that these peaks originate from resonant tunneling by the edge states. Although it has been reported that the electron transport through the edge states in CNT is suppressed owing to the symmetry mismatch between the edge states and conducting CNT states. However, our calculation reveals that the fluctuation

of the symmetry due to the presence of the doped atom leads to the spin-dependent resonant tunneling through the edge states (5). These results indicate that the atom substitution plays important roles for the electron transport through the edge states in addition to the spin-polarized electronic structure.

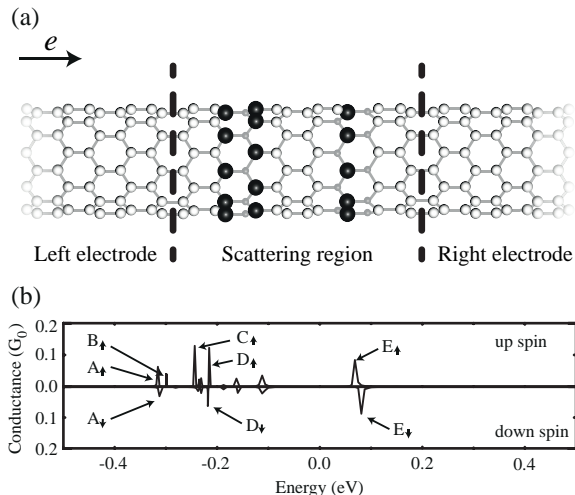


Figure 3: (a) Computational model for transport calculation. Meaning of symbols are the same with those in Fig. 1. (b) Conductance spectra as functions of energy of incident electrons. Zero energy was chosen as the Fermi level.

References

- [1] T. Ono, T. Ota, and Y. Egami: Phys. Rev. B **84** (2011) 224424.
- [2] S. Enouz, O. Stéphan, J.-L. Cochon, C. Colliex, and A. Loiseau: Nano Lett. **7** (2007) 1856.
- [3] T. Ono, Y. Egami, and K. Hirose: Phys. Rev. B **86** (2012) 195406.
- [4] K. Hirose, T. Ono, Y. Fujimoto, and S. Tsukamoto, First Principles Calculations in Real-Space Formalism, (Imperial College, London, 2005).
- [5] H. D. Nguyen and T. Ono: J. Phys. Chem. C **46** (2013) 117.

Ab-initio search of novel multiferroics based on manganites

Kunihiko Yamauchi¹ and Masayuki Toyoda^{1,2}

¹ *ISIR-SANKEN, Osaka University, Ibaraki, Osaka 567-0047*

² *CREST, JST, Kawaguchi, Saitama, 332-0012*

By means of density-functional simulations for various transition-metal oxides, we discuss the electronic mechanism of magnetism and ferroelectricity. DFT simulations were performed by using the VASP code and the Hi-LAPW code within the GGA+ U formalism.

Based on multiferroic HoMnO_3 , where the exchange striction induces the large ferroelectric polarization, we predicted new multiferroic compounds $\text{Ho}_{1/2}\text{A}_{1/2}\text{MnO}_3$ ($\text{A} = \text{As, Sb, Bi}$) with enhanced polarization. We found that doping of lone pair cations with different ionic radii, at the A-site of orthorhombic HoMnO_3 , results in a marked increase of the electronic polarization and its development along the b -axis.[1]

Half-doped manganites are known to exhibit ferroelectricity with CE-type charge-ordered states together with antiferromagnetic spin configuration. In bilayer $\text{PrCa}_2\text{Mn}_2\text{O}_7$, we clarified that the displacement of apical oxygens bonded to either Mn^{3+} or Mn^{4+} ions plays an important role in the rising of ferroelectricity. Importantly, local dipoles due to apical oxygens are also intimately linked to charge and orbital ordering patterns in MnO_2 planes, which in turn contribute to polarization. Besides, an important outcome of our work consists in proposing Born effective charges as a

valid mean to quantify charge disproportionation effects, in terms of anisotropy and size of electronic clouds around Mn ions.[2, 3]

A-site-ordered perovskites $\text{AA}'_3\text{B}_4\text{O}_{12}$ are expected to give rise to intriguing magnetic structure, as having magnetic transition-metal ions both at A' site and B site. We comprehensively studied magnetism of $\text{CaCu}_3\text{B}_4\text{O}_{12}$ ($\text{B} = \text{Ti, Ge, Zr, and Sn}$) and evaluated the magnetic exchange coupling constants between Cu spins. The experimentally observed magnetic orders of these compounds are reasonably explained by delicate balance of the ferromagnetic nearest coupling and the antiferromagnetic long-range coupling.[4]

参考文献

- [1] S. S. Subramanian, K. Yamauchi, T. Ozaki, T. Oguchi and B. Natesan, *J. Phys.: Condens. Matter* **25**, 385901 (2013).
- [2] K. Yamauchi and S. Picozzi, *J. Phys. Soc. Jpn.* **82**, 113703 (2013).
- [3] K. Yamauchi and P. Barone, *J. Phys.: Condens. Matter* **26**, 103201 (2014).
- [4] M. Toyoda, K. Yamauchi, and T. Oguchi, *Phys. Rev. B* **87**, 224430 (2013).

First-principles studies on a reaction mechanism of Nylon-oligomer hydrolase

Yasuteru SHIGETA

Graduate School of Pure and Applied Sciences,

University of Tsukuba, 1-1-1 Tennodai, Tsukuba, Ibaraki 305-8577

The active site of 6-aminohexanoate-dimer hydrolase, a nylon-6 byproduct-degrading enzyme with a β -lactamase fold, possesses a Ser112/Lys115/Tyr215 catalytic triad similar to the one of penicillin-recognizing family of serine-reactive hydrolases but includes a unique Tyr170 residue [1] as shown in Fig. 1. By using a reactive QM/MM approach [2], we work out its catalytic mechanism and related functional/structural specificities. At variance with other peptidases, we show that the involvement of Tyr170 in the enzyme-substrate interactions is responsible for a structural variation in the substrate-binding state. The acylation via a tetrahedral intermediate is the rate-limiting step, with a free-energy barrier of ~ 21 kcal/mol (see Fig. 2), driven by the catalytic triad Ser112, Lys115, and Tyr215, acting as a nucleophile, general base, and general acid, respectively. The functional interaction of peculiar Tyr170 with this triad leads to an efficient disruption of the tetrahedral intermediate,

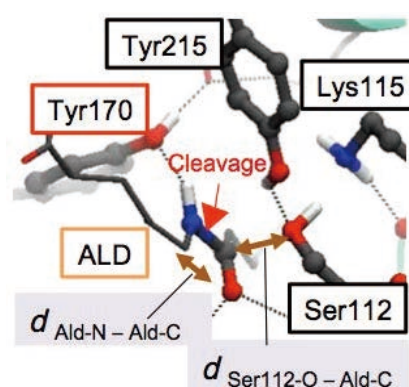


Fig. 1 Active site and reaction coordinates for QM/MM analyses

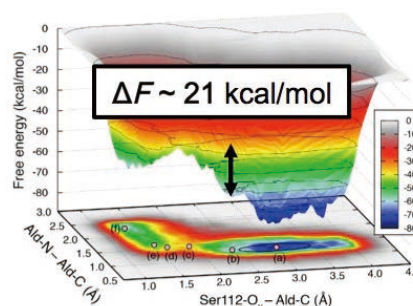


Fig. 2: Free energy surface along two-dimensional reaction coordinates

promoting a conformational change of the substrate favorable for proton donation from the general acid [3].

References

- [1] S. Negoro, *et al. J. Mol. Biol.* **370**, 142 (2009).
- [2] CPMD ver 3.15 .
- [3] K. Kamiya, *et al. J. Phys. Chem. Lett.* **5**, 1210 (2014).

First-principles calculation of electrochemical properties of redox-active monolayers: Counter anion effects

Ken-ichi FUKUI

*Department of Materials Engineering Science, Graduate School of Engineering Science,
Osaka University, Machikaneyama, Toyonaka, Osaka 560-8531*

A microscopic understanding of electrochemical properties is of fundamental importance for future electrochemistry. We have revealed that the electrochemical properties of ferrocene (Fc) terminated self-assembled monolayers (SAMs) can be obtained by first-principles molecular dynamics (FPMD) in the case of hydrophilic environment. In this study, we calculated the hydrophobic systems with including counter anions explicitly.

FPMD calculations were performed using the program “STATE”. Fig. 1 shows our Fc SAM systems. Two FPMD runs (more than 0.5 ps) with vertical energy calculations were carried out for neutral (Fc) and positively charged (Fc⁺) cases 300 K for each system to estimate the free energy difference ΔA [1].

The obtained values are summarized in Table 1. In contrast to the previous study, FcC4 system showed smaller ΔA value compared to FcC7, indicating that the microscopic environment of the Fc moiety in the FcC4 system is more susceptible to oxidation. This tendency is consistent with the experimental results [2]. These results indicate that the electrostatic interaction between Fc⁺ moiety

and ClO₄⁻ in the hydrophobic environment has a significant role in determining ΔA values. Quantitative estimation of anion dependencies is in progress.

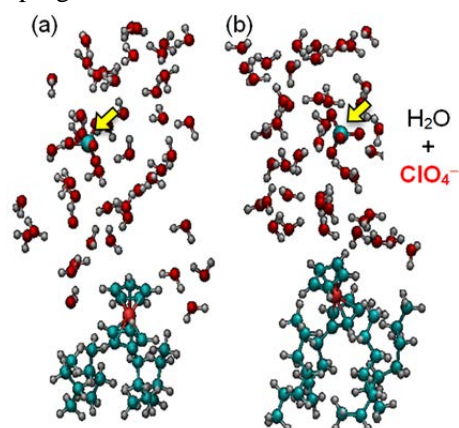


Fig. 1: Snapshots of Fc SAM systems taken from each MD simulation. The Fc-terminated molecule is surrounded by (a) *n*-butane as a standard system (FcC4) and (b) *n*-heptane to represent a hydrophobic environment (FcC7). Each system includes a ClO₄⁻ anion (see arrows).

Table 1. Values of the free energy difference, ΔA , obtained from MD simulations (unit: eV)

Anion	FcC4		FcC7	
	no	yes	no	yes
ΔA	1.87	1.40	1.73	1.50
$\Delta\Delta A$	-	-	-0.14	+0.10
$\Delta\Delta A$ exp ^[2]	-	-	-	+0.25

References

- [1] Y. Tateyama, et al., *J. Chem. Phys.*, **122**, 234505 (2005).
[2] S. E. Creager, G. K. Rowe, *J. Electroanal. Chem.*, **291**, 420 (1997).

Theoretical Analyses on Electron/Ion/Thermal Transport Properties toward Nano-devices

Satoshi WATANABE

*Department of Materials Engineering, the University of Tokyo
7-3-1 Hongo, Bunkyo-ku, Tokyo, 113-8656*

1 Introduction

The electrical properties of nanostructures have been extensively investigated in the last few decades. However, further studies on complicated situations and phenomena, such as multi-terminal electronic transport, time-varying electronic transport, and the interplay among electronic, thermal and ionic transport at nanoscale, are strongly desired toward the design and control of nanoscale electronic devices. We have been performing investigations on these topics using theoretical analyses based on atomic/electronic level simulations. In the followings, some of our results in the fiscal year (FY) 2013 are described.

2 AC transient transport in nanostructures

The understanding on responses to AC signals of nanostructures is crucial for realizing next-generation ultrafast devices. So we have been theoretically studying AC transport properties of nanostructures.

Previously, we studied AC transport properties of metallic carbon nanotubes (m-CNTs) with a single atomic vacancy and seamless contact with lead regions using nonequilibrium Green's function (NEGF) method based on simple tight binding calculations [1]. Recently, we have examined the same system more closely, based on the density functional theory (DFT) calculations [2]. In the calculations, we used our homemade code for the

NEGF and the SIESTA code. We have found that the two states induced by the vacancy, the π -orbital-origin vacancy state and the σ -orbital-origin dangling-bond state, show different susceptance behaviors at first sight. That is, besides capacitive peaks seen in both of the two states, satellite inductive peaks are clearly seen adjacent to the main capacitive peak only around the dangling-bond state. Our analysis with a simple resonant scattering model reveals that the origin and the magnitude of these satellite inductive peaks can be understood by just one parameter, i.e., the lifetime of electrons at a defect state.

We have also examined AC transport properties of 1, 4-Benzenedithiol molecule sandwiched between semi-infinite one-dimensional gold electrodes using the same method (NEGF based on DFT). In the calculated susceptance spectrum, we have found two types of features; one corresponding to conductance peaks/dips and the other not related to those. We have found that the former can be understood similarly to the case of the above m-CNTs, while the latter, which is seen at the energies having small conductances, correlates with the DOS of the electrodes.

3 Conductive filaments in oxide-based resistive switching devices

Oxide-based resistive switching devices, especially amorphous-TaO_x (a-TaO_x) based ones, have attracted much attention as strong can-

didates of next-generation memory cells. Their switching behavior is understood based on the formation/rupture of conductive filaments (CFs), but microscopic details of the CF structures and their formation/rupture processes have not been well clarified yet.

Previously, we have examined CFs in Cu/a-TaO_x/Pt from first principles within the DFT [3]. Recently, we have examined CFs in Pt/a-TaO_x/Pt heterostructures [4]. Calculations were performed using the VASP. Amorphous TaO_x structures were obtained by simulated annealing method. Since the resistance change of a-TaO_x is controlled by the O concentration, we perform systematic investigation on the structures and properties of a-TaO_x ($0.75 \leq x \leq 2.85$). We have found the strong correlation among Ta/O coordination number, Ta–Ta/Ta–O bond lengths, and O concentration in a-TaO_x. With the decrease of O concentration, Ta atoms tend to merge together and finally form a continued Ta-rich region in a-TaO_{0.75}, which suggests that not O vacancies, but the Ta–Ta bonding mainly contributes to the CF in a-TaO_x based resistive switches.

4 Thermoelectric properties of carbon nanostructures

Our previous study on thermal transport properties of various carbon nanostructures, single walled carbon nanotubes (SWNT), graphene nanoribbons (GNR), conical-helix nanofiber (CHNF) and cup-stacked carbon nanofibers (CSNF), by classical nonequilibrium MD simulations revealed that the thermal conductivities of CHNF and CSNF are two orders of magnitude lower than SWNT and GNR [5]. Since the low thermal conductivity is favorable for thermoelectric materials, we have recently investigated the thermoelectric figure of merit, ZT, of conical carbon nanofibers theoretically [6]. We adopted non-equilibrium Green's function (NEGF) method with the semi-empirical Hückel method implemented in

the ATK code.

Our results show that the CSNF behaves like a semiconductor while the CHNF is metallic. CSNF electrical conductance is very low at the Fermi-level, which corresponds to remarkably high thermopower of $S > 1.5$ mV/K. The maximum thermopower calculated for CHNF was less than 0.5 mV/K. The estimated values of ZT depend on the Fermi level position, and the maximum values are 5.2 and 2.8 for the CSNF and CHNF, respectively. These high ZT values suggest that further experimental and theoretical studies are worthy.

References

- [1] D. Hirai T. Yamamoto and S. Watanabe: Appl. Phys. Express **4** (2011) 075103.
- [2] D. Hirai T. Yamamoto and S. Watanabe: J. Appl. Phys., in press.
- [3] B. Xiao T. Gu, T. Tada and S. Watanabe: J. Appl. Phys. **115** (2014) 034503.
- [4] B. Xiao and S. Watanabe: submitted to Nanoscale.
- [5] D. A. Thomas, T. Yamamoto, T. Tada and S. Watanabe: Trans. Mater. Res. Soc. Jpn. **38** (2013) 183.
- [6] D. A. Thomas, Doctoral thesis, The University of Tokyo (2014).

Self-Poisoning Dynamical Effects in the Oxygen Reduction Reaction on Pt(111) from a Top-down Kinetic Analysis and First-Principles Calculations

Nicephore Bonnet and Minoru Otani

*National Institute of advanced Industrial Science and Technology (AIST),
1-1-1 Umezono, Tsukuba, Ibaaki 305-8568*

The oxygen reduction reaction (ORR) is critical to a variety of processes such as combustion, corrosion, energy conversion, and storage. However, the detailed mechanism of the ORR at the atomic level remains unknown owing to the difficulty in probing intermediate species in reactive conditions. Although first-principles techniques have been intensively used to assess different reaction pathways, it is still not possible to rationalize all experimental measurements, which illustrates the persistent difficulties to account for all aspects of the ORR in a first-principles bottom-up approach.

Alternatively, in this project, we have conducted a top-down kinetic analysis of the ORR on Pt(111), in which electrochemical measurements are used to explore the possible reaction pathways at the atomic level, while ensuring that results of this analysis are consistent with first-principles computations, either from existing literature, or performed additionally by using the STATE code on available computational resources.

This dual approach allows us to shed some light on the relative efficacy of the ORR by comparing its free energy landscapes along the alternative associative and dissociative pathways (Fig. 1).

Specifically, we find that although the ORR proceeds preferentially through the associative pathway at high electrode potentials, a dissociative pathway becomes possible at lower potentials. However, the latter is gradually hampered by the products of the oxygen dissociation, such that the associative pathway again becomes dominant in the steady-state regime. The present study thus illustrates the impor-

tance of dynamical and self-poisoning effects in the ORR, motivating further characterization by the application of highly space and time-resolved probing techniques. This project also illustrates the intimate synergy between experimental data (here used as the basis for the top-down analysis) and first-principles computations.

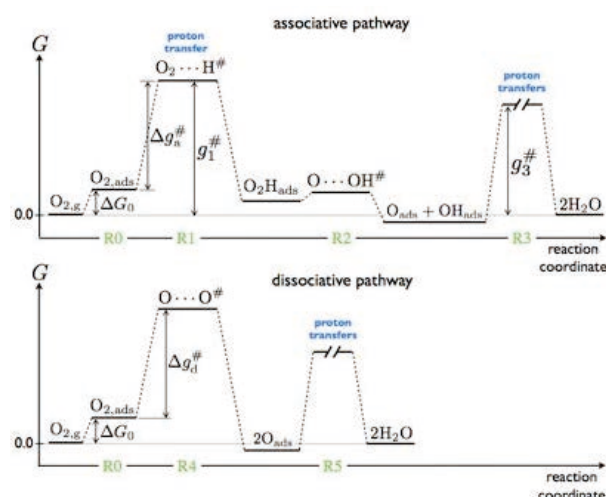


Figure 1: Free energy diagrams of ORR associative (top) and dissociative (bottom) pathways.

[C class; 10000 K (B), 2000 K (C)]

First principles calculations on magnetism and transport properties at surfaces/interfaces and in molecules

Kohji NAKAMURA

*Department of Physics Engineering, Mie University
Tsu, Mie 514-8507*

Progresses on i) perpendicular magnetocrystalline anisotropy (PMA) of 3d transition-metal thin films, ii) magneto-transport properties of Fe thin films in an external electric field (E -field), and iii) magnetism of metal-phthalocyanine (MPc) molecules, by means of first principles full-potential linearized augmented plane wave method, are presented.[1]

PMA of 3d transition-metal thin films — In searching transition-metal thin films with a large PMA that overcomes the shape in-plane magnetic anisotropy and thermal fluctuations for ultrahigh density and nonvolatile spin-electronics, we systematically calculated the MA energies of Fe-based thin films consisting of magnetic 3d elements (Mn, Fe, Co, and Ni). The results predicted that giant PMA can be achieved by tuning the atomic-layer alignments in an Fe-Ni thin film with a bcc-like-layer stacking of Fe₂Ni/Fe/Ni/Fe₂, which arises from the spin-orbit coupling interaction between occupied and unoccupied Ni $d_{x^2-y^2,xy}$ bands crossing the Fermi level.

Magneto-transport properties of Fe thin films in an E-field — Magnetism induced by an E -field has received much attention as a potential approach for providing a new pathway for controlling magnetism. Here, we investigated the magneto-transport properties in an E -field, where the conductivity tensor is obtained by applying the Kubo formula of linear response theory. For the free-standing Fe monolayer, results predict a reduction (enhancement) of the in-plane dc electric and intrinsic Hall conductivities for E -field less than about 1 V/Å, due

to the change in the band structure around Fermi level (E_F). An abrupt change in these conductivities around 1.1 V/Å appears where the magnetization reorients from the out-of-plane direction to the in-plane direction. The interband conductivity in the low energy region (<0.3 eV from E_F) is modified by the E -field. Small changes in the magneto-transport properties were also confirmed in the Fe monolayer on MgO substrate.

Magnetism of MPc molecules — A challenge to miniaturize devices for novel magnetic application now extends to treating the extreme limit of a single atom or molecule. For organometallic molecules with transition-metals, multiplets are essential aspects of their electronic structure. Here, we investigated electronic structures and magnetism of single MPc molecules, in which multiplets are treated by imposing a density matrix constraint on the d -orbital occupation numbers. We found that for the MnPc, the ground state is the 4E_g (d_{xy} , d_{z^2} , $d_{xz(yz)}^3$) state with the perpendicular magnetic anisotropy with respect to the molecular plane, while for the FePc and CoPc, the ground states are the $^3A_{2g}$ (d_{xy}^2 , $d_{z^2}^2$, $d_{xz(yz)}^2$) and $^2A_{1g}$ (d_{xy}^2 , $d_{z^2}^2$, $d_{xz(yz)}^3$) states, respectively, with a planar magnetic anisotropy.

References

- [1] K. Hotta et. al., PRL **110** (2012) 267206; K. Nakamura et. al., J. Korean Phys. Soc. **63** (2013) 612; Y. Kitaoka et. al., J. Appl. Phys. **113** (2013) 17E130.

First-principles investigation on thermophysics of nano structures

Shinji TSUNEYUKI^{1,2}

¹*Department of Physics, The University of Tokyo
Hongo, Bunkyo-ku, Tokyo 113-0033*

²*Institute for Solid State Physics, The University of Tokyo
Kashiwa-no-ha, Kashiwa, Chiba 277-8581*

Lattice thermal conductivity of crystals is governed by the anharmonicity of interatomic potentials. It is an essential ingredient of the figure of merit for thermoelectric materials, where lower thermal conductivity is preferred. On the other hand, higher thermal conductivity is preferred in electronic devices for thermal stability. From the viewpoint of materials design for these purposes, we have developed a new scheme to calculate lattice thermal conductivity from first principles.

So far three methods have been proposed for computational study of thermal conductivity: a method based on Boltzmann's transport equation and diagrammatic evaluation of lifetime of phonons, molecular dynamics (MD) simulation with the Kubo-Greenwood formula and non-equilibrium MD simulation of heat transfer. In any case, first-principles simulation is highly difficult because of the large system size either in real space or in \mathbf{k} space necessary for reliable calculation. Thus we decided to develop an accurate, efficient and versatile method for modelling anharmonic interatomic potentials with first-principles MD based on the density functional theory (DFT).

The model potential is just a Taylor expansion of the total energy of the system calculated by DFT,

$$V(\mathbf{u}) = V_0 + \frac{1}{2} \sum_{i,j} \Phi_{ij} u_i u_j + \frac{1}{3!} \sum_{i,j,k} \Phi_{ijk} u_i u_j u_k + \dots$$

$\mathbf{u} = (u_1, u_2, \dots)$ are the displacements in xyz direction of each atom from its potential minimum, Φ_{ij} is a harmonic force constant and $\Phi_{ijk\dots}$ is called an anharmonic force constant. Practically the Taylor expansion is terminated at a low order and the force constants are

determined so that the model potential minimizes the deviation from first-principles potential energy for some sampling points under crystalline symmetry constraints [1]. In this study, we adopt up-to the sixth-order force constants for the parameter fitting. For efficient sampling of the potential energy hyper-surface, we use the locus of atoms obtained by first-principles MD at a fixed temperature [2]: the temperature should be high enough to reflect anharmonic character of the potential but low enough to avoid unphysical sampling. We find the third-order force constants determined in this way are comparably accurate as those carefully obtained by numerical differentiation of the potential energy.

Once the force constants are determined, phonon dispersion, group velocity and the lifetime of each phonon mode are calculated, with which lattice thermal conductivity and its temperature dependence is obtained within the relaxation-time approximation. We applied the scheme to Si, Mg₂Si, PbTe, Bi₂Te₃ and Ba₈Ga₁₆G₃₀ and found that material dependence and temperature dependence of the thermal conductivity are quantitatively reproduced in a wide range from 10⁰ to 10³ W/mK.

The program package we developed will be published at the portal site for materials science simulation "MateriApps" [3] in FY2014.

References

- [1] K. Esfarjani and H.T. Stokes, Phys. Rev. B77, 144112 (2008); Phys. Rev. B86, 019904 (2012).
- [2] T. Tadano, Y. Gohda and S. Tsuneyuki, J. Phys. Condens. Matter, in press.
- [3] <http://ma.cms-initiative.jp/>

First-Principles Molecular-Dynamics Study of Structural and Electronic Properties of Covalent Liquids under Pressure

Fuyuki SHIMOJO, Akihide KOURA, Arifin RIZAL, Daiki FUKUNAGA, Kenta IDEUE

Department of Physics, Kumamoto University, Kumamoto 860-8555

To clarify the microscopic mechanism of changes in the structural and dynamic properties of amorphous or liquid covalent materials under pressure, we have carried out first-principles molecular-dynamics simulations [1-3]. To investigate the pressure dependence of the static structure, we obtain the structure factors, the pair distribution functions, and the distribution of the coordination numbers as a function of pressure. The bond-overlap populations and the Mulliken charges as well as the electronic density of states show the change in the covalent character in the materials due to compression.

In the static structure factor of amorphous silica at ambient pressure, there is a first-sharp diffraction peak (FSDP) at a wavenumber of about 1.6 \AA^{-1} , which indicates the existence of an intermediate-range structural correlation between the tetrahedral units. Our calculations show that FSDP disappears under pressure over 10 GPa, suggesting that the intermediate-range correlation vanishes. Under further compression, the tetrahedral units collapse accompanied with an increase of the coordination number. While the nearest-

neighbor distance of the silicon-silicon pair decreases up to 10 GPa, it increases at higher pressures. In the amorphous state, unlike in the crystalline phase, the structural change occurs gradually under pressure.

The concentration dependence of the dynamic properties of liquid thallium-selenium alloys has been also investigated. At low thallium concentrations, fairly long selenium chains exist in the liquid state. Upon the addition of thallium atoms, the self-diffusion coefficients of both selenium and thallium decrease despite the shortening of the selenium chain length. We clarify that this behavior is due to the suppression of self-diffusion by the increase in the strength of electrostatic interactions between thallium and selenium atoms.

References

- [1] A. Koura and F. Shimojo: *J. Phys. Soc. Jpn.* **82** (2013) 094602.
- [2] S. Ohmura, *et al.*: *J. Phys. Soc. Jpn.* **82** (2013) 074602.
- [3] A. Koura, S. Ohmura, and F. Shimojo: *J. Chem. Phys.* **138** (2013) 134504.

Effects of doping on atomic structures and electronic properties of nanocarbon materials

Yoshitaka FUJIMOTO

Department of Physics, Tokyo Institute of Technology

Oh-okayama, Meguro, Tokyo 152-8551

Introduction of defects such as atomic vacancies and chemical impurities could often change the electronic properties and enhance chemical reactivity of carbon-based materials. The nitrogen and atomic vacancy complex defects in carbon-based materials has received much attention from nanoscience and nanotechnology, and graphene and carbon nanotubes with such nitrogen defects are expected to produce the new device materials used in catalyst for oxygen reduction reactions, capacitors for energy storages and hydrogen storages.

Here, we study the adsorption effects of hydrogens on nitrogen-vacancy complex defects in graphene using a first-principles total-energy calculation within the framework of the density-functional theory. As nitrogen-vacancy complexes, we use two kinds of pyridine-type defects: one is trimerized pyridine-type defects consisting of three nitrogen atoms around a single vacancy and the other is tetramerized pyridine-type defects consisting of four nitrogen atoms around a divacancy [1, 2]. The adsorption energies of hydrogen atoms on N-doped graphene are calculated as a function of the number of hydrogen atom, and it is found that the two hydrogen atoms adsorptions become energetically the most favorable for the trimerized as well as the tetramerized pyridine-type defects.

To discuss the stabilities of H atoms adsorption onto a graphene sheet, the adsorption energy is defined as

$$E_a = E_{tot} - E_{sub} - nE_{H_2}/2, \quad (1)$$

where E_{tot} and E_{sub} are total energies of pyridine-type N-doped graphene with and without hydrogen atoms, respectively, E_{H_2} is

also total energy of an isolated H_2 molecule, and n is number of adsorbed H atoms.

The adsorption energies of H atoms on N-doped graphene are calculated as a function of number of H atoms. It is found that adsorptions of two H atoms on the trimerized and the tetramerized pyridine-type defects become energetically the most favorable. It is also found that when H_2 molecules are setting near not only the trimerized pyridine-type but also the tetramerized pyridine-type defects, the H_2 molecules are dissociated and two H atoms are adsorbed to N atoms in the pyridine-type defects. Thus, the pyridine-type defects are expected to act as a highly reactive site.

In summary, the adsorptions of hydrogen atoms onto the pyridine-type defects in graphene have been investigated using first-principles density-functional calculations. The dissociative adsorptions of H_2 molecule on the trimerized as well as the tetramerized pyridine-type defects are found to become favorable energetically.

References

- [1] Y. Fujimoto and S. Saito, *Phys. Rev. B* **84**, 245446 (2011).
- [2] Y. Fujimoto and S. Saito, *Physica E* **43**, 677 (2011).

First-principles study on Pt and oxide electrocatalyst

Osamu SUGINO

Institute for Solid State Physics,

The University of Tokyo, Kashiwa-no-ha, Kashiwa, Chiba 277-8581

We have investigated the properties of two different electrocatalysts for the oxidation (reduction) of oxygen/hydrogen molecules, i.e., platinum (Pt) and zirconium oxide (ZrO_2). On the Pt catalyst, despite a large number of theoretical researches the understanding is still far from complete. This is especially the case for the electro-adsorption of hydrogen (H) on Pt(111), which is by far the most studied subject. The research has been hampered by the small difference in the stability among adsorption sites, e.g., top, hollow, and bridge sites and by the limited number of available measurements. In this context, the aim of our study is to overcome this problem by (1) performing an intensive comparison of the adsorption sites within the density functional theory (DFT) and the generalized gradient approximation (GGA) and by (2) utilizing a recent detailed measurement on the effective lateral interaction of the adsorbed H atoms for an honest comparison with the simulation.

It was found that the top site and the fcc hollow site compete with each other as the most stable site, as has been discussed in many researches, but the relative adsorption energy depends very sensitively on the computational

parameters, i.e., the thickness of the slab model and the k -point used for the Brillouine zone integration. With this in mind we have increased the thickness up to 18 layers and the number of k -point up to 24×24 per lateral (1×1) cell to reach the convergence. The relative energy for the full coverage condition was found to be almost degenerated unless the zero-point energy (ZPE) correction was included but, after including the correction, the fcc hollow site was found more stable by 70 meV. The relative energy is thus originated from the quantum effect.

To investigate the relative energy at lower coverage conditions, we have calculated the DFT-GGA total energy for many different configurations realized within a (3×3) lateral cell and mapped the result to a lattice gas model. The model was then used to conduct a Monte Carlo simulation using a (10×10) cell. The result was analyzed to obtain the thermally averaged H-H interaction energy, which is called the g -value, to be compared with the measurements. To see a parameter dependence, we have also done the simulation using different set of parameters for the lattice gas model.

The theoretical g -value was found slightly

smaller than the measured one and can be fitted well to the experiment when the H-H interaction parameter was increased by 20 %. This suggests that the interaction is underestimated by DFT-GGA by that amount. Here we admit that our calculation completely neglected the hydration effect considering that the effect has been conjectured small; we cannot therefore exclude the possibility that the hydration effect may play an important role in strengthen the H-H interaction.

Regarding the relative energy of H on the top site and that on the fcc hollow site, the g-value remained unchanged when the fcc hollow site had been virtually lowered in energy and, on the other hand, it deviated from the experiment when the site had been shifted upward. This result can be naturally understood by dominated fcc hollow site in the whole coverages.

This study have advanced a DFT-GGA level description on the H electroadsorption on Pt(111). The theory is found consistent with experiment reasonably well although slight discrepancy from experiment can be seen in the H-H interaction. The next target will be to go beyond the accuracy of DDF-GGA and to take into account the hydration effect.

Regarding the zirconia, we examined the mechanism for oxygen reduction reaction on zirconia surface using first-principles molecular dynamics. In our calculation model, we introduced an oxygen vacancy on tetragonal zirconia (101) surface, adsorbed an oxygen

molecule near the vacancy site, introduced water molecules near the surface, and simulated how the system evolves when a hydrogen atom (proton + electron) nears the surface. We found that the oxygen molecule is easily split after being adsorbed at the vacancy site. As a result of this reaction, however, the vacancy is filled by one of the oxygen atoms and thus loses activity as a reaction center. Hydrogen quickly attacks the other oxygen atom and a water molecule is formed when a second hydrogen atom is introduced in the simulation. This suggests that desorption of surface oxygen ions (formation of vacancies) is the rate-limiting step for ORR at the zirconia surface.

References

- [1] T. T. H. Tran, Y. Takimoto, and O. Sugino, *Surf. Sci.* 625, 104 (2014).

Computer Simulations of Nano-Fe Magnetizations

Shuji OBATA

School of Science & Engineering, Tokyo Denki University
Ishizaka, Hatoyama, Hiki, Saitama 350-0394, Japan

Relating with the main subject of the investigations of the electronic states in nano-materials, characteristics of magnetic dipole moment interactions induced from 3d and 4s orbitals in Fe metal are discussed in this work.

Using the ISSP system A (shii), the Fortran programs of the nano-Fe magnetizations are executed by about 500 line programing compiled with xsf90. The used times are about p4- 18 hours par job drawing domain structures and magnetization curves. The magnetic domain structures are determined by the classical dipole moment interactions as shown in Fig. 1. Setting distance vector $\mathbf{d}_{ij}=\mathbf{e}_{ij}d_{ij}$ between dipole moments at i and j , the interaction energies are equated as

$$W_{ij} = \frac{1}{4\pi\mu_0 d_{ij}^3} \{ (\boldsymbol{\mu}_i \cdot \boldsymbol{\mu}_j) - 3(\boldsymbol{\mu}_i \cdot \mathbf{e}_{ij})(\boldsymbol{\mu}_j \cdot \mathbf{e}_{ij}) \}. \quad (1)$$

Crystal Fe takes the BCC structure with the lattice constant $a=2.86 \times 10^{-10}$ [m] up to 911 °C and have 2 atoms in a lattice. This Fe metal has the dipole moments of $2n_b\mu_0\mu_B$ per a lattice, where $n_b=2.22$, μ_0 and μ_B are permeability and the Bohr magneton respectively. In our simulations, the magnetic moments are set to have freedom of 26 directions as shown in Fig. 2.^{[1][2]}

The nano-magnets depend on the system structure. The Barkhausen effects are observed in detail magnetization curves as in Fig. 3.

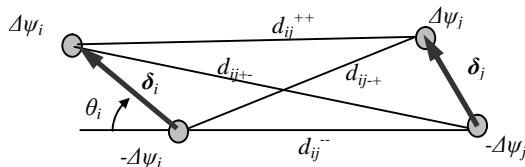


Fig. 1. Two magnetic moment interactions. The dipole moments are equated as $\boldsymbol{\mu}_i = n_b\boldsymbol{\mu}_B^0 = \delta_i\Delta\psi_i$

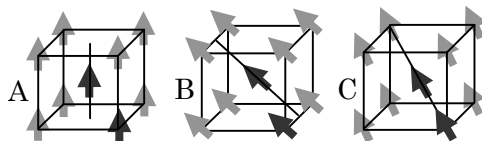


Fig. 2. Magnetic moment directions in a BCC lattice.

The domain structures at the jump points in a circle in Fig. 3 are drawn in Fig. 4. The results in the last year are obtained in the 6 freedoms of the easy axis directions. Comparing to those results, the domain structures in Fig. 4 in 26 freedom directions become a little bit complex, but the Barkhausen effects and the magnetization curves are similarly obtained.

The comparison of BCC & FCC Fe is also investigating now, where the similar results are obtained. The results of Fe₃O₄ are also obtained, where the domain structures are difficult to draw.

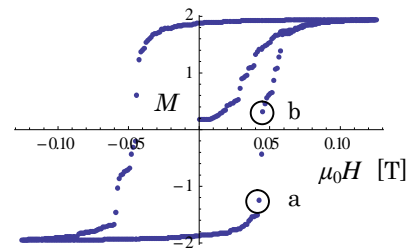


Fig. 3. The magnetization curve in a nano-belt system of the $N_xN_yN_z=16 \times 4 \times 64$ lattice points in z direction field with $n_b=2.0$.

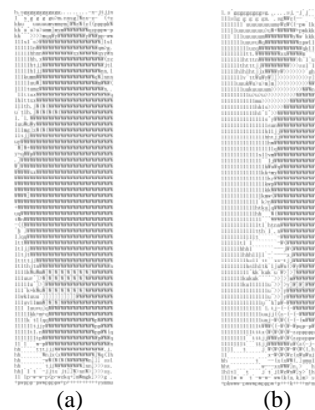


Fig. 4. The domain structures of the second y layer at the jump points in a circle in Fig. 3. (a)~(d) correspond to a~d respectively.

[1] S. Obata : IEEJ Trans. FM. **133** (2013) 489-499.
[2] S. Obata : Materials Transactions. **54** (2013) 1661-66.

First-Principles Calculation of Transition-Metal Compounds

Tamio OGUCHI, Masayuki TOYODA,

Keisuke ISOYAMA, Masataka DEGUCHI, Akihiro FUJII

Institute of Scientific and Industrial Research, Osaka University, Ibaraki 567-0047

A first-principles density-functional-theory method has been applied to various condensed matter and surface systems for the last few decades. In this project, we study the electronic properties of several transition-metal compounds and explore their chemical trends and effects associated with crystal structure and symmetry. In addition, continuous developments of numerical methods related to the first-principles calculations are also pursued. In FY2013, we mainly studied the electronic structure of transition-metal oxides.

The A-site ordered perovskites $AA'B_4O_{12}$ are known to be a derivative of the standard perovskite oxides ABO_3 , where relatively large cations occupy the A site while relatively small transition-metal cations are accommodated at the B site. In the A-site ordered perovskites, Jahn-Teller active cations such as Cu^{2+} and Mn^{3+} are located at the A' site with a peculiar square planar coordination. Among them, $CaCu_3B_4O_{12}$ (B=Ti, Ge, Zr, and Sn) (CCBO) consist of non-magnetic B-site ions and may be suitable for a study on the magnetic ordering associated with the A' sites. Magnetic couplings between Cu ions in CCBO were evaluated by total-energy calculations within an effective Heisenberg model [1]. It is found that the nearest and second-nearest neighbor couplings J_1 and J_2 are relatively weak ferromagnetic, almost independent of the B-site ions while the third-nearest neighbor coupling J_3 is also so in B=Ge and Sn but strongly antiferromagnetic in the cases of B=Ti and Zr, leading to the stable antiferromagnetic order. The antiferromagnetic coupling J_3 originates from the long-range superexchange interactions via Cu-O-Ti(Zr)-O-Ti hopping paths. Very strong

hybridization between $Cu-d_{x^2-y^2}$ and O- p orbitals is a peculiar feature in these A-site ordered perovskite oxides.

The electronic structure of the A-site ordered perovskite $LaCu_3Fe_4O_{12}$ (LCFO) is also investigated by means of first-principles calculations [2]. LCFO reveals metal-to-insulator and paramagnetic-to-antiferromagnetic transitions with a volume expansion by 1.3% at 393K as temperature decreases. This is believed to be associated with a charge transfer as $3Cu^{2+} + 4Fe^{3.75+} \rightarrow 3Cu^{3+} + 4Fe^{3+}$, according to a bond distance analysis. We found that the volume change at the transitions is a key for understanding the changes in the electronic structure and magnetism.

Some other first-principles applications to transition-metal compounds have been carried out for $PdCoO_2$ [3], $PdCrO_2$ [4], $FeTe_{1-x}Se_x$ [5], and so on, in collaboration with experimental groups.

References

- [1] M. Toyoda, K. Yamauchi, T. Oguchi: Phys. Rev. B **87** (2013) 224430.
- [2] K. Isoyama, M. Toyoda, K. Yamauchi, T. Oguchi: JPS Meeting (2014) 28aPS-97.
- [3] H. Takatsu, *et al.*: Phys. Rev. Lett. **111** (2013) 056601.
- [4] J. M. Ok, *et al.*: Phys. Rev. Lett. **111** (2013) 176405.
- [5] H. Okazaki, *et al.*: Euro. Phys. Lett. **104** (2013) 37010.

First-Principles Calculations of Electron and Spin Properties in Solid Materials

Hiroyoshi MOMIDA

*Institute of Scientific and Industrial Research, Osaka University
8-1 Mihogaoka, Ibaraki, Osaka 567-0047*

We have performed first-principles electronic structure calculations to study material properties of several kinds of solid systems at bulk, surface and interface environments with or without considerations of defect influences. Thanks to the support of computer resources, three refereed papers were published in the fiscal year 2013 [1, 2, 3]. To elucidate the nature of a brittle fracture process in steel materials, we have studied microscopic mechanism of hydrogen-enhanced vacancy embrittlement of grain boundaries in α -Fe [1]. Our computations partly contribute to show x-ray absorption spectra of FeS₂ which is a technologically important material such as secondary batteries [2], and to conduct physical guiding principles for high quality resistive random access memory stack with an Al₂O₃ insertion layer [3].

In the fiscal year 2013, we have mainly used the supercomputers to predict topologically-insulating phases of Sb₂Te-based materials, to study surface band structures of the topological insulator Bi₂Se₃ with several defects, and to estimate magnetic hyperfine interactions at Sn nuclei in Co₂MnSn Heusler alloys. Last two topics are in collaboration with experimental groups. Computations were done using the HiLAPW code which utilizes the all-electron full-potential linearized augmented plane-wave method based on the density functional theory. For the topological insulator systems in which the spin-orbit couplings (SOC) have essential roles on their electronic structures, SOC were included as the second variation procedure.

We computed mostly with the MPI-only parallelizations, and code optimizations are still in progress to improve performances.

As a main scientific achievement of this project, we find that Sb₂Te-based materials can have topological insulator phases controlled by external strains or element substitutions. Sb₂Te is known as a semimetal in its equilibrium structure, and the structure has two Sb₂ bilayers between Sb₂Te₃ quintuple layers. Our result shows that an in-plane strain expanding in the layer direction can induce a band gap, and that element substitutions by a larger atom can also induce a band gap. Calculated Z_2 topological invariants of the insulating phases are $Z_2 = 1$ showing that they can be a strong topological insulator.

This work was done in collaboration with Eriko Takasaki, who partly did computations, and Tamio Oguchi. I would like to thank Takahisa Ohno for all of the help and support.

References

- [1] H. Momida, Y. Asari, Y. Nakamura, Y. Tateyama and T. Ohno: Phys. Rev. B **88** (2013) 144107.
- [2] T. Oguchi and H. Momida: J. Phys. Soc. Jpn. **82** (2013) 065004.
- [3] M. Y. Yang, K. Kamiya, B. Magyari-Köpe, H. Momida, T. Ohno, M. Niwa, Y. Nishi and K. Shiraishi: Jpn. J. Appl. Phys. **52** (2013) 04CD11.

First-Principles Calculations Concerning Spintronics

Mineo SAITO

Institute of Science and Technology, Kanazawa University

Kakuma, Kanazawa, 920-1192 Japan

In spintronics, the spin-orbit interaction (SOI) plays an important role. Therefore, fully-relativistic density functional calculations are necessary to evaluate spintronics materials. ZnO forms two-dimensional electron gas which has a good quality and thus its device application is desired. In this study, we carry out first-principles calculations on ZnO which is a wide gap semiconductor.

Since we have studied the conduction band bottom previously [1], we here study the valence band top (Fig. 1). At the Γ point, the highest occupied band belongs to the two-dimensional irreducible representation of E_2 and the next highest occupied band belongs to the irreducible representation of A_1 . This energy splitting originates from the crystal field. When the SOI is considered, the E_2 level splits into the upper $E_{1/2}$ level and the lower $E_{3/2}$ level. This energy order was unexpected and thus the negative spin orbit coupling has been considered to occur in this system, previously.

However, we find that this energy order originates from the strong SOI. i.e., we find that two $E_{1/2}$ levels originating from E_2 and A_1 are strongly mixed. This strong mixture can be confirmed that the atomic orbitals of p_x and p_y

(E_2) and that of p_z (A_1) are strongly mixed. Therefore, we conclude that the SOI in ZnO is strong. This finding is important in spintronics application of ZnO.

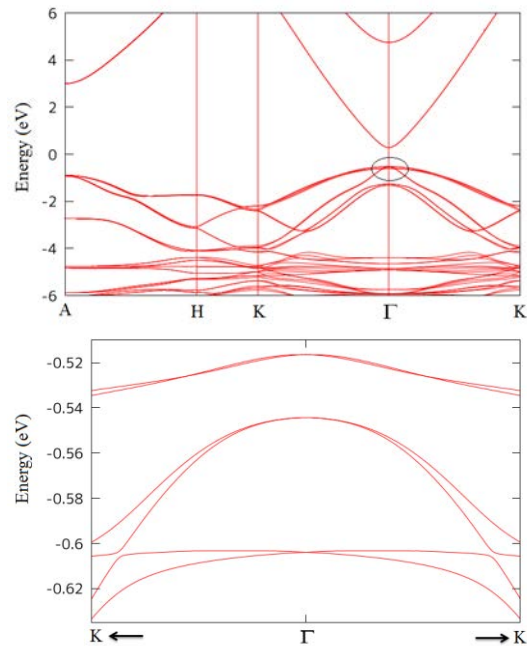


Fig. 1 Band structure of ZnO (SOI is included)

References

- [1] M. A. Adhib, H. Kotaka, F. Ishii, and M. Saito: Appl. Phys. Exp. 7 (2014) 053002.

Hybrid *ab initio* QM/MM calculations of biological macromolecular systems

Masaru TATENO

Graduate School of Life Science, University of Hyogo

In this study, hybrid *ab initio* quantum mechanics (QM) / molecular mechanics (MM) calculation was employed to investigate electronic structures of crucial biological macromolecular systems. Here, we used our QM/MM interface program, which connects highly-parallelized engines for QM and MM calculations. Employing our calculation system, we computationally analyzed catalytic mechanisms of crucial biological macromolecular systems. The followings are parts of the results that we obtained in this FY.

To obtain unknown structures, such as intermediate structures in catalytic reaction processes that are exerted by enzymes, we performed structural modeling to obtain the atomic-resolution structures that are experimentally inaccessible [1]. For the calculations in the modeling, we performed hybrid QM/MM simulations of the enzyme, and thereby built parameter sets of non-standard chemical structures (assigned as the QM regions) that were included in the enzyme, by improving our previous parameter values that were obtained by full QM calculations.

The following is another achievement. For every organism, responses of each cell to

signals from the environmental outside are crucial to optimize its states. Thus, the cellular signal transduction systems are essential to the organisms to transduce the outside signal to the nucleus, where genome DNA is located. In fact, the defects of this function lead the system to fatal errors, such as cancer.

The hydrolysis reaction of GTP to GDP by Ras, which is the product of the RAS oncogene (cancer gene), constitutes one of the most critical reactions for cellular signal transduction. Since this hydrolysis reaction, which acts as a crucial switch in various signaling cascades, is activated by binding of the GTPase activating protein (GAP) of Ras, the mechanisms of this reaction by the Ras-GAP complex have intensively been investigated for decades. However, even the reaction scheme has not yet been positively identified.

Last FY, we performed docking simulations of GTP and the Ras-GAP complex by classical MD simulations and hybrid *ab initio* QM/MM MD simulations. In this FY, employing the obtained structural model, we further conducted hybrid *ab initio* QM/MM MD simulations to investigate the catalytic reaction mechanisms [2]. The activation barriers that were estimated

by our computational analysis were comparable with respect to the two reaction pathways, i.e., the dissociative and associative mechanisms (see Fig. 1). Thus, we revealed that the catalysis by the Ras•GAP complex operates by both dissociative and associative mechanisms. To our knowledge, this is the first finding of a “dual-mechanism/pathway” hydrolase.

Then, based on the more detailed catalytic processes that were elucidated in the present analysis, we investigated other various hydrolysis reactions by enzymes, with the use of crystal structures that were previously reported. Thereby, we built a novel and simple scheme for identifying the catalytic mechanisms of such various hydrolase reactions, which enabled us to predict the reaction mechanisms of

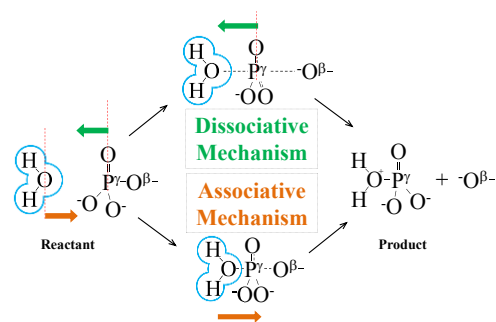


Fig. 1. The fundamental schemes of the catalytic reaction of hydrolysis by various enzymes (hydrolases). The upper and lower represent the dissociative and associative mechanisms, respectively. For the Ras-GAP complex, we investigated whether these two catalytic reaction pathways are plausible or not, employing hybrid *ab initio* QM/MM MD simulations in this FY [2].

hydrolases. Thus, we can now provide the explanation of the reason why the mechanism operates in a hydrolase. Thus, our present work also provides a solid basis for engineering applications such as enzyme design, etc., based on the detailed hydrolase mechanisms.

References

- [1] Kubo, M., etc.: Effective pumping proton collection facilitated by a copper site (Cu_B) of bovine heart cytochrome c oxidase, revealed by a newly developed time-resolved infrared system, *J. Biol. Chem.*, **288** (2013), 30259-69.
- [2] Itagaki, T., Kang, J., and Tateno, M.: Dual catalytic reaction mechanisms by the oncogenic Ras and RasGAP complex, *submitted*.

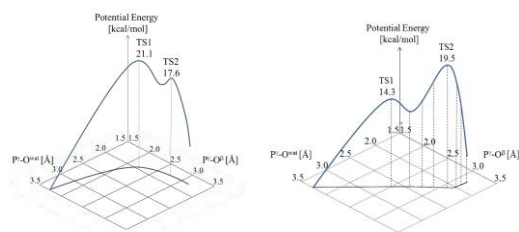


Fig. 2. The energy profiles that were obtained by our hybrid *ab initio* QM/MM MD simulations of the Ras-GAP complex. The analysis revealed that the activation barriers obtained are comparable. Therefore, we concluded that the two reaction pathways are both plausible. This is the first finding that these two catalytic pathways are involved in a hydrolysis reaction by an enzyme (hydrolase).

Theoretical investigation of the initial growth process of organic semiconductor thin films

Kazume NISHIDATE and Masayuki HASEGAWA

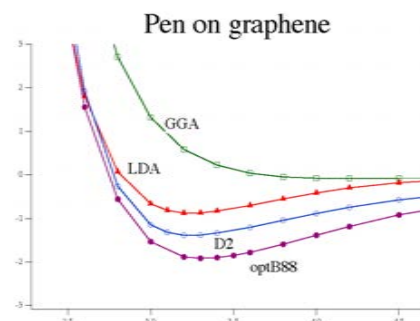
Faculty of Engineering, Iwate University

Ueda 4-3-5, Morioka, Iwate 020-8551

A pathway of carriers in an organic semiconductor device is formed at the interface between the organic thin film and the gate insulating thin film. Controlling the arrangement of organic molecule at the first layer on the gate plays a crucial role not only in the device characteristics but also in the crystallinity of the organic thin film.

Pentacene (Pn) is an aromatic molecule composed of five benzene rings. It has been regarded as a very likely candidate for organic semiconductor since it displays high carrier mobility. In recent years, acceleration of the carrier mobility has also been tried by forming Pn layers on a graphene sheet which is placed on the insulating gate.[?]

There are two types of interactions between the Pn molecules. One is the long range van der Waals (vdW) interaction, and the other is the repulsive interaction between the outer hydrogen atoms. The competition of the interaction among the Pn molecules result in the formation of the characteristic herringbone pattern of the organic crystal. To assess the early stages of the formation of Pn layers on graphene, we have performed large scale vdW density functional electronic structure calculation (vdW-DFT) of the Pn on graphene system. We also performed the Grimms D2 calculation (DFT-D2) where vdW force is empirically implemented. Both of the Local density approximation (LDA) as well as the generalized gradient approximation (GGA/PW91) were performed as complement calculations.



The supercell contains a graphene sheet with the dimensions of 11×11 benzene nucleus units. Large vacuum region above the graphene sheet is taken ($\sim 15\text{\AA}$) to minimize the unphysical interaction through the boundary. We placed Pn molecule above the graphene sheet with changing the Pn to graphene distance. The configuration is similar to the AB stacking form of graphite; i.e. an apex of the benzen nucleus of Pn is arranged alternately to be on the hole of the benzen nucleus of graphene. The equilibrium distances from Pn to graphene are 3.2\AA (LDA), 3.2\AA (DFT-D2) and 3.3\AA (vdW-DFT). Adsorption energies are -0.87 eV (LDA), -1.38 eV (DFT-D2) and -1.91 eV (vdW-DFT). However, Pn was not adsorbed on the graphene in the GGA computation demonstrating lack of capability to evaluate the long range forces. α

References

- [1] Wi Hyung Lee *et al.*: J. Am. Chem. Soc. **133**, 4447-4454 (2011).

First principles based analysis of reactions on solid surfaces/interfaces

Hideaki Kasai

Department of Applied Physics, Osaka university

Center for Atomic and Molecular Technologies, Osaka university

2-1, Yamadaoka, Suita city, Osaka, Japan, 565-0871

Understanding reactions on surfaces and interfaces is important for developing advanced materials and technologies. Various interesting physical and chemical phenomena are discovered at surfaces and interfaces, ranging from fundamental phenomena like tunneling effects to applications like catalytic reactions and migration of oxygen.

In 2014, several studies on surfaces and interfaces based on density functional theory (DFT) have been carried out in our group [1]. Due to the availability of powerful and useful ISSP computational facilities, it has been possible for us to investigate various interesting and complex problems which can be difficult to deal with experimentally.

Research areas that can be highlighted from our recent works include clean energy related issues such as photocatalysts [2] and solid oxide fuel cells (SOFCs) [3, 4, 5, 6, 7].

The interaction of olefins with various kinds of solid surfaces has been studied extensively over the last few decades. Among many olefin-solid surface interaction systems, ethylene adsorption on solid surfaces is a topic that has attracted a great deal of interest, mainly due to its simplicity in structure and high reactivity. Hence, ethylene adsorption can be regarded as a benchmark study in order to investigate the interaction involving olefin-solid surfaces. It is also worth to be noted that the ethylene interaction with solid surface plays an important role in many kinds of technological, indus-

trial and environmental applications such as separation of light olefins from paraffins, various transformations of hydrocarbons in chemical industries, production of clean transportation fuels, and degradation of various harmful volatile organic compounds (VOCs) derived from ethylene. Therefore, a strong understanding on the physicochemical aspect of olefin-solid surface interaction is necessary. In this work, we investigated the adsorption of C_2H_4 (ethylene) on anatase TiO_2 (001) surface by means of first-principles calculation. Four adsorption configurations that correspond to two main types of interaction of ethylene-solid surface, namely π -bonded and di- σ -bonded interactions, are studied. We found that ethylene adsorbed on top of unsaturated Ti5c (five-fold coordinated Titanium) is the most stable configuration and this configuration corresponds to the π -bonded interaction. In this configuration, the adsorption energy is calculated to be - 0.2 eV and ethylene retains its initial sp^2 planar configuration upon adsorption. Vibrational frequency analysis shows that some small modifications are observed for each reported vibrational modes of ethylene. These findings suggest that ethylene is weakly adsorbed on clean TiO_2 surface and vdW interaction is found to have a significant contribution to the total binding energy of ethylene.

Development of novel fast ion conductors is a crucial issue for SOFCs which can operate at low temperatures. Experimental stud-

ies on fast ion conductors in the recent twenty years have established that rare-earth-based oxides are the most promising materials for solid electrolytes and air electrodes (as cathodes in discharging processes). However, the currently available solid electrolyte materials run at high temperature while one of the main challenges is to reduce the operating temperature below 600°C. Therefore, in our group, we have studied several promising materials that offer possibilities of realizing low operating temperature SOFCs, which includes La_2GeO_5 [3, 4], CeO_2 [3, 5], Pr_2NiO_4 [6], and LaGaO_3 [7] as solid electrolyte materials. The studies on La_2GeO_5 -based materials are still in the early stage and their properties are being clarified one by one. Here, four of five oxygen atoms are bonded covalently while the other is ionically bonded. This hybrid characteristic is expected to yield in novel ideas that have not been discovered yet. On the other hand, the studies on CeO_2 -based materials have entered a mature stage that involved proper conditions of doping and strains toward practical applications. Simple laws are developed on the formation and migration energies and dopant atomic radii. This simpleness is attributed to the ionic nature of O bonding. However, currently we try to increase the complexities of our calculations to also include the description of 4f-electrons in the interaction to gain deeper understanding in the ionic migration. On the other hand, Pr_2NiO_4 -based ceramic oxides are known as promising MIEC cathode material for SOFC owing to its experimentally found good ionic and electronic conductivity compared to other known materials. Substitutional doping at the cation site [$\text{Pr}_{2-y}\text{R}_y\text{Ni}_{1-x-y-z}\text{E}_x\text{T}_z\text{O}_4$ (R=La, and E=Cu and T=Ga)] shows change in both structural and electronic properties. Higher concentration of La doping increases the lattice parameter while maintaining the electronic property of the host system. On the other hand, Cu doping causes tilting of the nickelate

octahedral substructures so as to stabilize the whole structure, but is accompanied by emergence of states which contributes to electronic conduction. However, Ga doping has indication of high O ion diffusion and lower electronic conductivity. Lastly, for the case of LaGaO_3 -based materials, we have investigated the influence of Mg^{2+} doped into Ga^{3+} and Sr^{2+} doped into La^{3+} ions (LSGM). The study is still ongoing and current results indicate that this doped system is semiconductor-like material. Substitution of Ga with Mg weakens the bond leading to the elongating the Mg-O bond length and explains the oxygen migration around Mg dopant.

References

- [1] <http://www.dyn.ap.eng.osaka-u.ac.jp>
- [2] Ganes Shukri, et al: Surface Science **619** (2014) 59.
- [3] Mamoru Sakaue, et al: ECS Transactions, **57** (2013) 1077.
- [4] Tran Phan Thuy Linh, et al: ECS Transactions, **57** (2013) 2411.
- [5] Musa Alaydrus, et al: ECS Transactions, **57** (2013) 2753.
- [6] Susan Meñez Aspera, et al: ECS Transactions, **57** (2013) 2733.
- [7] Triati, et al: ECS Transactions, **57** (2013) 2715.

Density functional theory study of stability and dynamics of metal nanoclusters on a silicon surface

Ikutaro HAMADA

National Institute for Materials Science

Tsukuba 305-0044, Japan

Small atomic clusters are of technological as well as fundamental importances. They are potential components of future microelectronics devices, high density storage devices, and catalysts. Furthermore, it may be possible to realized intriguing physical properties in the small clusters, because of the quantum size effects. Recent progress in scanning probe microscopy enable one to manipulate atoms and molecules one by one, and it is becoming possible to fabricate well defined small atomic clusters on surfaces. Although the control of the number of constituent atoms in the cluster is possible, it is difficult to determine the atomic structures only the experiment. I perform density functional theory calculations of Pb_n ($n=1-4$) on Si(111)(7×7), to clarify the atomic structures of the Pb_n clusters, and the mechanism of the atomic switching realized by the scanning tunneling microscopy (STM).

All the calculations were performed using the STATE[1] code. We used a plane-wave basis set to expand the wave functions and ultrasoft pseudo potentials to describe electron-ion interactions. The surface was modeled by a slab composed of eight atomic layers, and a thick enough vacuum was inserted between the neighboring slabs. The silicon atoms in the bottom layer are terminated by the hydrogen atoms. The effective screening medium method[2] was used to eliminate spurious electrostatic interactions with the image slabs.

In this work, special attention has been paid for Pb_3 , because the atomic switching is in-

duced by STM for Pb_3 . To clarify the mechanism of the atomic switching, it is essential to determine the most stable atomic structure. I have examined more than 20 configurations, and investigated the stable atomic structure of Pb_3 . STM topographies for the most stable configuration were simulated by using the Tersoff-Hamann theory[4]. I found that the simulated STM topography for the occupied states is in reasonable agreement with experiment. Simulated topography for unoccupied states is similar to the occupied one. In the experiment, however, STM topography shows significant bias dependence, suggesting that the structures of Pb_3 examined in the calculations so far cannot explain the experimentally observed Pb_3 . Further investigation is needed to clarify the structure and dynamics of the Pb_3 cluster on Si(111).

References

- [1] Y. Morikawa, H. Ishii, and K. Seki, Phys. Rev. B **69** (2004) 041403(R).
- [2] M. Otani and O. Sugino, Phys. Rev. B **73**, (2006) 115407.
- [3] I. Hamada, M. Otani, O. Sugino, and Y. Morikawa, Phys. Rev. B **80**, 165411 (2009).
- [4] J. Tersoff and D.R. Hamann, Phys. Rev. Lett. **20** (1983) 1998.

First-Principles GW +Bethe-Salpeter Calculations for Photoabsorption Spectra of $M^+@C_{60}$

Yoshifumi NOGUCHI

Institute for Solid State Physics,

The University of Tokyo, Kashiwa-no-ha, Kashiwa, Chiba 277-8581

Fullerene is known as a very good acceptor, thereby finding application in organic solar cell. Additionally, recent experiments have shown that metal encapsulation into a fullerene molecule, such as in $Li^+@C_{60}$ enhances its accepting potential owing to the stabilization of the fullerene frame by the metal ion encapsulated inside. A theoretical investigation to understand the structural and optical properties of the $Li^+@C_{60}$ molecule is necessary, for further advances in the field of organic solar cells.

The talented first-principles method, in particular for simulating the optical properties, is a Green's function method based on the many-body perturbation theory (GW +Bethe-Salpeter), not a standard DFT-based method. However since the Green's function method is computationally more expensive than DFT, there is a strict limitation on the treatable system size.

Recently, we developed a hybrid (OpenMP and MPI) parallel version of the GW +Bethe-Salpeter program code. Fig. 1 shows the result of the benchmark test measured performed on the Fujitsu FX10 supercomputer. The MPI

parallel efficiency in weak scaling reaches about 97 % with 1536 MPI parallel execution. With this high parallel efficiency, the present program code can handle systems with more than 100 atoms.

In this study, we employed the first-principles GW +Bethe-Salpeter method to calculate the photoabsorption spectra of $M^+@C_{60}$, where $M=H, Li, Na, \text{ and } K$. The calculated spectra are in good agreement with the available experiment. We discussed the effect of M^+ encapsulation into fullerene on the photoabsorption spectra [1].

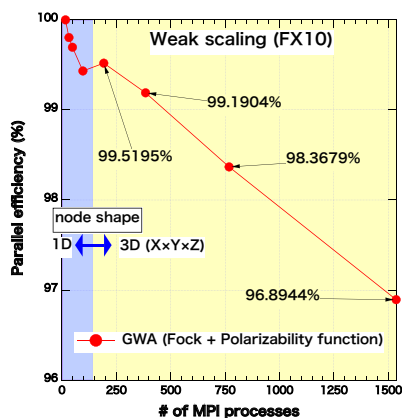


FIG. 1. MPI parallel efficiency.

References

- [1] Y. Noguchi, O. Sugino, H. Okada, and Y. Matsuo, *J. Phys. Chem. C*, **117**, 15362 (2013).

Microscopic Understanding of Electric Double Layer at Solid-Liquid Interfaces

Kazuto AKAGI

WPI-AIMR, Tohoku University

Katahira, Aoba-ku, Sendai, Miyagi 980-8577

H^+ ions play various important roles in functional materials/devices such as catalyst, fuel cell, and also in more complex biological systems. Elucidation of spatial distribution and dynamics of H^+ ions at the interfacial region in these systems is one of the important subjects for computational materials science. In this project, microscopic picture of H^+ ions in an acid aqueous solution is studied based on the first-principles molecular dynamics (MD) calculations and a series of hydrogen-bond network analyses. Each simulation cell has an appropriate size with more than 110 water molecules to describe not an adsorbed water film but a solid-liquid interface. The PBE functional was used at 400K (\approx SPC/E water at 280K) with the plane wave basis set of $E_{\text{cutoff}} = 400\text{eV}$ and the PAW scheme for valence electrons. 100ps MD trajectories were used for the analysis of each system.

First, the microscopic picture how H^+ ions are bound around counter anions in 2mol/l H_2SO_4 solution was investigated by comparison of the potentials of mean force (PMF) evaluated in two ways: the radial distribution functions and integration of the averaged forces, respectively. It turned out that the picture that a hydrogen ion can be described as a hydronium ion (H_3O^+) is well justified and the typical binding free-energy around HSO_4^- was 4 kcal/mol (Fig.1a). This is almost the same strength as the attractive interaction between Na^+_{aq} and Cl^-_{aq} .

Next, the interfaces between Pt surfaces and

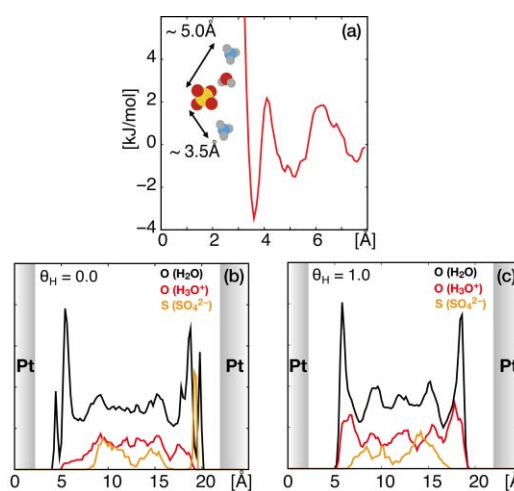


Figure.1 (a) Potential of mean force for H_3O^+ around HSO_4^-/SO_4^{2-} . (b)(c) Spatial distribution of H_2O [black], H_3O^+ [red] and HSO_4^-/SO_4^{2-} [orange] along the depth direction.

2mol/l H_2SO_4 solution were studied. As the Pt(111) surface changed from hydrophilic to hydrophobic with increase in the adsorbed hydrogen atoms, the hydronium ions escaping from the hydrophilic surface (Fig.1b) were getting localized at the most interfacial region with the hydrophobic surface (Fig.1c). They were strongly bound by SO_4^{2-} compared to those in a bulk solution, and their accumulation leads to the stability of adsorbed hydrogen atoms on a Pt surface. While the mechanism of change in spatial distribution of H_3O^+ and HSO_4^-/SO_4^{2-} is still unclear, several interesting relations with the topology of hydrogen-bond network by surrounding water molecules were also found. It will be reported after the detailed analyses are done.

Study on Nano-scale Carbon Materials

Susumu Okada

*Graduate School of Pure and Applied Sciences, University of Tsukuba
1-1-1 Tennodai, Tsukuba, Ibaraki 305-8577*

Pentagons embedded into hexagonal sp^2 (threefold-coordinated) carbon networks play a crucial role in determining the geometric and electronic properties of the resulting nanoscale carbon allotropes. In the infinite planar hexagonal C network, pentagons should be appeared with the appropriate number of polygons. For example, an isolated pentagon embedded in graphene induces the formation of a heptagon adjacent to it to maintain a planar sp^2 network, as is found in Stone-Wales type and fused pentagon type topological defects. Since pentagons and other polygons disrupt the AB bipartite symmetry of graphene, such topological defects in graphene occasionally induces an unusual electronic structure at or near the Fermi level in addition to the characteristic electronic structure of graphene. Localized states and flat dispersion bands associated with the topological defects are expected to occur around them. Therefore, it is interesting to explore the geometric structure and electronic properties of graphene containing many topological defects. In this study, we explore the geometric and electronic structures of a 2D sp^2 C allotrope consisting of pentagons and dodecagons, as a representative structure of the limit of topological defects in sp^2 networks, based on first-principles total energy calculations.

We found that the 2D sp^2 carbon allotrope retains its planar structure at the equilibrium lateral lattice parameter $a = 7.1 \text{ \AA}$. At the equilibrium lattice constant, the calculated total energy of the sheet is 0.66 eV/atom with respect to the energy of graphene, indicating that the structure is energetically stable. Further *ab initio* molecular dynamics simulations confirmed that the sheet was kinetically stable up to a temperature of 1000K for simulation

times of a few picoseconds. We found that the sheet is a metal with a flat dispersion band that crosses the Fermi level. Owing to the flat dispersion band at the Fermi level, the state is split into majority and minority spin states, respectively, leading to spin polarization on the sheet. The polarized electron spin is ferromagnetically ordered and distributed throughout the whole network of the sheet with a magnetic moment of $0.62 \mu_B/\text{nm}^2$. In addition to the magnetism arising from the flat dispersion band, although the network does not contain any hexagonal rings, the sheet still exhibits the characteristics electronic properties of graphite and graphene. The fused pentagon sp^2 C sheet has a pair of massive Dirac dispersion bands at the K point. Detailed analysis on the wave function indicated that the states possess non-bonding π electron nature on the honeycomb network of fused pentagons.

Study on material search and electrode interfaces for next-generation secondary batteries

Yasunobu ANDO

*Department of Materials Engineering, The University of Tokyo
7-3-1, Hongo, Bunkyo-ku, Tokyo 113-8656*

Basic researches for secondary batteries through the use of computer simulation have been studied actively. Especially, Li-ion batteries have been attracted much interest because of their broad applications. To advance improvements of performance of the batteries, obscure fields such as ion dynamics at electrochemical interfaces should be worked on. In order to understand the nature of ion dynamics at the interfaces, we focus on the functional binders-electrode interfaces. It is reported that functional binders modulate the insertion process that makes us possible to design the performance of batteries.

We model the interfaces including poly(vinylidene fluoride) (PVdF) and single-graphene electrode. *Ab initio* molecular dynamics with electric field is performed by OpenMX (Open source package for Material eXplorer) [1]. Electric field is considered in the system by using Effective Screening Medium (ESM) method. In ESM scheme, atoms must not go across the cell edge along the z-direction because periodic boundary condition is not satisfied. Therefore, we have to impose an artificial wall near the cell edge that is controlled by the value “wall.position” in an input file.

In a process of the research, we find some bugs corresponding to setting the wall position. We have to write “ESM.wall.switch ON” on an input file to valid an ESM wall, which is not written in a official manual. We show the time evolution of position of the topmost H

atoms along the z-direction in figure 1. Without the keyword, the topmost atoms expand gradually as is shown by a solid line. On the other hand, with the keyword, the wall is worked appropriately. A broken line in figure 1 suggests that the topmost position is converged to 26.2 Å after about 300 fs. We also find that wall position is not worked appropriately because actual wall position is relative to the grid origin that is set automatically in the program. All of them have already been reported to developers.

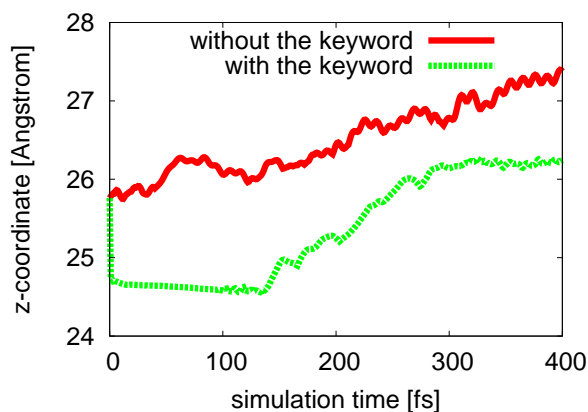


Figure 1: Time evolution of the topmost position of H atoms in PVdF. Solid and broken lines represent the results without and with the keyword “ESM.wall.position ON”, respectively.

References

- [1] <http://www.openmx-square.org>

Itinerant electronic states at rare-earth-magnet interfaces

Yoshihiro GOHDA*

*Department of Physics, The University of Tokyo
Hongo 7-3-1, Bunkyo-ku, Tokyo 113-0033, Japan*

Electrons in rare-earth magnets can be classified as two types: itinerant electrons and localized ones. Fe $3d$ as well as Nd $5d$ electrons are examples of the former, while Nd $4f$ electrons are the latter. In particular, itinerant magnetic states dominate interactions among magnetic sites directly. Thus, itinerant d states are expected to be sensitive to lattice strain, although the current status of the understanding on this issue is being far from complete, in particular for the magnetic anisotropy [1]. In this project, we have investigated strain effects on magnetic properties on the basis of density functional theory. We focused on $\text{Y}_2\text{Fe}_{14}\text{B}$ as shown in Fig. 1 (a), because Y is a prototypical rare earth element without having f electrons. First-principles calculations are performed using the OpenMX code [2], where pseudo-atomic orbitals and norm-conserving pseudopotentials are used.

We changed the lattice constants a and c from the equilibrium values in various manner. We found that the uniform compression enhances the perpendicular magnetic anisotropy. To clarify the origin of this enhancement, we developed a new method to decompose the magnetic-anisotropy energy into contribution from each atomic site as well as from couplings among specific atomic orbitals. This method employs second-order perturbation theory and an on-site approximation for the spin-orbit coupling: the exact form of the scalar triple product of the electric field, the electronic momentum, and the spin direction is approximated as the form of $\xi \mathbf{l} \cdot \mathbf{s}$ neglecting any

off-site interactions. The coupling constant ξ is fixed to the atomic value [3]. The spatial parts of non-perturbed states are Kohn-Sham states obtained by calculations without spin-orbit coupling, whereas the spin part is rotated with the collinearity. As a result, we clarified that the Fe j_2 site plays a significant role in enhancing the magnetic anisotropy. Furthermore, couplings among $3d_{x^2-y^2}$ and $3d_{xy}$ components at this site contribute dominantly, where both the effect of the local density of states shown in Fig. 1 (b) and the matrix elements among atomic orbitals are essential. Our method enables us to study the interface anisotropy quantitatively.

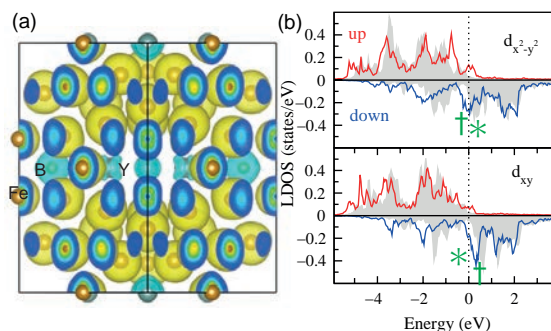


Figure 1: (a) Crystal structure and spin-density distribution of $\text{Y}_2\text{Fe}_{14}\text{B}$. (b) Local density of states (LDOS) projected onto $3d_{x^2-y^2}$ and $3d_{xy}$ components of the Fe j_2 site. The LDOS of the unstrained $\text{Y}_2\text{Fe}_{14}\text{B}$ are depicted by shades, whereas the strained ones are drawn by solid lines. Pairs of † and * indicates anisotropy coupling, respectively.

*Present address: Department of Materials Science and Engineering, Tokyo Institute of Technology, J1-3, Nagatsuta-cho 4259, Midori-ku, Yokohama 226-8502, Japan

- [1] S. Hirosawa *et al.*, J. Appl. Phys. **59**, 873 (1986).
- [2] T. Ozaki, Phys. Rev. B. **67**, 155108 (2003).
- [3] Y. Yanase and H. Harima, Solid State Phys. (in Japanese) **46**, 229 (2011).
- [4] Z. Torbatian, Y. Gohda, T. Ozaki, and S. Tsuneyuki, in preparation.

Expansion of the first principle electronic structure calculation with hybrid method

Takeo FUJIWARA

*Center for Research and Development of Higher Education, University of Tokyo
Hongo, Bunkyo-ku, Tokyo 113-0033*

The aim of our project is the development of a method applicable to the large-scale molecular dynamics (MD) simulation and investigation of slow dynamics of new materials, such as solid state fast ion conductors.

(I) Automatic parametrization for tight-binding molecular dynamics simulation method: We propose the transferable tight-binding parametrization procedure,[1] based on the extended Hückel approximation and the charge self consistent scheme, and applied to the quantum molecular dynamics simulation for long-time dynamics of large-scale systems of liquid and solid fast ion conductors.

We have also developed the algorithm and coding program package for automatic determination of parameters of tight-binding method. This program will be open.

(II) Dynamical behavior of lithium ions in thio-Lisicon: Microscopic origin of the high conductivity at room temperatures in lithium superionic conductors has remained the fundamental un-solved problem, though the recent discovery of $\text{Li}_{10}\text{GeP}_2\text{S}_{12}$ took a great step toward the application of solid electrolytes.[1, 2, 3, 4, 5] We achieve long-time (2ns) tight-binding molecular dynamics simulations of $\text{Li}_{4-x}\text{Ge}_{1-x}\text{P}_x\text{S}_4$, and observe the diffusion process where lithium atoms collectively hop into neighboring lithium sites by kicking the lithium atoms occupying these sites out. Furthermore, it is found out that excess lithium atoms or doped lithium vacancies trigger a new diffusion process and drastically reduce the activation energy. We discuss the dynamic properties of lithium atoms in these materials, such as the diffusion constant, the activation energy and the diffusion path.

References

- [1] S.Nishino and T.Fujiwara: "Parametrization scheme with accuracy and transferability for tight-binding electronic structure calculations with extended Hückel approximation and molecular dynamics simulations", *J. Molecular Modelling*. **19** (2013) 2363-2373 .
- [2] T. Fujiwara, S. Yamamoto, S. Nishino and H. Yamasaki, "Electronic structures and characteristics of Li ionic positions in thio-LISICON by the first principles calculation", The 19th International Conference on Solid State Ionics, Kyoto, Japan, June 2 - 7, 2013.
- [3] S. Nishino, T. Fujiwara, H. Yamasaki and S. Yamamoto, "Long Time Tight-Binding Molecular Dynamics Simulations of Li_4GeS_4 ", The 19th International Conference on Solid State Ionics, Kyoto, Japan, June 2 - 7, 2013.
- [4] T. Fujiwara, S. Nishino H. Yamasaki, and S. Yamamoto, "Electronic structures and Li ion dynamics in thio-LISICON, Li_4GeS_4 and Li_3PS_4 ", International Symposium on Electronic-Structure Theories and Related Experiments, Stuttgart, Germany, 12-15 June 2013.
- [5] S. Nishino, T. Fujiwara, S. Yamamoto, and H. Yamasaki, "Lithium Ion Dynamics in Li_4GeS_4 and Li_3PS_4 ", The 8th Pacific Rim International Congress on Advanced Materials and Processing, August, 2013, Hawaii, USA
- [6] 西野信也, 藤原毅夫, 山崎久嗣, "固体電解質 $\text{Li}_{4-x}\text{Ge}_{1-x}\text{P}_x\text{S}_4$ におけるリチウム拡散機構", 日本物理学会, 2014年3月27日-30日、東海大学

Development of ab initio GW code

Kazuma Nakamura

Quantum Physics Section, Kyushu Institute of Technology,

1-1 Sensui-cho, Tobata, Kitakyushu, Fukuoka, 804-8550

Using ab initio GW calculations, we study plasmaron states of various materials. The plasmaron state is defined as a coupled state of free electron and plasmon. This state can be observed as the ground state in a system which has “isolated low-energy bands” near the Fermi level. Electrons in materials interact via a long-ranged Coulomb interaction with each other, which can generate collective charge excitation, i.e., plasmon excitation. In general, the energy scale of the plasmon excitation is the order of 10 eV and therefore it is believed that such excitations are irrelevant to the low-energy physics of the order of 0.1-1 eV. However, in the isolated-band materials, low-energy bands around the Fermi level tend to isolate from other high-energy bands and, as a result, the Fermi velocity, or equivalently plasma frequency, is dominated by the bandwidth and occupancy of the isolated low-energy bands. Their bandwidth is ~ 1 eV and the plasma frequency is usually smaller than this value. In this case, this plasmon excitation can renormalize the bare band structure via the self-energy effect and generate a coupled state of free electron and plasmon.

In this report, we present a study for the low-energy plasmaron state of two compounds with

the isolated low-energy band structure: One is an organic compound $(\text{TMTSF})_2\text{PF}_6$ [1], and the other is the transition metal oxide SrVO_3 . Both materials are known as a strongly correlated system and effects of onsite Coulomb repulsion on the electronic structure has actively been discussed. On the other hand, for these materials, the low-energy plasmon excitation are experimentally observed in electron energy loss spectroscopy (0.4-1.0 eV for $(\text{TMTSF})_2\text{PF}_6$ and 1.4 eV for SrVO_3). The bandwidth estimated by density-functional calculations are 1.2 eV for $(\text{TMTSF})_2\text{PF}_6$ and 2.7 eV for SrVO_3 , and thus, the plasmon-excitation energy are smaller than the bandwidth. So, it is interesting to calculate the self-energy effect due to the plasmon excitation with the GW approximation calculations from first principles. To this end, we have developed a GW code based on the plane wave basis set with the pseudopotential approximation, and calculated the spectral function to see the formation of the plasmaron state. The code is massively parallelized, capable to treat huge systems such as organic compounds. All Calculations were done at Supercomputer center at Institute for Solid State Physics, University of Tokyo.

Figure 1 is our calculated reflectance as a function of frequency of $(\text{TMTSF})_2\text{PF}_6$ ((a)) and SrVO_3 ((b)). The drop from 1 to 0 specifies the plasma frequency. For $(\text{TMTSF})_2\text{PF}_6$, the values are 1.0 eV for the $E//x$ polarization right (red) and 0.4 eV for the $E \perp x$ one (green). For SrVO_3 , the value is 1.4 eV. We found that our spectra well reproduce the experimental ones.

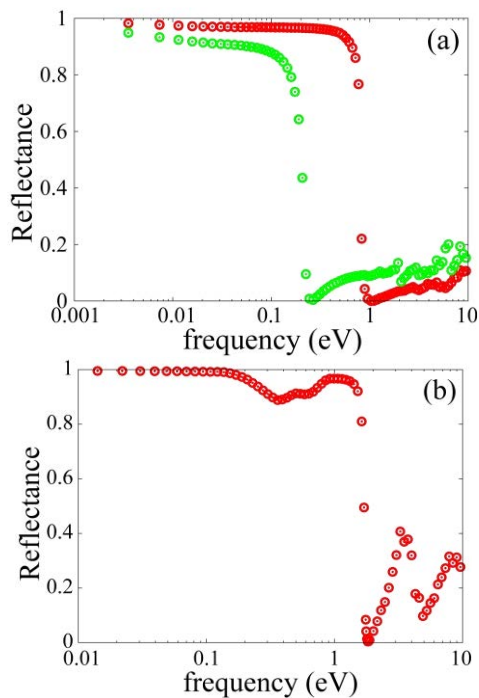


Fig.1 Calculated reflectance of $(\text{TMTSF})_2\text{PF}_6$ (a) and SrVO_3 (b). In (a), red and green describe results for the $E//x$ and $E \perp x$ polarization rights, respectively.

Figure 2 is the GW spectral function of $(\text{TMTSF})_2\text{PF}_6$ ((a)) and SrVO_3 ((b)). The density-functional band and the Fermi level are drawn by red and yellow solid lines, respectively. The bright regions below the

occupied bands and upper the unoccupied ones indicate the formation of the plasmaron states.

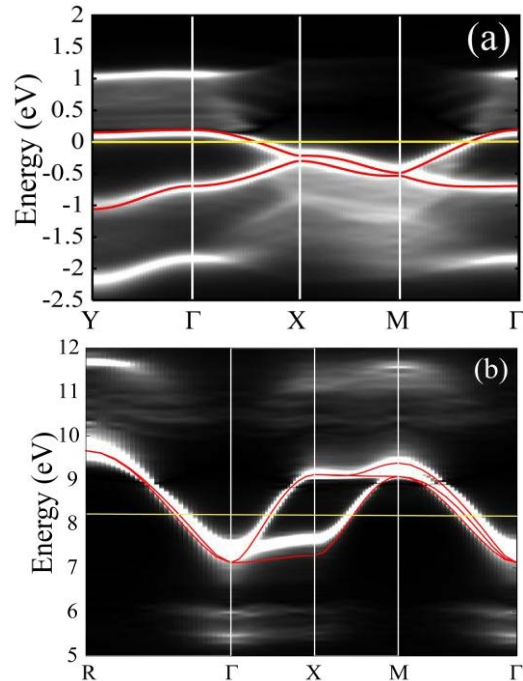


Fig.2 Calculated GW spectral function of $(\text{TMTSF})_2\text{PF}_6$ (a) and SrVO_3 (b). Red curves is the density-functional results.

In summary, we find low-energy plasmon excitations comparing to the energy scale of the bandwidth for the “isolated-low-energy-band” materials, reproducing experimental reflectance. By calculating GW self energy and spectral function, we find that this low-energy plasmon excitation leads to the formation of the plasmaron states.

[1] K. Nakamura, S. Sakai, R. Arita, and K. Kuroki, Phys. Rev. B 88, 125128 (2013)

Study on physicochemical properties for proton conductivity in lanthanum tungstate

Yohei Shono, Junichiro Otomo

*Department of Environment Systems, Graduate School of Frontier Science,
The University of Tokyo, Kashiwa-no-ha, Kashiwa, Chiba 277-8581*

Fuel cells have been taught to be a promising alternative power source these days. As commercial products, polymer electrolyte fuel cells (PEFC) and solid oxide fuel cells (SOFC) have been developed in past years, however, both of the fuel cells still have some serious problems in terms of material durability and power generation efficiency. In this sense, intermediate temperature fuel cells (ITFC) with proton conducting solid electrolyte have been proposed, which is expected to have high material durability and power generation efficiency. Nevertheless, there is no promising proton conducting solid electrolyte for ITFC, which should be developed further.

In the previous studies^[1-3], there have been some reports about Lanthanum tungstate (LWO) as a promising candidate for proton conducting solid electrolyte for p-ITFC. LWO was reported to have intrinsic oxygen vacancies in its crystal structure, resulting high proton conductivity. Although these reports on crystal structure in LWO, there have been no report on proton conducting mechanism in LWO crystal structure.

In this study, we investigate the proton conducting mechanism in LWO using density functional theory (DFT) and nudged elastic band (NEB) method. DFT calculations were carried out with the SIESTA code^[4]. The double- ζ split-valence basis set with polarization orbitals (DZP) was used in the calculations. The generalized gradient approximation (GGA) using the RPBE functional^[5] was used as the exchange correlation function, and k-points were sampled with $2 \times 2 \times 2$ grids using the Monkhorst–Pack method^[6].

Crystal structures were optimized until the maximum atomic forces became smaller than 0.04 eV/\AA . We also calculated the proton-conducting barriers in LWO with the NEB method^[7] using the revised SIESTA code developed by Ohto et al^[8]. Crystal structures were visualized with VESTA software^[9]. All calculations in this study were carried out in System B in the super computer center of Institute for Solid State Physics, using 32 to 64 MPI parallel calculations.

Before study on the proton diffusion mechanism in LWO, the crystal structures of LWO70 ($\text{La}_{28}\text{W}_4\text{O}_{56}$) and LWO54 ($\text{La}_{27}\text{W}_5\text{O}_{56}$) were optimized with the conjugated gradient method. The results indicated that the crystal structure of LWO54 is more stable than that of LWO70. This result is consistent with the reported experimental results; LWO can be synthesized only when the La/W ratio is lower than 5.7^[1].

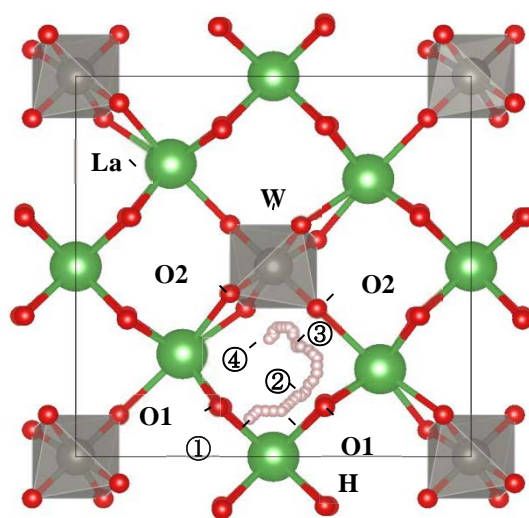


Figure 1. Projected crystal structure of LWO70 with proton diffusion paths calculated in this study.

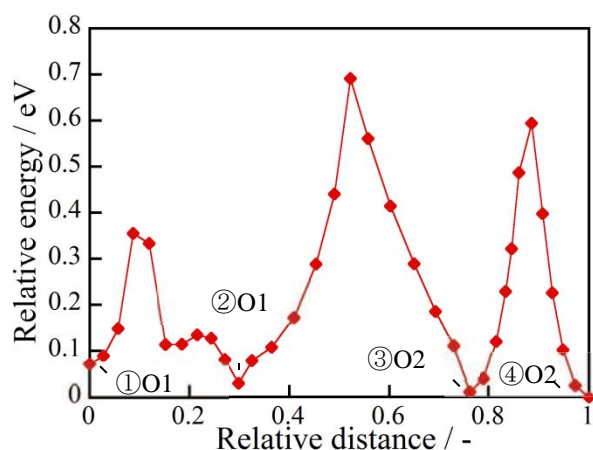


Figure 2. The results of NEB calculation for proton diffusion in LWO70.

To investigate the proton diffusion barrier in LWO, we employed the NEB method and in the LWO70 crystal structure as shown in Figure 1. Because of the locally distorted crystal structure of LWO, there are many possible proton diffusion paths in LWO70. To simplify the calculations, we employed oxygen at the O2 site with average O1–O2 and O2–O2 distances (see Figure 1). Figure 2 shows the results of the NEB calculations. The calculated relative energy was plotted as a function of the relative distance. As shown in Figure 2, the barrier of proton diffusion in the O1–

O1 jump is the lowest among the considered paths. This result means that, in the LWO70 crystal structure, long-range proton conduction most likely to occur as O1–O1 jumps, rather than O1–O2 and O2–O2 jumps. Thus, protons in LWO diffuse over a long range through cycles of O1–O1 jumps until becoming trapped in other O2 sites.

The results from the DFT calculations in this study explain the reported experimental observations well. To improve the proton conductivity in LWO, the proton concentration should be increased without disturbing the proton-conducting paths around the O1 sites next to La atoms.

References

- [1] A. Magrasó et al.: *Dalton Trans.*, **46**, (2009) 10273-10283.
- [2] A. Magrasó et al.: *J. Mater. Chem.*, **22(5)**, (2012) 1762-1764.
- [3] A. Magrasó et al.: *J. Mater. Chem. A*, **1**, (2013) 3774-3782.
- [4] J. M. Soler et al.: *J. Phys.: Condens. Matter.*, **14**, (2002) 2745-2779.
- [5] Y. Zhang, W. Yang: *Phys. Rev. Lett.*, **80(4)**, (1998) 890.
- [6] H. J. Monkhorst and J. D. Pack: *Phys. Rev. B*, **13**, (1976) 5188-5192.
- [7] G. Henkelman et al.: *J. Chem. Phys.*, **113 (22)**, (2000) 9901-9904.
- [8] T. Ohto et al.: *Phys. Rev. B*, **87**, (2013) 205139.
- [9] K. Momma, F. Izumi: *J. Appl. Crystallogr.*, **44**, (2011) 1272-1276.

Synthesis of proton conducting electrolyte and evaluation of ion conductivity of interfaces

Aki Iwanaga, Junichiro Otomo

Department of Environment Systems, Graduate School of Frontier Sciences, The University of Tokyo, 5-1-5 Kashiwanoha, Kashiwa, Chiba 277-8563, Japan

Proton conducting intermediate temperature fuel cells with proton-conducting solid electrolyte (p-ITFC) have been proposed, which is expected to have high material durability and power generation efficiency. In order to utilize it, it is needed to improve its efficiency. For this mission one of the bottleneck is proton conductivity of electrolyte. To improve proton conductivity, I focused on hetero interface between other kinds of electrolytes. There are some reports that oxide ion conductivity was promoted in hetero interface, so in this study I try to check if promotion of proton conductivity in hetero interface occur or not.

As electrolyte SrZrO₃ and SrTiO₃ was chosen. To think what happens in hetero structure, there are some phenomenon that affect to proton conductivity. One is segregation of dopant. It was proved by a experiment^[1] that dopants segregate in hetero structure. In this study energy level and proton diffusion in SZO was investigated using density functional theory (DFT) and nudged elastic band (NEB) method. DFT calculations were carried out with the SIESTA code^[2]. The double- ζ split-valence basis set with polarization orbitals (DZP) was used in the calculations. The generalized gradient approximation (GGA) using the RPBE functional^[3] was used as the exchange correlation function, and k-points were sampled with 2 \times 2 \times 2 grids using the Monkhorst–Pack method^[4].

First, energy level of system in which dopants are segregated and non-segregated were compared. Then proton diffusion barrier was calculated in both system using nudged elastic band method.

Because two electrolytes are also n-type and p-type

semiconductor, there is a p-n junction in hetero interface. If the electric field affects level of the system was studied.

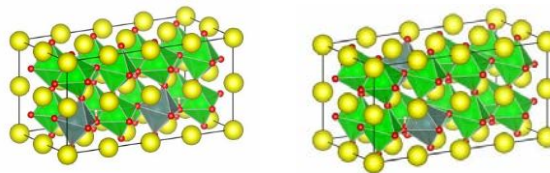


Fig1. 12.5%Ydope SrZrO₃; (left) dopant is segregated; (right) Y is not segregated energy

sample	DFT total energy (eV)	Potential (eV)	Binding (eV)	Binding/cell (eV)
Non-segregated	-13985.3	-12767.3	-1218.0	-152.2508
segregated	-27970.6	-25534.6	-2436.0	-152.2503

Table 1. energy level of 12.5% Y dope SrZrO₃

The picture of the system and their energy level were showed in Fig.1 and Table1. In segregated and non-segregated system, energy levels were almost same. Electric field also did not affect to energy level.

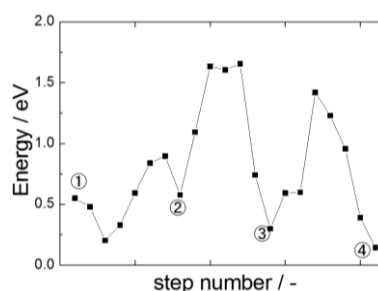
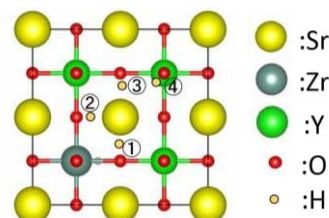


Fig2. Proton diffusion barrier

Proton diffusion barrier is shown in Fig.2. Proton diffusion barrier around dopant is low comparing with other area depart from dopant. From this result, segregated dopant

may have good effect to proton conductivity.

In order to find the reason why ionic conductivity is promoted around hetero interface, further study is needed.

Other reasons for promotion of proton conductivity are distortion of lattice structure caused by lattice mismatch, and generation of new diffusion pathway. These possibilities are needed to be checked.

Reference

- [1] P.F. Yan et al.:Solid State Ionics 31-37 (2012) 222-223
- [2] J. M. Soler et al.: J. Phys.: Condens. Matter., 14, (2002) 2745-2779.
- [3] Y. Zhang, W. Yang: Phys. Rev. Lett., 80(4), (1998) 890.
- [4] H. J. Monkhorst and J. D. Pack: Phys. Rev. B, 13, (1976) 5188-5192.
- [7] G. Henkelman et al.: J. Chem. Phys., 113 (22), (2000) 9901-9904.

First-principles study for adsorbed metallic atoms on quasicrystal surface

Kazuki NOZAWA

*Department of Physics, Chuo University
Kasuga, Bunkyo-ku, Tokyo, 112-8551*

Quasicrystals (QCs) are long-range ordered materials with rotational symmetries incompatible with the translational symmetry operation. More than 100 binary or ternary metallic QC systems have been found so far, but there is no report about the single-element QC. Recently, it was reported that Pb atoms deposited on a five-fold surface of a ternary QC Ag-In-Yb show different quasiperiodic arrangement depending on deposition time, implying a possibility of forming a multi-layered quasiperiodic film.

We carried out first-principles density functional calculations to determine the adsorption structure of Pb atoms on the Ag-In-Yb QC surface. To handle the aperiodic surface within the first-principles calculation, we used a slab model composed of a disc-shaped cluster with 30Å diameter and 4Å thickness as a model of the five fold surface of the Ag-In-Yb QC. The topmost layer is chosen to intersect the center of the rhombic triacontahedral cluster, which is a structural building unit of this QC, and the atomic positions are extracted from a X-ray diffraction data of isostructural Cd-Yb QC. In order to avoid decreasing accuracy of calculation at the cluster edge, we evaluated adsorption energy as the difference of cohesive energies between adsorbed- and non-adsorbed-systems calculated using a cluster, which is centered at each calculated site. Interactions between ionic cores are approximated using the projector-augmented wave potentials, and the GGA-PBE functional was

employed for the exchange-correlation term. A 40Å×40Å×18Å tetragonal super-cell is used to isolate each cluster by sufficient vacuum layer and the gamma point is used for Brillouin-zone sampling. The MPI parallelization method is used to speed up the calculation.

Calculation reveals that experimentally observed quasiperiodic patterns are made from Pb atoms adsorbed at different height from the surface. Additional layers, which were not observed in STM experiments but confirmed by XPS experiment afterward, are found and it was demonstrated that those layers play important role for stabilization of the layered structure. Furthermore, it was determined that the adsorbed Pb atoms occupy the atomic sites of the Ag-In-Yb QC used as a template, meaning Pb atoms are stacking with imitating the crystal structure of the template. Because there are some unoccupied atomic sites, the adsorption height of Pb atoms does not correspond exactly to the atomic sites of QC, but the lateral position is completely agree with the atomic sites of QC. The obtained structure does not have sufficient thickness yet, but this is the first instance of crystal growth of a single element quasicrystal [1].

References

- [1] H. R. Sharma, K. Nozawa, J. A. Smerdon, P. J. Nugent, I. McLeod, V. R. Dhanak, M. Shimoda, Y. Ishii, A. P. Tsai, R. McGrath, *Nat. Commun.*, **4**, (2013) 2715.

Local structure of organo-complexes adsorbed on metallic surfaces

Ken-ichi SHUDO

*Faculty of Science/Engineering, Yokohama National University
Tokiwadai 79-5, Hodogaya-ku Yokohama 240-8501 JAPAN*

Our group observed real-time molecular vibration adsorbed on metal surface using ultrafast pulse lasers. [1] The very high optical sensitivity even at the monolayer film is ascribed to surface enhancement of Raman scattering (SERS) [2] if the substrate surfaces are inhomogeneous [3]. Fourier spectra of pyridine adsorbed on Ag nanoclusters (estimated diameter is 50 nm), peaks shifted due to the adsorption and lifetime of the vibronic decay changes according to the colloidal density.

For the cluster models (Fig. 1), we estimated the peak shifts with diagonalization of potential matrices obtained by means of first principles calculation. The eigenfrequencies, corresponding to the experimentally stringest optical peak, shift to the lower energy on the flat surface, while at the vortex site this shifts to the higher energy. This accounts for the observed result that the peak splits into two components.

In the case of 15-carboxyl-1-pentadecanetriol adsorbed to the Ag nanoclusters, transient peak shifts in the time-windowed spectra are suggested to be corresponding to the femtosecond-scale vibronic propagation from

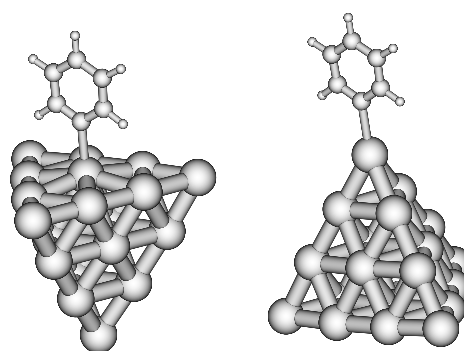


Fig. 1 Cluster model of pyridine adsorbed on a flat surface (left) and at the vortex-atom (right).

Ag to carbon chain, in comparison with the calculated eigenfrequencies.

References

- [1] K. Shudo, I. Katayama, S. Ohno (eds): "Frontiers in Optical Methods: Nano-Characterization and Coherent Control" (2013, Springer-Verlag GmbH, Berlin/ Heidelberg) ISBN 978-3-642-40593-8
- [2] J. Takeda, K. Ikufumi, K. Shudo, M. Kitajima: *Journal of Luminescence*, *in press* (2014).
- [3] M. Shindo, T. Sawada, K. Doi, K. Mukai and K. Shudo: *J. Phys.: Conf. Ser.* **441**, 012044 pp.6 (2013).

First Principles Based Analysis of Electronic Structures and Reactions on Surfaces/Interfaces

Yuji KUNISADA

*Center for Advanced Research of Energy and Materials, Faculty of Engineering,
Hokkaido University, Sapporo, Hokkaido 060-8628*

We investigated the electronic structures and reactions on surfaces/interfaces, with the aid of the first principles calculation based on the density functional theory (DFT). In addition, we developed the quantum state calculation code for atomic nuclei to consider the quantum mechanics behaviors of the hydrogen isotopes (H, D, T, muonium).

At first, we investigated the electronic structures of Pd/ZnO interfaces, which is considered as prospective materials for electronic devices. [1] The full-potential linearized augmented plane wave (FLAPW) calculation based on DFT was carried out through WIEN 2k [2] on F16 queue in system B. We installed parallelized WIEN 2K with Intel® MPI Library and Intel® Math Kernel Library. We calculated the O-K edge electron energy-loss spectra at Pd/ZnO interfaces with the corresponding supercell, which consists of 108 atoms. We found that the sharp peak, which corresponds to the bonding orbitals formed by the overlapping of Pd 4d and O 2p orbitals, appears in the vicinity of 530 eV energy loss. This result shows the good agreement with our experimental O-K edge electron energy-loss

spectra. Thus, we could determine electronic structures of Pd/ZnO interfaces from the results from first principles calculation and electron energy-loss spectroscopy (EELS) experiment.

We also investigated the hydrogen isotope adsorption states on fcc Fe(111) surfaces to understand the hydrogen embrittlement mechanism of iron-based steels. We adopted the slab model with 2x2 fcc Fe(111) five atomic layers. We obtained the potential energy surfaces (PES) of H/fcc Fe(111) systems through the repeated ab initio total-energy calculations with various adsorption configurations. We performed the repeated ab initio total-energy calculations with Vienna Ab initio Simulation Package (VASP) [3-6] on P1, F4, F8 and F16 queue in system B. We installed parallelized VASP with Intel® MPI Library and Intel® Math Kernel Library. We consumed most of our budget to obtain the PES, because we have to calculate more than 10,000 ab initio total-energy calculations with various parameters. When we calculated the corresponding PES, we set 12x12 grids for in-plane direction and 26 grids for the direction perpendicular to the surface. We also performed

the quantum state calculations for the hydrogen isotopes to consider the quantum mechanics behaviors of hydrogen isotopes due to their small mass. We adopted the Gaussian basis for the wave function of hydrogen isotopes. [7] In order to obtain the three-dimensional quantum states of hydrogen isotopes on fcc Fe(111) surfaces, we solved the Schrödinger equation for atomic nuclei based on the corresponding PES results. The corresponding eigenstates and eigenenergies includes the influence of non-locality and zero-point energies. The diagonalization of up to 40500x40500 matrix was performed on P1 and F4 queue in system B to obtain the hydrogen isotope adsorption states on 2x2 fcc Fe(111) surfaces. In order to fasten our original code with the large scale diagonalization, we applied appropriate optimization and parallelization with Intel® MPI Library and Intel® Math Kernel Library. From these calculations, we found H and muonium show the delocalized adsorption

states on the fcc Fe(111) surfaces.

References

- [1] N. Sakaguchi, K. Watanabe, and Y. Kunisada: *Kenbikyo* **48** (2013) 195.
- [2] P. Blaha, K. Schwarz, G. Madsen, D. Kvasnicka, and J. Luitz, WIEN 2k, Augmented Plane Wave + Local Orbitals Program for Calculating Crystal Properties, Vienna, Austria, 2001.
- [3] G. Kresse and J. Hafner: *Phys. Rev. B* **47** (1993) 558.
- [4] G. Kresse and J. Hafner: *Phys. Rev. B* **49** (1994) 14251.
- [5] G. Kresse and J. Furthmüller: *Comput. Mat. Sci.* **6** (1996) 15.
- [6] G. Kresse and J. Furthmüller: *Phys. Rev. B* **54** (1996) 11169.
- [7] N. Ozawa, T. Roman, H. Nakanishi, W. A. Diño, and H. Kasai: *Phys. Rev. B* **75** (2007) 115421.

Dissociation mechanism of multiple-charged molecules irradiated by X-FEL: first-principles molecular-dynamics simulation

Satoshi Ohmura

Department of physics, Kyoto University, Sakyo-ku, Kyoto, 606-8502

With the advent of X-ray free electron laser (X-FEL), many interesting phenomena in which molecules are highly charged due to strong laser fields were observed. The highly charged molecules are quite unstable because of the Coulomb repulsive force and destroyed on a subpicosecond (Coulomb explosion). Recently, dissociation of several highly-charged aromatic molecules has been investigated by position-sensitive time-of-flight measurements. These studies suggest that the momenta of the fragment ions after the explosion reflects the structure of the parent molecules even for the dissociation channels for which the dissociations are not described by the simple Coulomb explosion model. For the application of Coulomb explosion such as Coulomb explosion imaging, it is highly desirable to clarify the charge state dependence of dissociation mechanism in coulomb explosion.

In this study, we performed *ab initio* molecular dynamics simulation to clarify the details of coulomb explosion mechanism of aromatic molecules. We took particular note of the charge-state dependence of the explosion mechanism.

The target system is the 4-bromophenol, in which a bromine atom and a hydroxyl group are located on the opposite sides of the carbon ring. To calculate charged molecular system in reciprocal space, we used cluster boundary conditions imposed with the method of Martyna and Tuckerman [1].

From our simulation, it is found that the dissociation mechanism has charge-state dependence. When the charge state is 6 or 7, one or two hydrogen atoms dissociate in the first stage (at times shorter than 20 fs after the molecule takes charges) while all hydrogen atoms dissociate when the charge state is over 7. After the hydrogen dissociation, the carbon ring breaks up. The mechanism of the carbon-ring breaking also has charge-state dependence. When the charge state is 6 or 7, the ring breaks with molecular expanding. On the other hand, molecule shrinks during the ring breaking when the charge state is over 7.

References

- [1] G. J. Martyna, *et al.*, *J. Chem Phys* **110** (1999) 2810
- [2] S. Ohmura *et al.*, *J. Phys.: Conf. Ser.* *accepted*

Large scale *ab initio* calculations on the fundamental processes of energy convergence devices and on their optimization for high conversion efficiency

Koichi Yamashita

Department of Chemical System Engineering,

The University of Tokyo, Hongo, Bunkyo-ku, Tokyo 113-8656

1. *ab initio* study of fast Na diffusion in Na₃P

Considering the limited resource of lithium, Na ion batteries are the attractive alternative due to the abundant resource of Na. So far the amorphous red P and carbon nanocomposite has been shown to be a very promising anode material for Na ion battery. Ionic conductivity and electronic conductivity are the critical factors that determine the speed of charging and discharging process. In this study, *ab initio* calculation was used to study the ionic conductivity and electron property in the fully charged state of P (Na₃P). This study aims to theoretically estimate the electrochemical performance of P as anode in the discharge process.

The density functional theory (DFT) calculations were performed with VASP. The electron-ion and electron-electron interactions have been described by PAW potentials and the GGA exchange-correlation functional of PBE, respectively. The Nudged Elastic Band method was employed to find the saddle point and minimum energy paths for Na diffusion.

We found that three possible independent and asymmetric Na diffusion paths exist. In the first

two, Na diffusion occurs within the same kind of sodium atom; while in the third path, Na diffusion occurs within sodium atoms of different kind.

Moreover the activation energies of Na diffusion in the first two paths are much smaller than that of the third. Besides, with the introduction of Na vacancy, a hole state deep in the valence region appears which is responsible for the valence band-edge raising in the center of the Brillouin zone.

This sodium vacancy is very likely to play a role in the electron transfer in Na₃P. The fast ionic conductivity and considerable electronic conductivity make P a promising anode material in the first step of Na de-intercalation process.

2. The role of methylammonium cation in the organic-inorganic lead iodide

Several papers have been recently appeared in literature reporting the enhanced photoconversion efficiency (PCE) up to 15% for solar cells formed by sandwiches of perovskite compounds, i.e the light harvester, mesoporous TiO₂, and a polymeric hole conductor. The usage of these 3D MAPbX₃ (MA= methylammonium, CH₃NH₃⁺, X=halide, Cl-, Br-, I-) perovskites, is strictly dependent by

their chemical stability and optimal transport characteristics in the device. It is astonishing, anyway, that materials with so high applicability in PV and with many undisclosed features still find scarce attention among theoreticians. We here disclose and characterize such class of lead-iodide organic-inorganic mixed perovskites.

DFT calculations are performed with VASP and SIESTA. The electron-ion and electron-electron interactions have been described by projector augmented waves potentials and the GGA exchange-correlation functional of Perdew-Burke-Ernzerhof, for the former, Plane Wave based, approach. Atomic Orbitals are at variance used in the case of SIESTA, still through a pseudopotential approach.

We performed a theoretical estimation of effective masses of photocarriers in the pseudocubic $\text{CH}_3\text{NH}_3\text{PbI}_3$, both with and without taking into account spin-orbit coupling effects. Predicted values of photogenerated electrons and holes are comparable to those for silicon used in inorganic commercially available solar cells[1].

3. *ab initio* study on the electronic double layer of transition metal oxide and water interface

Interface structure of electrocatalysts and water plays important role on electrochemical reaction. Attempts to reveal interface structure and distribution of potentials have been made both theoretically and experimentally, however they are still challenges because of the complicated system of electrochemistry. Our research interest

lies in an interface structure of RuO_2 /water as an (photo)electrocatalysts for oxygen evolution reaction under given pH and electrode potential. The basic concept of the method used in this research is comparing Gibbs Free energies of many different interface structures including effects of pH and electrode potential to find the most stable one.

All the calculations were performed with GPAW Software with PAW setups. We used GGA/RPBE functional. RuO_2 /water interfaces are modeled by 4layer slab $\text{RuO}_2(110)$ and surface proton concentrations range from 2.0 to 0.0. In case of high coverage conditions, we classified the water structure by their orientations as up (proton is pointing out from the RuO_2 surface), parallel and down (proton is pointing to surface).

The results demonstrated that in the range of low potential region (~ 0.5 V), almost all surface oxygen atoms become water and in the region around 1.0 V, rapid de-protonation occurs. The difference between acid and base conditions is the water orientation in low potential region. These results are in good agreement with experimental ones. From our studies, it can be proposed that the mechanism of oxygen evolution reaction is different between electrochemical condition (around 1.5 V) and photoelectrochemical condition (expected at low potential region), and between acid and base conditions.

References

- [1] G. Giorgi, J.-I. Fujisawa, H. Segawa, K. Yamashita: J. of Phys. Chem. Lett. **4** (2013) 4213.

Theoretical analyses for thermal conductance of interfaces of the gold surfaces and self-assembled monolayers

Koichi Yamashita

*Department of Chemical System Engineering,
The University of Tokyo, Hongo, Bunkyo-ku, Tokyo 113-8656*

Self-assembled monolayers (SAMs) which have stable and well-order structures are expected as candidates of materials for nanoscale devices. Thermal properties of the interface have particularly attracted attention because they are related to various functions, such as thermal storages and thermal transistors. It is, therefore, required to elucidate the thermal properties of the SAM-metal structures.

This study aims to analyze the structural effects on the thermal properties at the interface of the SAMs sandwiched between gold substrates. For this purpose, we attempted to perform the thermal transport calculations for the SAM-gold-substrate-systems by using the non-equilibrium Green's function (NEGF) method. In particular, we focused on the effects of the anchor atoms sticking to the gold substrates.

In the last year, we investigated of stability of some structures of the SAM-gold-substrate-systems in which sulfur atoms were adopted as the anchor atoms like previous studies [1,2]. For the gold substrates, clean (1 1 1) surfaces were used (Fig. 1). Structural optimizations were performed by using SIESTA [3] with the local

density approximation.

As a result, we have revealed that the adsorption structure is not so stable. Namely, the sandwich structures can be easily collapsed

and stable carbon chains are not retained. This instability seems to result from that the van der Waals (VdW) interactions between the carbon chains were not considered explicitly. Therefore, we are planning to investigate VdW effects on the structural stability by using the latest unstable version of SIESTA which is able to consider the VdW interactions explicitly. Then, thermal properties should be investigated by the NEGF.

References

- [1] M. D. Losego, M. E. Grady, N. R. Sottos, D. G. Cahill, P. V. Braun: *Nat. Mater.* **11** (2012) 502.
- [2] T. Frederiksen, C. Munuera, C. Ocal, M. Brandbyge, M. Paulsson, D. Sanchez-Portal, A. Arnau: *ACS Nano* **3** (2009) 2073.
- [3] J. M. Soler, E. Artacho, J. D. Gale, A. García, J. Junquera, P. Ordejón, D. Sánchez-Portal: *J. Phys. Condens. Mater.* **14** (2002) 2745.

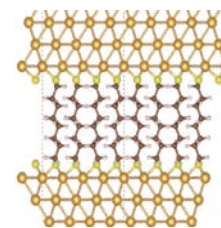


Fig. 1 A structure of the SAM-gold-substrate.

First-principles study on the defects in semiconductors

Jun YAMAUCHI

Faculty of Science and Technology, Keio University

3-14-1 Hiyoshi, Kohoku-ku, Yokohama-shi, Kanagawa 223-8522

As the size of devices on integrated circuits decreases, the behavior of dopant atoms make relatively larger effect on the device performance. Especially, it is very important to understand the unfavorable defects including the dopant atoms. The experimental observations on each defect is extremely difficult. One of the major difficulties for detecting dopant configurations is the very weak signals from the defects of very low concentration comparing to those from the matrix semiconductors. However, recently, as a solution for the above problem, it is suggested to use powerful synchrotron radiation facilities to measure the X-ray photoelectron spectroscopy (XPS) signals of defects. On the other hand, there have been few reliable first-principles core-level XPS calculations for impurity defects in semiconductors, because the local potential boundary condition of defect model systems has not yet been sufficiently evaluated. To obtain reliable shifts in the XPS binding energy, it is necessary to take a sufficiently large supercell for a defect.

We carried out a comprehensive study on the arsenic (As) 3d core-level XPS binding energies for As defects in crystalline Si using a first-principles calculation with careful evaluation of the local potential boundary condition for the model system, where convergence within 0.1 eV was confirmed for the supercell size. The code used in this study is xTAPP, which is a hybrid paralleled density functional theory calculation program with plane-wave basis[1]. Figure 1 shows the calculated As 3d core level

XPS binding energies for the As defects in silicon crystals. It is found that the experimentally observed spectra (~ 1.2 eV) is explained by the combination defects of substitutional As atoms and a vacancy[2].

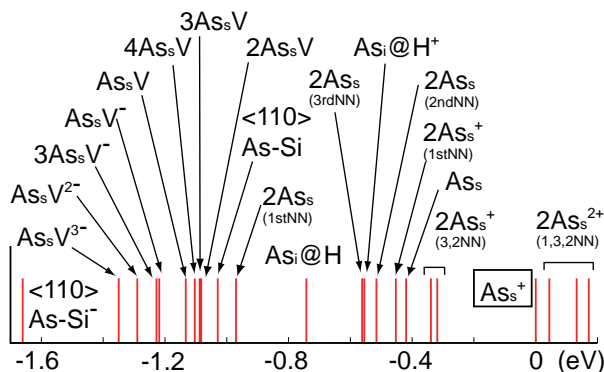


Figure 1: Calculated As 3d core level XPS binding energies for the defects in silicon crystals. The origin of the binding energy is that of the ionized substitutional As, which is surrounded by a square.

References

- [1] xTAPP (eXtended Tokyo Ab initio Program Package) (<http://frodo.wpi-aimr.tohoku.ac.jp>)
- [2] H. Kishi, M. Miyazawa, N. Matsushima, and J. Yamauchi: AIP Conf. Proc. **1583** (2014) 226.

Exploring low-dimensional honeycomb nano materials

Noriaki TAKAGI¹, Ryuichi ARAFUNE², Mao KANNO¹, and Emi MINAMITANI³

¹*Department of Advanced Materials Science, University of Tokyo
Kashiwa-no-ha, Kashiwa, Chiba 277-8561,*

²*International Center for Materials Nanoarchitectonics, National Institute for Materials,
Science, 1-1 Namiki, Ibaraki 304-0044,*

³*RIKEN, 2-1 Hirosawa, Saitama 351-0198, Japan.*

Since the discovery of exotic graphene, unraveling the hidden properties of honeycomb lattice materials is of great importance. Silicene, a two-dimensional honeycomb sheet of consisting of Si atoms, has attracted lots of attention. It is theoretically predicted that a freestanding silicene possesses Dirac fermion features [1] and that silicene is also topological insulator due to the sizable spin-orbit coupling [2].

We investigated the stability of silicene on Cu(111) covered with a hexagonal boron nitride (h-BN) layer by using density functional theory (DFT) calculations. The DFT calculations were carried out by the plane-wave-based Vienna Ab initio Simulation Package (VASP) [3, 4] with the projected augmented wave method [5]. The silicene on h-BN/Cu(111) was modeled by using a supercell which consists of a silicene layer lying on h-BN layer on top of a 5-layer Cu slab with a vacuum of 15 Å thick along the surface normal. The supercell are composed 35 Cu, 7 B, 7 N and 6 Si atoms. The positions of atoms in silicene, h-BN, and top four layers of Cu slab were optimized without any

constraint until the forces on individual atoms were less than 0.01 eV/Å. In order to weak interface couplings, van der Waals correction was included. From the total energy calculations for various configurations of silicene lattice relative to the h-BN lattice, we found that the silicene is stable, and that Dirac fermion feature survives similarly to the freestanding silicene. These results demonstrate that the h-BN/Cu(111) is a promising candidate for realizing Dirac fermion silicene.

Reference

- [1] S. Cahangirov et al.: Phys. Rev. Lett. **102**, 236804 (2009).
- [2] M. Ezawa, Phys. Rev. Lett. **109**, 055502 (2012).
- [3] G. Kresse and J. Furthmüller: Phys. Rev. B **56** (1996) 11169.
- [4] G. Kresse and J. Furthmüller: Comput. Mater. Sci. **6** (1996) 15.
- [5] P. E. Blöchl: Phys. Rev. B **24** (1994) 17953.

Spin state of organic molecules on solid surfaces

Noriaki TAKAGI¹, Ryouichi HIRAOKA¹ and Emi MINAMITANI²

¹*Department of Advanced Materials Science, University of Tokyo*

Kashiwa-no-ha, Kashiwa, Chiba 277-8561

²*RIKEN, 2-1 Hirosawa, Saitama 351-0198, Japan.*

Manipulating quantum state of matter is central issue in condensed matter physics and material science. Scanning tunneling microscopy (STM) junction where a single molecule connects with two electrodes, i.e., an STM tip and a substrate, is a model of single molecule quantum dot. By changing the tip-molecule distance to tune coupling strengths of the molecule with the two electrodes, the STM junction offers a possibility to manipulate the quantum state of the molecular dot.

We tried to manipulate the Kondo resonance states of iron(II) phthalocyanine (denoted as FePc) on Au(111) [1,2] experimentally by precisely controlling the tip-molecule distance. When the tip was far away from the FePc molecule on Au(111), a Fano-Kondo (F-K) antiresonance was observed. As the tip approached to the central Fe ion of the molecule, the F-K antiresonance gradually became symmetric and a pair of conductance steps appeared in the dI/dV spectrum

finally when the tip touched with the molecule. This spectral evolution was reversibly observed when the tip moved away from the molecule. These results indicate that the Hamiltonian of the molecular quantum dot is changed from Kondo-type to the zero field splitting type and vice versa by the perturbation of the tip.

In order to understand the reversible spectral evolution, we calculated the geometric structure, electronic structure and spin state of FePc in the STM junction by the plane-wave-based Vienna Ab initio Simulation Package (VASP) [3, 4] with the projected augmented wave method [5]. The STM junction was modeled by using a supercell. The STM tip was modeled by a 6-layer trigonal pyramid consisting of 56 Au atoms. The FePc molecule is located on a four-layer Au slab. To describe the Coulomb interaction at the Fe ion, we used local density approximation + U method. We calculated two limiting configurations. One is the configuration where the tip is

1.5-nm apart from the molecule such that the coupling of the tip with the molecule is negligible. The other is the configuration where the tip is contacted with the Fe ion in the molecule. When the tip is far away, the position of the Fe ion is slightly displaced into the substrate and the electronic charges are accumulated in between the molecule and Au substrate. In the contact configuration, the Fe ion moves to the tip and the electron charge accumulation is reduced at the molecule-substrate interface and instead appears at the tip-molecule contact region. In addition, the spin states of Fe ion for both configurations are not drastically changed. These calculated results partly explain the spectral evolution observed experimentally, and indicate that the position of the Fe ion is a key to understand the reversible switching of the Hamiltonian. 17953.

Reference

- [1] N. Tsukahara *et al.*: Phys. Rev. Lett. **106** (2011) 187401.
- [2] E. Minamitani *et al.*: Phys. Rev. Lett. **109**, 086602 (2012).
- [3] G. Kresse and J. Furthmüller: Phys. Rev. B **56** (1996) 11169.
- [4] G. Kresse and J. Furthmüller: Comput. Mater. Sci. **6** (1996) 15.
- [5] P. E. Blöchl: Phys. Rev. B **24** (1994)

First-Principles Study of Magnetic Materials and Magnetism

Takashi MIYAKE

Nanosystem Research Institute, AIST, Umezono, Tsukuba, Ibaraki 305-8568

Rare-earth magnet $\text{NdFe}_{11}\text{TiN}$ [1]

Performance of a hard magnet is characterized by magnetization and coercivity, and the latter has a strong correlation with the magnetocrystalline anisotropy (MCA) energy. Among rare-earth magnets, $R\text{Fe}_{12-x}M_x$ compounds are potentially strong hard magnets, because large magnetization will be achieved if x can be reduced. Although $R\text{Fe}_{12}$ does not exist, $R\text{Fe}_{12-x}\text{Ti}_x$ is thermodynamically stable for relatively small $x < 1$. Titanium substitution suppresses magnetization significantly. On the other hand, magnetization is enhanced and strong uniaxial anisotropy is induced by interstitial nitrogenation, which makes the compound strong hard magnet.

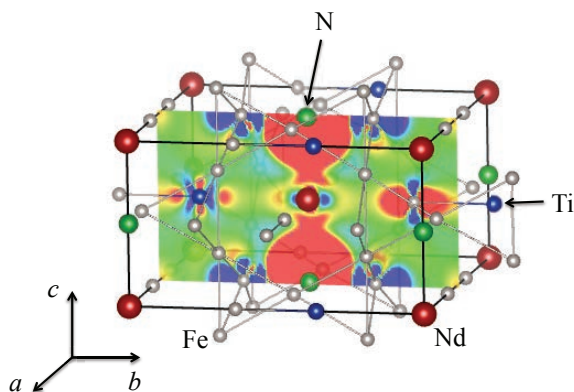


Figure 1: Charge density difference between $\text{NdFe}_{11}\text{Ti}$ and $\text{NdFe}_{11}\text{TiN}$.

We have investigated the effect of Ti substitution and interstitial nitrogenation on magnetic properties from microscopic viewpoint by means of the density functional theory in

the generalized gradient approximation using QMAS [2]. The Nd-f electrons are treated as open-core states. We found that by nitrogenation, electron density is increased in the c direction from Nd (Figure 1). The Nd-f electrons feel repulsive force and extend in the ab directions, leading to large crystal-electric field coefficient A_{20} . This is the cause of uniaxial magnetic anisotropy. We also found that virtual bound state appears above the Fermi level by titanium substitution. Substantial reduction of magnetization is explained by Friedel's sum rule.

Magnetocrystalline anisotropy from transition-metal sublattice [3]

It is widely believed that anisotropy of the orbital moments (OMs) induced by the spin-orbit interaction (SOI) around each atom are physical origin of the MCA. Bruno derived an approximate formula that relates the MCA energy and the OMs by assuming large exchange splitting. However, the MCA energies and OMs of real materials obtained by first-principles calculations are often inconsistent with Bruno's formula.

We have derived a second-order perturbation formula for the MCA. The energy correction by SOI can be split into the spin-conserving and the spin-flip contributions. We have applied the formula to $L1_0$ alloys. It is found that the formula reproduces qualitatively the behavior of their MCA energies as a function of the lattice constant. While the MCA of FePt, CoPt, and FePd mainly orig-

inates from the spin-conserving contribution, the spin- $\uparrow\downarrow$ term is major in MnAl and MnGa. In FePt, CoPt, and FePd, the variation of the MCA energy against the lattice constant can be explained from the variation of the spin- $\uparrow\downarrow$ contribution. These results indicate that not only the anisotropy of OMs but also the spin- $\uparrow\downarrow$ contributions must be taken into account for the understanding of the MCA of the L1₀ alloys.

References

- [1] Takashi Miyake, Kiyoyuki Terakura, Yosuke Harashima, Hiori Kino and Shoji Ishibashi: *J. Phys. Soc. Jpn.* **83** (2014) 043702.
- [2] <http://qmas.jp/>
- [3] Taichi Kosugi, Takashi Miyake, and Shoji Ishibashi: *J. Phys. Soc. Jpn.* **83** (2014) 044707.

Electronic Transport Simulation of Edge-Disordered Graphene Nanoribbons

Takahiro YAMAMOTO

Dept. of Electrical Engineering, Tokyo Univ. of Science Katsushika-ku, Tokyo 125-8585

Graphene is expected to be a channel material of field effect transistors (FETs) because of their high carrier mobility. However no band gap of the graphene is a serious problem for its FET application. One possible way to overcome the gap-opening problem is to process it in the form of a nanometer width ribbon. They have been successfully applied to FETs with high on-off ratio. A recent experiment reported that the resistance of GNRs increases exponentially with their length even at the room temperature [1]. This non-Ohmic behavior is due to the edge-roughness of GNRs. The effects of edge-roughness become more remarkable when the ribbon width becomes narrower in the future.

In this study, we have computationally investigated the coherent electronic transport in narrow edge-disordered armchair GNRs (ED-AGNRs) using the nonequilibrium Green's function method combined with a tight-binding model. We calculated the conductance with various edge-disorder configurations with changing the electron energy from -2eV to 2eV , the amount of edge carbon-pair vacancies from 4% to 30% and the ribbon-width from 0.74 nm

to 2.95 nm. We confirmed that the averaged conductance of ED-AGNRs decreased exponentially with their lengths, which is consistent with a previous experimental report [2]. We also examined (i) a relation between the localization length ξ and the edge-vacancy concentration, and (ii) the ribbon-width dependence of ξ . As is expected, ξ increases with decreasing the edge-vacancy concentration and with increasing the ribbon width.

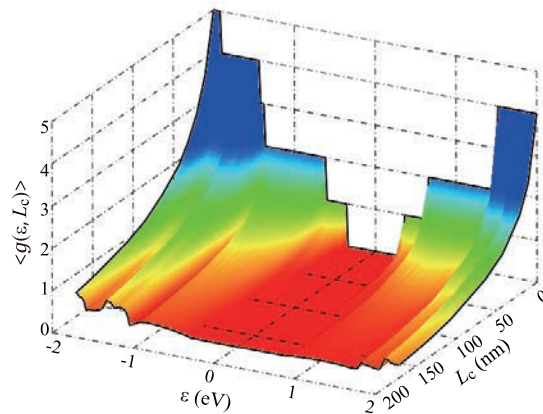


Fig. 1: The length and energy dependences of the averaged conductance of 1.48 nm-width ED-GNRs with 4% edge vacancies.

References

- [1] Xu et al., *Nano Lett.* **11** (2011) 1082.
- [2] K. Takashima and T. Yamamoto: *Appl. Phys. Lett.* **104** (2014) 093105.

Ab initio study of thermoelectric properties of molecules between magnetic electrodes

Tatsuhiko OHTO

Graduate School of Engineering Science,

Osaka University, 1-3 Machikaneyama, Toyonaka, Osaka 560-8531

The molecular junction is a promising system to achieve maximum thermoelectric efficiency due to the quantum confinement of the molecular orbital (MO) into the nanoscale gap [1]. The difference in the energy between the MO and the Fermi level of the electrode is called as the carrier injection barrier. As the Seebeck coefficient S of a molecular junction is related to the differential conductance, smaller carrier injection barrier is desirable. To achieve a small injection barrier, we propose to use molecular junctions with ferromagnetic electrodes as it can induce the spin polarization of MOs. The reduction of the injection barrier due to spin splitting of MOs should be larger than that induced by the change in work functions of metal electrodes. To test this hypothesis, we investigate the transport properties of Ni-benzenedithiol (BDT) -Ni molecular junction with the nonequilibrium Green's function method based on density functional theory. Result revealed that one of the spin split highest occupied MO of BDT appears just above the Fermi level, indicating an increase in the magnitude of S (compared to when Au electrode was used) and a change in

the sign as well. We obtained negative and large S for Ni-BDT-Ni junctions. We further investigated the effect of spin configuration of electrodes and surface roughness on S . The structural optimization performed with the SIESTA program [2] on System B was very helpful to advance our research.

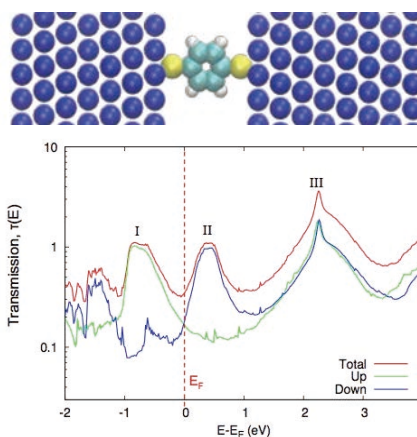


Fig. 1: Structure and transmission coefficient per spin of Ni-BDT-Ni junction.

References

- [1] H. Park, Nat. Mater. **6** (2007) 330
- [2] J. M. Soler: E. Artacho: J. D. Gale: A. Garcia: J. Junquera: P. Ordejon: D. Sanchez-Portal, J. Phys.: Condens. Matter **14** (2002) 2745

Development and Application of First-Principles Electron-Transport Simulators for Massively Parallel Computer

Yoshiyuki EGAMI

*Division of Applied Physics, Faculty of Engineering, Hokkaido University
Kita 13, Nishi 8, Kita-ku, Sapporo, Hokkaido 060-8628*

Electron-transport simulations are important to investigate and develop new electronic devices. Recently, to obtain more practical knowledge on electron-transport properties of nanoscale materials, large-scale transport simulations have attracted much interest. In this subject, we developed an efficient first-principles electron-transport simulator systems based on the Lippmann-Schwinger (LS) equation within the framework of the real-space finite-difference scheme[1].

In the conventional LS method, scattering wave functions are expressed in the Laue representation, where a 2-dimensional plane-wave expansion and a real-space discretization are combined. However, one may frequently encounter a numerical problem due to the appearance of evanescent waves exponentially growing and decaying. On the other hand, in our LS method based on the fully real-space algorithm (grid LS), the numerical collapse due to the evanescent waves and the computational costs can be restrained by using the ratio expression of the retarded Green's function obtained analytically or by incorporating the self-energy matrices and the recursive formulas of the ratio matrices[2]. Furthermore, the real-space algorithm is suitable for massively parallel computing.

In order to examine the performance of the grid LS method, the electron-transport simulations for the semiconductor/insulator membranes sandwiched between semi-infinite elec-

trodes are demonstrated on the Sysyem B and/or Systme C of the Supercomputer Center at the Institute for Solid State Physics. Here, the transport properties of electrons flowing across the (001)Si/SiO₂ and (001)Ge/GeO₂ membranes containing danglingbond (DB) defects around interfaces. In each model, one of the DBs is passivated by a hydrogen atom while the other remains with the Si (Ge) atom of the center back-bonded to two neighboring Si (Ge) atoms and an oxygen atom. As the result, the Si/SiO₂ model exhibits much larger currents, while the Ge/GeO₂ membrane avoid serious problems caused by the DB defects and is expected to reduce the leakage current. Consequently, it is confirmed that our procedure can precisely and efficiently extend a knowledge of the physics underlying the transport of electrons through nanoscale structures.

References

- [1] K. Hirose et al., *First-Principles Calculations in Real-Space Formalism*, (Imperial College Press, London, 2005).
- [2] Y. Egami, S. Tsukamoto, T. Ono, and K. Hirose, *Phys. Rev. B*, *submitted*.

First-Principles Calculation of Spin Splitting at Oxide Surfaces and Interfaces

Fumiyuki ISHII

*Faculty of Mathematics and Physics, Institute of Science and Engineering,
Kanazawa University, Kanazawa, 920-1192, Japan*

Ferlectrics are materials which possess spontaneous electric polarization associated with structural phase transition. The electric polarization in ferroelectrics can be controlled by external electric field and pressure. This electrical feature is applicable to several kind of electronic device such as nonvolatile ferroelectric memory. The ferroelectrics are also potential candidate for spintronics application such as spin field-effect-transistor (spin-FET) made of metal-oxide-semiconductor[1]. In conventional spin-FET, the spin is controlled by the Rashba effect caused by the external electric field [2]. By using the ferroelectrics for spin-FET, the spin can be controlled by electric polarization, i.e., internal electric field.

In this study, we have investigated structure and spin state of ferroelectric oxides $ATiO_3$ ($A=Pb, Ba$) and surface of $PbTiO_3$. We have performed the fully-relativistic first-principles calculations based on the non-collinear spin density functional theory implemented in OpenMX code[3]. We have evaluate the energy barrier for polarization rotation by using nudged elastic band method[4] as show in Fig. 1. By changing the direction of the electric polarization, the spin textures in the Bloch-wave vector space (momentum space) drastically change as show in Fig. 2. Based on the group theory, we also discussed relation between the symmetry of crystal structures and spin textures.

References

- [1] S. Datta and B. Das, *Appl. Phys. Lett.* **56**, (1990)665.

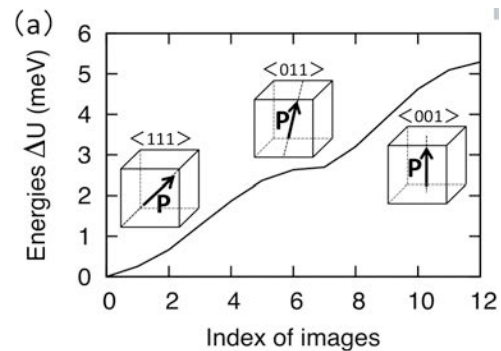


Figure 1: Total energy difference for $BaTiO_3$ with electric-polarization rotation.

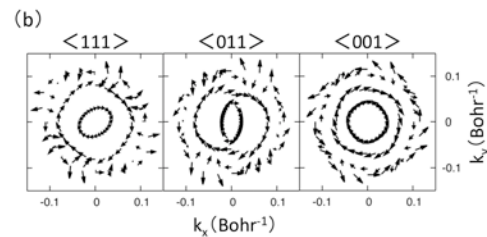


Figure 2: Spin textures for $BaTiO_3$ with electric-polarization rotation.

- [2] E. I. Rashba: *Sov. Phys. Solid State* **2**, (1960)1109.
- [3] T. Ozaki et al., [http:// www.openmx-square.org/](http://www.openmx-square.org/)
- [4] G. Henkelman and H. Jonsson, *J. Chem. Phys.* **113**, (2000)9978.

First-Principles Calculation of Transition Metal Oxide Superlattices

Fumiyuki ISHII

*Faculty of Mathematics and Physics, Institute of Science and Engineering,
Kanazawa University, Kanazawa, 920-1192, Japan*

Recently, artificial superlattices are extensively studied for the application to the spintronics device. In particular, heterostructures of perovskite-type transition-metal oxides attract attention because they exhibit a variety of physical properties[1]. For examples, high-mobility electron gas and tunable Rashba spin-splitting caused by internal electric field in nonmagnetic superlattice interface $\text{LaAlO}_3/\text{SrTiO}_3$ have been reported. Charge-orbital order and magnetic structure in magnetic superlattice $\text{LaMnO}_3/\text{SrMnO}_3$ were found to be strongly affected by substrate LaAlO_3 , $\text{La}_{0.3}\text{Sr}_{1.7}\text{AlTaO}_6$ (LSAT) and SrTiO_3 . The ferromagnetic order were observed in magnetic/nonmagnetic superlattice $(\text{LaMnO}_3)_n/(\text{SrTiO}_3)_8$ ($n=1,2,8$). The previous theoretical study clarified that the system $(\text{LaMnO}_3)_2/(\text{SrTiO}_3)_8$ show half-metallicity. These interesting new properties may originate from the interface of the artificial superlattice. However, the microscopic origin of the phenomenon and the atomic/electronic structure of these interfaces have not been understood sufficiently.

In this study, we clarify the electronic structure and the magnetic stability of artificial superlattice $(\text{LaMnO}_3)_n/(\text{SrTiO}_3)_m$ by using fully-relativistic first-principles electronic structure calculations. By using OPENMX code[2], we perform fully-relativistic first-principles electronic band structure calculations based on non-collinear spin density functional theory (DFT) within the generalized gradient approximation. Figure 1 shows the atomic structure of the ferromagnetic superlattice $(\text{LaMnO}_3)_3/(\text{SrTiO}_3)_3$ and the partial density of states (PDOS) of Mn atoms and Ti

atoms. While the states of Mn atoms show 100% spin-polarized as like half-metallic states, the states of Ti atoms show metallic by electron doping at the LaO interface. We also investigate the spin states on Fermi surfaces. As a result, we found that the Rashba spin-splitting and spin texture strongly depended on the Fermi surfaces. The Rashba parameters are evaluated by the nearly parabolic band obtained from our first-principles calculation. These results may provide understanding of electrical conductivity of this superlattice interface. We also study the superlattices $\text{LaAlO}_3/\text{SrTiO}_3$ and $\text{LaMnO}_3/\text{SrMnO}_3$.

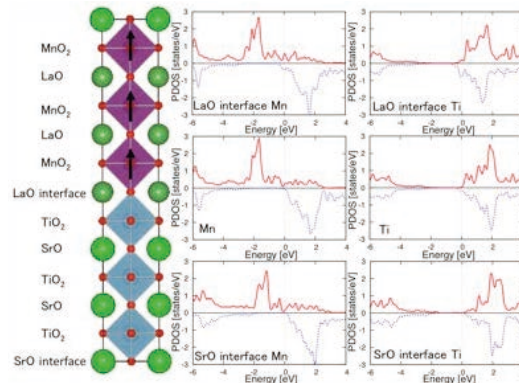


Figure 1: Atomic structure of ferromagnetic superlattice $(\text{LaMnO}_3)_3/(\text{SrTiO}_3)_3$ and partial density of states of Mn and Ti atoms.

References

- [1] H.Y. Hwang et al., *Nature Mater.* **11**, (2012)103.
- [2] T. Ozaki et al., [http:// www.openmx-square.org/](http://www.openmx-square.org/)

A study of the electron self-energy using $\text{GW}\Gamma$ scheme

Masahiro SAKURAI

*Institute for Solid State Physics, University of Tokyo
Kashiwa-no-ha, Kashiwa, Chiba 277-8581*

The electron self-energy Σ , which is a fundamental quantity in the many-electron problem, can be determined from the closed set of five equations derived by Hedin that relate the self-energy Σ , the dressed Green's function G , the dynamically screened Coulomb interaction W , the polarization function Π , and the vertex function Γ to each other. Hedin's approach to obtain self-consistent solution to the coupled equations begins with an approximation to the vertex function and it generates the self-energy in a perturbation series in terms of W . Within the lowest level approximation, Γ is taken as unity and Σ is given as a product of G and W . This approximation is called the GW approximation (GWA). The GWA (without self-consistency in practical calculation) has turned out to give an accurate quasiparticle energy for semiconductors and insulators. The GW method, however, has some serious drawbacks. For example, the GWA breaks the exact relation between Σ and Γ known as Ward identity (WI), which results in violation of local electron-number conservation law.

To address this problem, Takada proposed a non-perturbative algorithm yielding exact Σ and formulated self-consistent $\text{GW}\Gamma$ scheme based on it. [1]. In the iterations toward self-consistency, both Σ and Γ are simultaneously revised in such a way as to ensure that they always meet the WI. To perform numerical calculation, we need an approximate functional form for the electron-hole irreducible interaction $\tilde{I} = \delta\Sigma[G]/\delta G$ which is an integral kernel of the Bethe-Salpeter equation to determine Γ . To study the electron gas, we adopted the

functional form based on the local-field factor [2]. We developed our $\text{GW}\Gamma$ code using MPI and checked the MPI parallel efficiency on System B (Fig. 1). Computationally heavy multiple summations involved in calculating Σ are parallelized over momentum p and fermion Matsubara frequency $i\omega_n$. Using the improved code, convergence has successfully achieved beyond $r_s = 5.25$ where it appears the dielectric catastrophe associated with negative compressibility κ . We are also developing our code to apply $\text{GW}\Gamma$ scheme to two-dimensional electron gas.

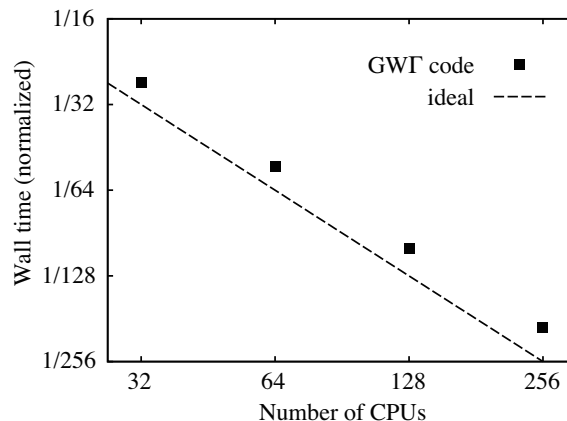


Figure 1: The wall time (normalized to that of 1 CPU) vs. the number of CPUs used for $\text{GW}\Gamma$ calculation on the electron gas ($r_s = 1$).

References

- [1] Y. Takada: Phys. Rev. B **52** (1995) 12708; Phys. Rev. Lett. **87** (2001) 226402.
- [2] S. Ishii, H. Maebashi, and Y. Takada: arXiv:1003.3342.

Study of hydrogen in intermetallic compound: thermodynamic property of vacancy and hydrogen in tungsten

Kazuhito Ohsawa

Institute for applied Mechanics, Kyushu University

Kasuga-koen 6-1, Kasuga-shi, Fukuoka 816-8580

Hydrogen (H) isotope retention is an important subject for safety operation of future fusion reactors. In particular, tritium (T) is a radioisotope whose physical half-life is about 12 years. Tungsten (W) and its alloys are promising as plasma facing materials installed in the fusion reactors due to the excellent properties, low hydrogen solubility and high melting point etc. However, H isotopes are trapped in vacancy (V) and some sorts of V-H complexes are nucleated. Besides, it has been reported that a maximum of 12 H atoms are trapped in the W vacancy at 0K¹⁾ according to first-principle calculations, as shown in Fig. 1. In the present work, we investigate thermodynamic properties of the V-H complexes in a bulk W. The V-H complex concentrations are calculated, assuming an

equilibrium thermodynamic model. Helmholtz free energy is $F=U-ST$. Internal energy U is composed of binding energy of H to W vacancy and formation energy of the vacancy. Entropy S is derived from the number of possible arrangement of H atoms and V-H complexes in the bulk W, i.e. configurational entropy. V-H complex concentrations are shown in Fig. 2 in a finite temperature. The V-H complex concentrations are equal to thermal vacancy density in the limit of low H concentration. While, the V-H complex concentrations rapidly increase as the H concentration increases. In the limit of high H concentration, the super-abundant vacancy formation induced by H is observed.

References

[1] K. Ohsawa: Phys. Rev. B 82, 184117 (2011)

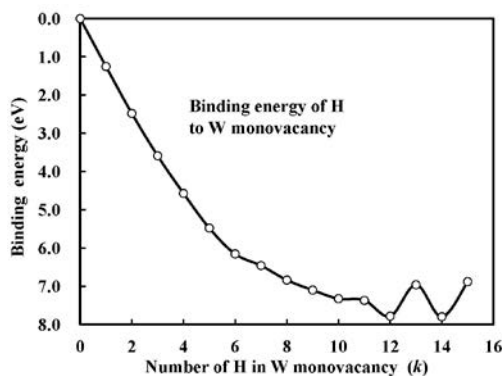


Fig. 1: Binding energy of H to W monovacancy estimated by first-principle calculations.

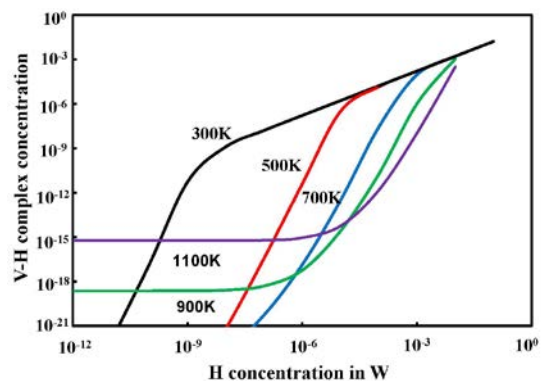


Fig. 2: Dependence of V-H concentration in W on H concentration in a finite temperature.

First-Principles Calculations of Photocatalytic Solid-liquid Interfaces

HIDETOSHI KIZAKI, TAKUYA NISHITANI, and YOSHITADA MORIKAWA

Graduate School of Engineering,

Osaka University, 2-1, Yamada-oka, Suita, Osaka 565-0871

LaFeO₃ is a promising material as a photocatalyst possessing a catalytic activity in visible light. In this study, our purpose is to investigate the stoichiometric stabilities under Fe and O vacancies in LaFeO₃. The relaxed lattice constants for *a*, *b* and *c* in bulk LaFeO₃ correspond to 0.559, 0.574 and 0.792 nm, respectively, which are in reasonable agreement with the experimental values of 0.558, 0.556 and 0.786 nm. At first, we calculated the formation energies of LaFeO₃ from La₂O₃ and Fe₂O₃ by GGA and GGA+U, and examined the effect of on-site coulomb U. The calculated formation energy of LaFeO₃ by GGA+U ($U_{\text{eff}} = 3.0$ eV) was -0.682 eV in good agreement with the experimental value of -0.669 eV, while it was -0.773 eV by GGA. Then, we modeled many kinds of structures that contained several vacancies of Fe or O, and calculated corresponding formation energies.

Furthermore we have also performed first-principles simulations for solid-liquid interfaces on Pt(322) stepped surface. As a result, we find that a H₂O dissociation and an adsorption of an OH molecule on stepped structure of Pt(322) w/o initial OH adsorptions as shown in Fig. 1. However, in case of the others, we cannot find the H₂O dissociation on not only Pt(111) flat surface w/ and w/o initial OH adsorptions but

Pt(322) stepped surface w/ initial OH adsorptions. These results are consistent with the energetics approach of only a hydroxyl adsorption on Pt(322) stepped surface and with experimental data if we consider that our simulation shows on the way to the final water reaction[1].

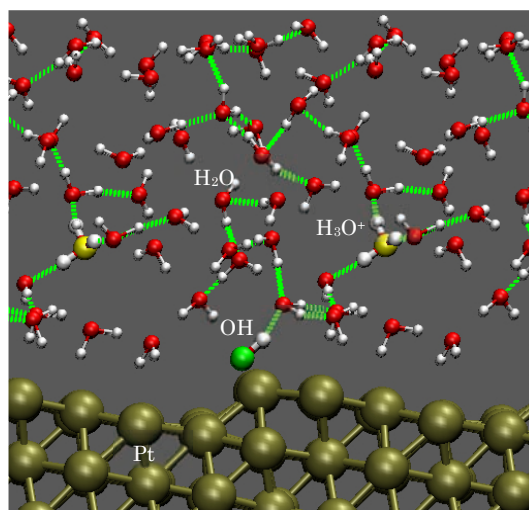


Fig. 1: H₂O dissociation and an adsorption of an OH molecule on Pt(322) stepped surface w/o initial OH adsorptions. Dotted line denotes H-bonding network.

References

- [1] Van der Niet, J.T.C Maria et. al. *Cat. Tod.* **2013**, 202, 105.

First principles calculation on defect structures in mixed conducting Perovskite oxides

Koji Amezawa

Institute of Multidisciplinary Research for Advanced Materials,

Tohoku University, 2-1-1 Katahira, Sendai 980-8577

Solid oxide fuel cells (SOFC) are expected as new energy generators due to their high efficiency of energy conversion. In order to realize SOFC operation at middle temperature ranges (773 ~ 973 K), performance of cathode materials need to be improved more. LaCoO_3 is one of the candidates as a cathode material [1-2]. In order to understand an origin of good performance of LaCoO_3 cathode, we computationally study defect formation behaviors in LaCoO_3 .

First principles total energy calculations were performed using VASP code. Local density approximation (LDA) and Hubbard U potential correction ($U_{\text{eff}} = 3.8$ eV for Co) implemented in VASP code is chosen as an exchange correlation potential for electrons. Cut off energy is set to be 500 eV. Firstly, a primitive cell of rhombohedral LaCoO_3 is fully optimized with k -point sampling meshes of $5 \times 5 \times 5$ until all residual forces acting on each ion become smaller than 0.02 eV/Å. Then, a supercell model containing 320 atoms is constructed. The supercell is optimized under the same condition of residual forces as the primitive cell. Sampling of k -point for the supercell is at Γ point. As defective models,

supercells containing an oxide ion vacancy or an interstitial proton are calculated as shown in the figure below.

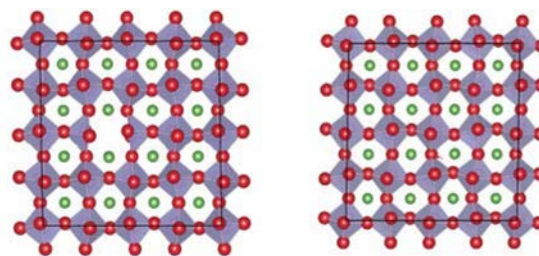


Fig. 1: Supercell models of LaCoO_3 with (left) an oxide ion vacancy and (right) an interstitial proton.

From total energy calculations of the supercells with an oxide ion vacancy and an interstitial proton, hydration enthalpy (ΔH_{hyd}) was evaluated. ΔH_{hyd} of LaCoO_3 is found to be -0.76 eV. This value is comparable with the case of proton conductive Y-doped BaZrO_3 , -0.82 eV. This results means that proton solution possibly affect properties of LaCoO_3 as a cathode.

References

- [1] K. Yashiro, *et al.*, *Electrochem. Solid-State Lett.*, **12**, B135 (2009).
- [2] Eva Mutoro, *et al.*, *Energy Environ. Sci.*, **4**, 3689 (2011).

Scanning tunneling microscopy simulation of β -FeSi₂(100) surface models

Ken HATTORI

*Graduate School of Materials Science, Nara Institute of Science and Technology
Takayama, Ikoma, Nara 630-0192*

Total energies of β -FeSi₂(100)1x1 with adatoms (66 atoms) and without adatoms (64 atoms) were calculated using Simulation Tool for Atom TEchnology (STATE)-Senri [1]. The substrate structure was assumed to be 1st-layer Si (8 atoms per (100)1x1 unit-cell)/2nd-Fe (2)/3rd-Fe (2)/4th-Si (8)/5th-Fe (4)/6th-Si (8)/7th-Fe (2)/8th-Fe (2)/9th-Si (8)/10th-Fe (4)/11th-Si (8)/12th-H (8). 20 adatom models (two Fe or two Si adatoms on 4 hollow sites, 4 bridge sites and 2 atop sites per (100)1x1 unit-cell) were considered to explain periodical atomic surface-protrusions observed by scanning tunneling microscopy. The in-plane lattice constants b and c , and the atomic positions in the last three layers were fixed to the calculated bulk values or stable surface-adsorption configurations. The film thickness was approximately 22 bohr in the total slab thickness of 60 bohr. The generalized gradient approximation proposed by Perdew, Burke, and Ernzerhof, and Troullier-Martins norm-conserving (Vanderbilt's ultrasoft) pseudo potentials for Fe and Si (H) atoms were used for the density functional theory (DFT) calculations. The wave functions and charge densities are expanded by a plane-wave set with cutoff energies of 25 and 225 Ry, respectively. The spin polarization was not considered. The k-mesh grid was 2x2x1 in the energy estimation. All atoms except the fixed ones were relaxed until all residual force components are less than 0.05 eV/Å.

Two hollow-site models (named as H3 and H4, and they were almost degenerated) were found to be stable for both Fe and Si adatom models. In this stage, the candidate models could be restricted to be WO (without adatoms), Fe-H3, Fe-H4, Si-H3, and Si-H4.

Next simulated STM patterns were compared to experimental images at filled ($E_F - 1$ eV) and empty ($E_F + 1$ eV) states. In the STM simulation the k-mesh grid was 5x5x1, and the dipole correction in the vacuum was inserted. The simulation mapped the iso-charge density surfaces at 10^{-8} e/bohr³.

In the WO model, four Si atoms in the 1st layer were considerably relaxed and form square-like positions, resulting in one protrusion in the STM patterns at both states. The patterns well explained the experimental images. In the Fe-H3/H4 models, one Fe adatom induced one STM protrusion, which were similar to those in the experiments. In the Si-H3/H4 models, Si adatoms also induced STM protrusions in both bias, however, in the empty state 2nd-layer Fe was also participated as brighter protrusions; this was not consistent with the experimental images. Thus, WO and Fe-H3/H4 models were proposed by the DFT calculations.

The calculations were performed in System A. The relaxation calculations were required over 10 hours in P1 process in each model. The dipole-correction calculations were several hours in P1 process. The STM-simulations were in D1 process.

The author thank Prof. Morikawa in Osaka University, Dr. Yanagisawa in Ryukyu University, and Dr. Hamada in NIMS for their great support in STATE-Senri calculations.

References

- [1] Y. Morikawa: Phys. Rev. B **63** (2001) 033405, and references therein.

Large scale first principles calculation of core loss spectroscopy

Teruyasu MIZOGUCHI

Institute of Industrial Science, University of Tokyo

Komaba, Meguro, Tokyo 153-8505

To achieve a comprehensive understanding of the chemical reactions, such as catalytic reaction at liquid–solid interfaces, analyses of the liquid properties with improved spatial resolution, temporal resolution, and sensitivity are needed. Among the existing analytical methods, core-loss spectroscopy using electrons or X-rays offers atomic-scale spatial resolution, nanosecond-level time resolution, and high sensitivity. Despite the advantages of core-loss spectroscopy, the practical application of this technique in liquid analysis has been limited, largely due to a lack of suitable theoretical methods for calculating the core-loss spectra of liquids.

In this study, the core-loss spectrum from the liquid was analyzed by combining MD simulations and first-principles band structure calculations in an effective approach for estimating the dynamic behavior of molecules from the core-loss spectrum.

First, two models were constructed for spectral calculations. The first model included an isolated methanol molecule inside a $10 \times 10 \times 10$ -Å box (Fig. 1). The methanol structure was optimised, and this model was thereafter called the ‘gas model’ because the methanol molecules were separated from each other. The second model, termed the ‘liquid model’, was constructed from an MD simulation. The validity of the MD simulation was confirmed using simulated melting and boiling temperatures. The liquid model obtained by the MD simulation at 313 K is shown in Figure 1.

The periodic boundary condition was used for the spectral calculations in this study, whereas prior studies used cluster calculations to generate the core-loss spectra of molecules and liquids, and one or several molecules were taken from independent MD calculations. However, the use

of the periodic boundary condition was important for reproducing the experimental spectra of liquids.

Through this study, we found that the calculated C-K edge spectrum of the isolated methanol molecule satisfactorily reproduces the experimental spectrum of methanol gas, while it is different from the experimental spectrum of liquid methanol. It was found that the reproducibility of the liquid spectrum is greatly improved by calculating C-K edge of the liquid model. This indicates that the spectral profiles of ELNES/XANES reflect molecule-molecule interactions and local structure fluctuations of molecules, such as stretching and bending [1].

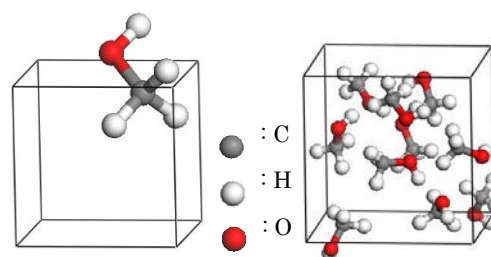


Figure 1: Models for ELNES/XANES calculation. (Left) gas-model and (right) liquid model. The methanol molecule in the gas model has the stable structure, whereas that in the liquid model was obtained by the MD simulation.

References

- [1] "An estimation of molecular dynamic behaviour in a liquid using core-loss spectroscopy", Y. Matsui, K. Seki, H. Hibara, T. Mizoguchi, *Scientific Reports*, 3 (2013) 3503-1-7.

First principles study on homo and hetero interface of photovoltaic materials

Teruyasu MIZOGUCHI

Institute of Industrial Science, University of Tokyo

Komaba, Meguro, Tokyo 153-8505

CIS is a direct energy-gap semiconductor and has a proper band gap for absorbing the solar ray, so it is expected to be the high efficiency photovoltaic cell. To absorb the solar ray more efficiently, the control of the band gap of CIS is indispensable. On the other hand, though the CIS is polycrystalline material and has a lot of GBs, the effect of GB on the band gap property is still under debate. Moreover, the electronic band bending at the GBs has been extensively studied, but many kinds of results were proposed. To clarify the effect of GB, we combined a first-principles calculation and a high-angle annular dark-field scanning transmission electron microscopy (HAADF-STEM).

In this study, we focused on $(112)[\bar{1}\bar{1}0]$ $\Sigma 3$ twin GB as a model. CIS has chalcopyrite structure which is like diamond structure and zinc-blende structure. Viewing the structure from $[\bar{1}\bar{1}0]$ axis, a dumbbell structure is observed where the dumbbell includes Se column and cation column. In the cation column, Cu and In are arranged in turns in the $[\bar{1}\bar{1}0]$ direction. Using this dumbbell structure, $(112)[\bar{1}\bar{1}0]$ $\Sigma 3$ twin GB is formed by tilting one side of grain along $[\bar{1}\bar{1}0]$ axis by 35.27° and the other side of grain by -32.27° . The number of atoms in the calculation periodic model was 96.

In STEM observation, HAADF-STEM was used (JEOL ARM-200CF). CIS thin film was deposited on MgO (001) substrate using pulsed laser deposition (PLD) method. In a first principles calculation, projector augmented wave (PAW) method was used within a Perdew-Burke-Ernzerhof (PBE) generalized gradient approximation using the Hubbard U correction (GGA+U) implemented in VASP code. The Heyd-Scuseria-Ernzerhof (HSE) hybrid functional scheme was applied in band gap calculations.

Figure 1 shows HAADF-STEM image of a GB in CIS. Dumbbell structure is clearly observed. From the brightness of those atomic columns, the kinds of the atomic columns can be identified. Thus, it is found that the bondings across the GB are between cation and Se columns. The

calculated structure was overlaid on the HAADF-STEM image. It is found that the calculated model is in good agreement with the observed image. Furthermore, similar twin boundary was frequently observed. This result matches the lowness of GB energy in calculation.

The effects of the atomic structure of the GB on the band gap and potential barrier were systematically investigated using hybrid functional calculation [1]. Furthermore, we also investigated the vacancy formation energetics at the GB [2].

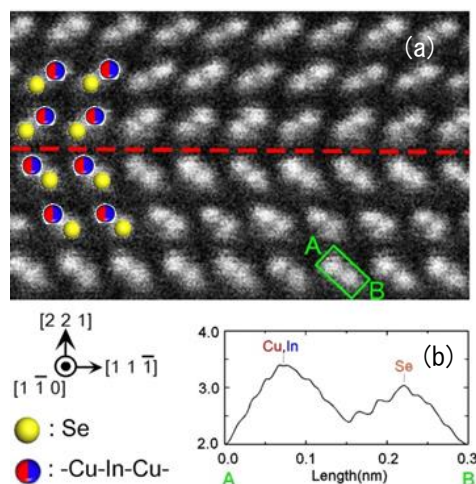


Figure 1: (a) HAADF-STEM images of CuInSe_2 and calculated model. The dot line represents the position of $\Sigma 3$ twin GBs. (b) Intensity profile HAADF image along A-B.

References

- [1] "The atomic structure, band gap, and electrostatic potential at the $(112)[1-10]$ twin grain boundary of CuInSe_2 " H. Yamaguchi, H. Hiramatsu, H. Hosono, and T. Mizoguchi, *Appl. Phys. Lett.*, 104, 153904-1-5 (2014).
- [2] "Defect formation energetics at the grain boundary in CuInSe_2 using first-principles calculations" H. Yamaguchi and T. Mizoguchi, *J. Ceram. Soc. Jpn.*, in press.

Analysis of the temperature dependence of the magnetic and electronic structures of Mn_3Pt on the basis of the first-principles molecular dynamics theory

Takashi UCHIDA

Hokkaido University of Science

4-1, 7-15, Maeda, Teine-ku, Sapporo 006-8585

The Mn-based ordered alloys Mn_3X (X=Pt, Rh, Ir), which all have Cu_3Au -type crystal structure, are frustrated itinerant magnets with an octahedral configuration of Mn local magnetic moments. Neutron diffraction experiments [1] suggest that at temperatures sufficiently below their Néel temperatures T_N , all these alloys reveal the triangular magnetic structure with Γ_{4g} symmetry (D-phase). On the other hand, it has been suggested that the D-phase of Mn_3Pt changes into collinear magnetic phase (F-phase) at 400 K before changing into paramagnetic phase at $T_N = 475$ K.

To clarify the physical origin of F-phase of Mn_3Pt , we have investigated and compared the temperature dependence of the magnetic and electronic structures of Mn_3Pt and Mn_3Ir by means of the first-principles molecular dynamics (MD) approach for itinerant magnets [2]. The theory is formulated by incorporating the first-principles TB-LMTO Hamiltonian into the MD approach for itinerant magnets on the basis of the functional integral method and the isothermal MD technique. The MD approach allows us to determine automatically the magnetic structure of a large system with several hundred atoms in a unit cell at finite temperatures.

In the first-principles MD approach, we calculate the thermal average of local magnetic moments by solving the isothermal MD equations of motion. The magnetic forces in the MD equations are determined at each time step by calculating the electronic structure by means of the recursion method. We utilize the

MPI parallel calculation scheme in the recursion calculation and this is found to be quite effective in saving computing time because more than 90 % of the CPU time concentrates on this process.

We have calculated the electronic and magnetic structure for a system with $4 \times 4 \times 4$ fcc lattice with fixing the crystal structure and lattice constant. At sufficiently low temperatures below T_N , Mn_3Pt and Mn_3Ir both exhibit the triangular magnetic structure (D-phase), being consistent with experiment. With increasing temperature from 25 K, Mn_3Pt exhibits a first-order transition to another ordered phase (F-phase) around 350 K, accompanying a development of Mn-Eg DOS at Fermi energy E_F . Mn_3Ir , on the other hand, shows a continuous decrease of Mn local moments up to T_N , indicating a second-order transition to paramagnetic phase. The Mn-Eg DOS of Mn_3Ir does not show appreciable development up to T_N . We conclude that the enhancement of the ferromagnetic couplings among the second-nearest neighbor Mn local moments (due to Mn-Eg states) are responsible for the emergence of F-phase in Mn_3Pt .

References

- [1] T. Ikeda and Y. Tsunoda, *J. Phys. Soc. Jpn.* **72** (2003) 2614.
- [2] T. Uchida and Y. Kakehashi, *J. Korean Phys. Soc.* **62** (2013) 1748.

First-principles calculations on atomic and electronic structure at oxide grain boundaries

Yukio SATO

Institute of Engineering Innovation,

The University of Tokyo, 2-11-16, Yayoi, Bunkyo, Tokyo 113-8656

Many of practical materials are used in the polycrystalline forms, and the grain boundaries (GBs) often play important roles in obtaining materials function. In the present study, we aim to add electrical conductivity to GBs of alumina (Al_2O_3), which is well-known electrical insulator and therefore used for insulating substrates in electrical circuit. This may allow us to build nano-patterned electrodes embedded within substrate materials. Doping a few 3d transition metal elements such as Co, Ni, and Cu, we tried to modify the electronic states formed in the GBs.

We have chosen an Al_2O_3 single GB for a case study. The GB has the geometrical orientation relationship of $\Sigma 13$ according to the coincidence site lattice (CSL) theory [1]. The adjacent crystals have common [11-20] axes in parallel and the GB plane is (1-104) [2].

Stable atomic arrangements of the Co, Ni, and Cu-doped Al_2O_3 GBs were simulated by first-principles PAW calculations under GGA approximation. Further, for the density of state calculations, hybrid functional was used for better description. The simulation cells included 120 atoms. All the calculations were done with the VASP code, and oxidation state of all the dopants was assumed to be +3.

Figure 1 shows the stable atomic arrangements of the GBs, where Al atoms at particular sites are replaced by Co, Ni, or Cu. After structural optimization, significant structural relaxation did not occur. On the other hand, there are noticeable differences in the density of states. For all the GBs, dopant elements form additional states in the band gap. Further, the lowest unoccupied levels formed in the Cu-doped case, which may allow us the biggest opportunity to obtain electrically

conductive GB.

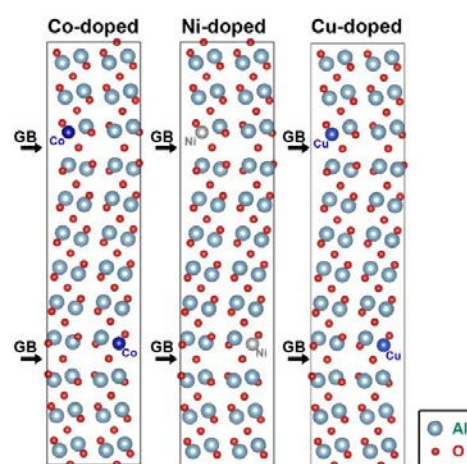


Fig. 1: Stable atomic arrangements in Co-, Ni-, and Cu-doped Al_2O_3 GBs.

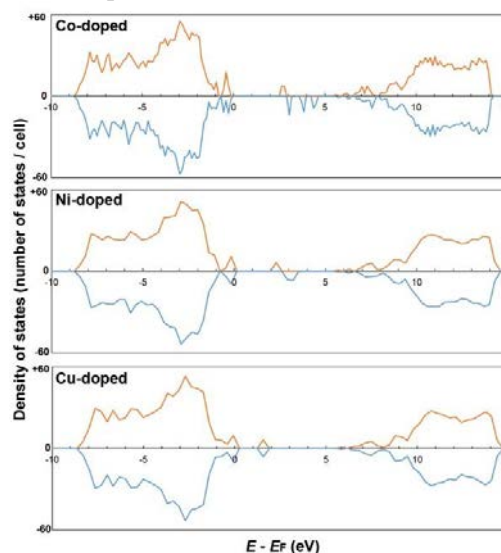


Fig. 2: Density of states of the Co-, Ni-, and Cu-doped Al_2O_3 GB supercells.

References

- [1] H. Grimmer, *Acta Cryst. A* **45** (1989) 505.
- [2] S. Fabris and C. Elsässer, *Acta Mater.* **51** (2003) 71.

First-principles calculations of the atomic arrangement at the interfaces in crystalline solids

Yukio SATO

Institute of Engineering Innovation,

The University of Tokyo, 2-11-16, Yayoi, Bunkyo, Tokyo 113-8656

Polycrystalline zinc oxide (ZnO) ceramics have found the application for varistor devices owing to the high nonlinearity in their current-voltage characteristics. It has been revealed that the nonlinearity is caused by grain boundaries (GBs) in ceramics. On the other hand, in recent years, ZnO films are intensively studied for transparent electrode application. In this case, GB may lower electrical conductivity via the reduction of electron mobility. In order to understand the GB effects on electrical property, we study atomistic structure of a ZnO GB.

We chose ZnO [0001]/(13 $\bar{4}$ 0) symmetric tilt GB for modelling. Simulation cells including the GBs constructed include approximately 210 atoms. First-principles PAW calculations were conducted using the VASP code, where the GGA-PBE exchange correlation potentials were used.

Figures 1 (a)~(d) show stable atomic arrangements of the GB obtained by the first-principles calculations together with their GB energies. The atomic arrangements are periodic as indicated by the dotted lines, and the arrangement are characterized as the combination of five, six, seven or eight-membered rings. Comparison of (a) and (c) reveals that the six- and eight-membered rings exhibit lower energy than the five- and seven-membered ones do. The same conclusion

comes out from the comparison of (b) and (d). Existence of dangling bonds in the case of five- and seven-membered rings case [1] would be a cause of extra energies in (c) and (d).

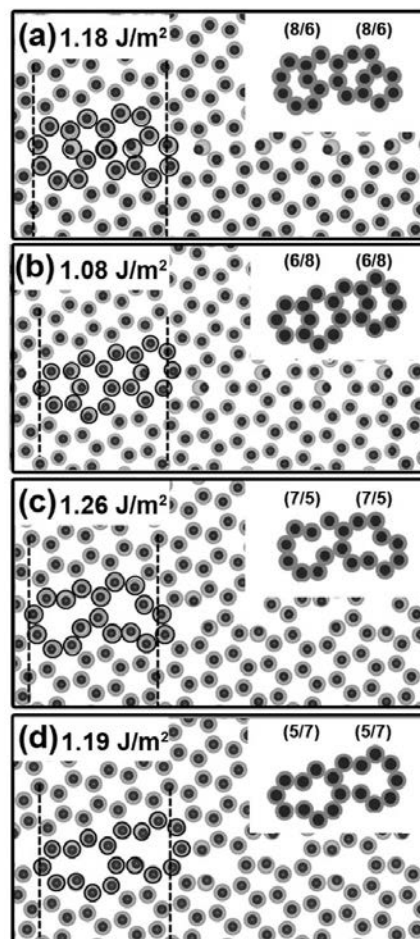


Fig. 1: Some stable atomic arrangements of ZnO [0001]/(13 $\bar{4}$ 0) symmetric tilt GB [1].

Reference

- [1] J. Roh *et al.*, *J. Am. Ceram. Soc.* **97** (2014) 617.

Search for new electronic properties of new nanoscale interfaces

Katsuyoshi KOBAYASHI

*Department of Physics, Ochanomizu University
2-1-1 Otsuka, Bunkyo-ku, Tokyo 112-8610*

Recently topological insulators are extensively studied. In 2013 we studied the electronic states of bismuth thin films.

It is theoretically predicted that a Bi film of one bilayer (BL) thickness is a two-dimensional topological insulator [1]. There is an experiment using scanning tunneling spectroscopy [2] that shows an evidence for the edge states of 1 BL Bi films. However, the energy range of the edge states observed in this experiment does not match with that of the theoretical calculation [3]. It has not been established that the edge states of 1BL Bi films are experimentally verified.

Another problematic point in 1 BL Bi films is that the dispersion of the edge bands is complex. There are three states in the edge bands that cross the Fermi energy. This property causes back scattering by scatterers with time-reversal symmetry. It makes the quantum spin Hall effect difficult to observe. In order to overcome this difficulty we try two theoretical investigations in 2013. One is making use of interactions with substrates. The other is decoration of the edges of 1 BL Bi films with atoms.

In the first investigation we calculated electronic states of 1BL Bi films on Bi_2Te_3 substrates. 1 BL Bi films have a bilayer structure. When Bi films are placed on substrates, the edge Bi atoms at two sides of wires are not equivalent. Our calculated results show that the degeneracy of the edge states localized at two sides of wires is lifted by the interaction with substrates. However, the splitting of the edge-state bands is not so large that the number of states crossing the Fermi energy changes. This is partially due to the fact that

the potential energy at Bi atoms in the 1 BL films is not symmetric.

In the second investigation we calculated electronic states of free standing 1 BL Bi wires with hydrogen atoms at edges. Figure 1 shows a calculated band structure. The band dispersion of the edge states of 1 BL Bi wires with hydrogen atoms are considerably different from those without hydrogen atoms. The former is like an ideal Dirac cone. There is only one state crossing the Fermi energy. Backscattering does not occur by scatterers with time-reversal symmetry. Therefore, the 1 BL Bi wires with hydrogen atoms at edges are promising systems for observing the quantum spin Hall effect.

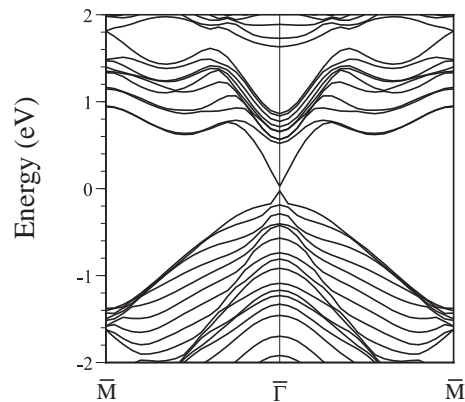


Figure 1: Band structure of a 1 BL Bi wire with hydrogen atoms at edges.

References

- [1] S. Murakami: *Phys. Rev. Lett.* **97** (2006) 236805.

- [2] F. Yang *et al.*: Phys. Rev. Lett. **109**
(2012) 016801.
- [3] M. Wada *et al.*: Phys. Rev. B **83** (2011)
121310(R).

Electronic State and Proximity Effects around Interface in Layered Superlattices

Kunitomo HIRAI

*Department of Physics, Nara Medical University
Kashihara, Nara 634-8521*

The purpose of the present research is to elucidate characteristics of electronic state in superlattices with layered structures, in particular, to illustrate proximity effects of each layer on adjacent layers in the superlattices. This research of a first-principles electronic structure calculation is performed by means of the Korringa-Kohn-Rostoker (KKR) Green function method within the framework of the local spin density (LSD) functional formalism.

The calculation by means of the KKR method was so far carried out for superlattices of ferromagnetic layers with nonmagnetic spacer layers such as Fe/Cr, Fe/V, Fe/Cu, . . . ones, with magnetizations of two successive Fe layers being aligned parallel or antiparallel. Oscillatory interlayer exchange coupling between ferromagnetic layers with respect to spacer thickness was investigated, and relation between bulk effects inherent in the spacer layer and the proximity effects due to the ferromagnetic layers was analyzed. In the calculation, every atom in a monolayer stacked in the superlattices is assumed to be equivalent, and there is one site in each monolayer. This assumption can be justified for the superlattices with ideal interfaces without structure, but not for those with realistic interfaces with structures like steps, islands, or such, and hence there are two or more sites in each monolayer for the superlattices with realistic interfaces.

A need of the calculation for superlattices with more sites in each monolayer arises also for layered superlattices of ordered alloys or

compounds, which now attract broad interests particularly in viewpoint of spintronics. We then start preparation of the calculation for superlattices with more sites in each monolayer, which results in increase of the number of atoms in a unit cell and involves vast increase of computation times. In the preparation of the calculation, installation of parallelization with use of the OpenMP into program codes of the KKR methods is intended, together with parallelization with use of the MPI which was already achieved, that is, installation of hybrid parallelization is intended.

The installation of the OpenMP is in progress and will be achieved in due course, and then the proximity effects in the superlattices with realistic interfaces will be investigated to elucidate the roles of the interfaces in the superlattices. The calculation will be carried out for Fe superlattices with steps, and magnetic frustration caused by the steps is investigated, in particular reference to possible mechanism of increase of total magnetization of the Fe layers, where fcc(001) or fcc(111) superlattices are considered together with usual bcc(001) ones and difference between those superlattices is to be analyzed. In addition, the calculation will be carried out for layered superlattices of ordered alloys, such as fcc(001) superlattices consisting of Fe and FePt layers, in particular reference to ferromagnetic or antiferromagnetic coupling between layers and within a monolayer.

First principles calculations of complex defect structures in oxide ceramics

Tetsuya TOHEI

Institute of Engineering Innovation,

The University of Tokyo, Yayoi, Bunkyo-ku, Tokyo 113-8656

α -alumina (α -Al₂O₃) is a popular oxide ceramics material with high mechanical strength, toughness, and corrosion resistance up to high temperatures, which are advantageous for application as high temperature structural materials. Rapid short-circuit diffusion process via grain boundaries in alumina is crucial for the material's high temperature properties such as creep deformation, densification in sintering, grain growth, and so on. Although diffusion phenomena along alumina grain boundary (GB) have been extensively studied, many questions remain unresolved [1]. In this study, we investigated atomic structures, vacancy formations and migration behaviors in alumina grain boundary by first principles theoretical calculations in order to understand the defect originated properties such as G.B. diffusion from an atomistic scale. We focused on Al₂O₃ Σ 11 (1-210)/[10-11] GB as a model grain boundary. Stable atomic configuration of the GB was firstly searched by the method of rigid body translation employing static lattice calculations. Then accurate atomistic structure of the GB was evaluated by first principles calculations within the framework of density functional theory (DFT). We used plane wave basis PAW method (VASP code) for structure optimization and total energy calculations. Supercells containing about 400 atoms were used for the calculations. Since oxygen diffusion in α -alumina is considered to occur mainly via oxygen vacancies, understanding the oxygen vacancy formation

behavior is essential. Formation energies of isolated oxygen (O) vacancies were calculated for various atomic sites around the GB and the bulk region. To evaluate atomic diffusion phenomena, we employed two classes of theoretical methods: First we performed classical molecular dynamics (MD) simulations to estimate dominant diffusion paths in alumina Σ 11 GB. For the MD calculations extended supercells with the GB and composed of about 3600 atoms were used, with several oxygen vacancies introduced into the atomic sites with low vacancy formation energies at the grain boundary. From the MD trajectories of the oxygen vacancy sites, it was confirmed that diffusion of oxygen vacancies predominantly occurs along the grain boundary. Then accurate geometry and activation energies for the dominant atomic migration paths were calculated by nudged elastic band (NEB) method using the first principles PAW method [2]. Calculations of phonon dispersion relations and phonon density of states were also performed on defect models in α -alumina to consider and discuss the lattice vibrational effects on the defect originated properties and phenomena in the material.

References

- [1] A. H. Heuer, J. Eur. Ceram. Soc., **28**, 1495-507 (2008).
- [2] N. Takahashi et al., Phys. Rev. B, **82**, 174302 (2010).

Thermo-Chemical Wear Mechanism of Diamond Cutting Tool

Yutaka Uda, Shoichi Shimada

Osaka Electro-Communication University, Hatsu-cho, Neyagawa, Osaka 572-8530

Sakuro Honda

Technology Research Institute of Osaka Prefecture, Ayumino, Izumi, Osaka 594-1157

Demand has been increasing for highly durable molds of heat-resistant materials for complex and precise optical components with high aspect ratio. Diamond is an ideal cutting tool material for high efficient ultraprecision metal cutting of complex three-dimensional metal works. However, it is well known that diamond cutting tool shows severe wear in cutting of heat-resistant materials such as ferrous metals and nickel.

On the other hand, in cutting of electroless nickel deposits (Ni-P), which is used as a material of precision molds of high performance optical components, remarkably less tool wear is observed than in case of pure nickel [1,2]. Phosphorous addition should have an important role for tool wear suppression. However, the essential mechanism of wear suppression has not yet been understood well.

Therefore, to understand the wear mechanism of diamond cutting tool in machining of nickel and ferrous metals is very much meaningful to realize useful fabrication technique of the precise molds of the metals with high accuracy and low cost.

Single grain cutting tests and erosion tests

suggest that the wear mechanism is not mechanical but thermo-chemical one [3-5]. Therefore, in order to reveal the mechanisms of the initial stages of wear process and wear suppression by phosphorous addition, ab initio molecular dynamics calculations of chemical reaction on diamond surface in contact with Ni and Ni-P surfaces were carried out using double-grid method for real-space electronic-structure calculations proposed by Dr. T. Ono of Osaka University [6].

The $C_{10}H_{14}$ Cluster is used as a model for a part of diamond (100) surface. Figure 1 shows the optimized atomic configuration of $C_{10}H_{14}$ cluster. The atom at the bottom of the model is the radical carbon interacting with metal surface. The dangling bonds of the other carbon atoms of diamond are terminated by hydrogen

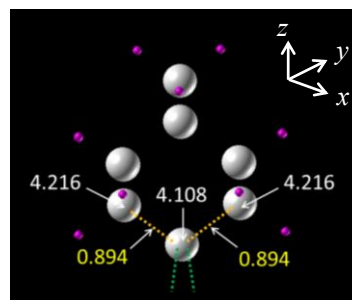


Fig.1. Model of diamond (100) surface

atoms. White and yellow figures express atomic and bond populations, respectively. The atomic population indicates the effective number of electrons belonging to individual atoms. The change between the bond population before and after a chemical reaction is an index of the change in the bond strength in covalent crystal. Figure 2 shows the model of Ni (100) surface. The model have periodic boundaries in x and y directions and aperiodic boundary in z direction. The atomic populations of all Ni atoms are almost 10.0.

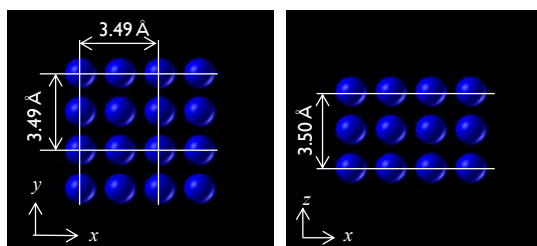


Fig.2. Model of Ni (100) surface

Figure 3 shows the optimized atomic configuration of the diamond cluster interacting with Ni and Ni-12wt%P surfaces. By the interaction with Ni, the atomic population of radical carbon increases to 4.91 from 4.11 and those of Ni decreases to 9.73. The result suggests that the strength of ionic bonding increases between carbon and Ni. The population of back bonds of radical carbon decrease to 0.76 from 0.89. The results suggest that the radical carbon has a chance to dissociate from the diamond surface when it has a large kinetic energy due to cutting temperature. On the other hand, in case of

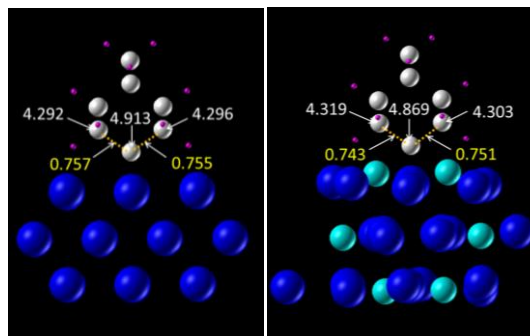


Fig.3. Effect of phosphorous addition to interaction with diamond

interacting with Ni-P, both of decrease of back bond population and increase of atomic population of radical carbon are remarkably suppressed. The result suggests that phosphorous addition reduces the dissociation of carbon atoms on diamond surface.

References

- [1] C.K. Syn, J.S. Taylor, R.R. Donaldson: Proc. SPIE, **676** (1986) 128.
- [2] J.M. Oomen, L. Eisses: Precision Engineering, **14**, (1992) 206.
- [3] T. Tanaka, N. Ikawa: Bull. JSPE, **7** (1973) 97.
- [4] S. Shimada, H. Tanaka, M. Higuchi, T. Yamaguchi, S. Honda, K. Obata: Annals of the CIRP, **53**, (2004) 57.
- [5] N. Furushiro, H. Tanaka, M. Higuchi, T. Yamaguchi, S. Shimada: Annals of the CIRP, **59**, (2010) 105.
- [6] T. Ono, K. Hirose: Physical Review Letters, **82** (1999) 5016.